Single-Electron Tunneling

Gerd Schön

Institut für Theoretische Festkörperphysik,
Universität Karlsruhe, D-76128 Karlsruhe, Germany

Chapter 3 of the book on
Quantum Transport and Dissipation
T. Dittrich, P. Hänggi, G. Ingold, B. Kramer, G. Schön, W. Zwerger
VCH Verlag

revised version, 1. October 1997

Contents

3 Single-Electron Tunneling

3.1 Introduction

In the last few years substantial progress has been achieved in micro-fabrication technology. It has become possible to fabricate in a controlled way metallic tunnel junctions with capacitances in the range of $C = 10^{-15}$F. In this case the charging energy associated with a single-electron charge, $E_C \equiv e^2/2C$, is of the order of 10^{-4}eV, which corresponds to a temperature scale $E_C/k_B \approx 1$K. This implies that electron transport in the sub-Kelvin regime is strongly affected by charging effects. Similar properties have been observed in semiconductor nanostructures, for instance in quantum dots in 2-dimensional electron gases. The Coulomb energy in these systems can be characterized by a capacitance which depends on the size of the dot and also may lie in the range of 10^{-15}F or less. Charging effects play a role in granular materials and ultimately even in molecular systems. Here the capacitance may be as low as 10^{-18}F, making single-electron tunneling observable even at room temperatures. This opens spectacular perspectives for future applications.

In this Chapter we will describe single-electron tunneling in the presence of charging effects. For definiteness we will consider metallic systems with a large density of quantum states, although the concepts described here are equally important for semiconductor or molecular systems. We will first study in Section 3.2 how the charging energy depends on the number of electrons and on transport and gate voltages applied to various parts of the system. The simplest model systems which demonstrate these features are the so-called "single-electron box" and the "single-electron transistor".

We will then derive in Section 3.3 within perturbation theory the single-electron tunneling rates. In low capacitance systems it is crucial to account for the change in the charging energy associated with the tunneling process. A master-equation description accounts for the large-scale features of the current-voltage characteristic of the single-electron transistor. In the Coulomb-blockade regime, where single-electron tunneling is suppressed, higher-order processes such as coherent "cotunneling" of electrons through several junctions become observable.

The mesoscopic junction systems studied here are small such that charging effects and higher-order quantum processes play a role. On the other hand, they are large enough such that macroscopic current and voltage probes and sources can be coupled to the system. This makes the mesoscopic system susceptible to the influence of the

electric circuit. It is therefore necessary to include in a complete description the external circuit and to investigate the influence of the electrodynamic environment on single-electron tunneling (Section 3.4).

We begin by studying tunnel junctions with two normal metal leads (NN). If part of the system is superconducting further highly interesting effects are found (Section 3.5). At subgap voltages the single-electron tunneling is suppressed. This makes higher-order processes such as Andreev reflection in normal-superconductor (NS) junctions the leading transport process. Furthermore, the energy of excitations created in one tunneling process can be regained if in a later tunneling process two excitations recombine into a Cooper pair. This leads to "parity effects", which distinguish between states with even or odd electron number in the superconducting electron box. They also lead to interesting structure in the I-V characteristics of superconducting (NSN or SSS) SET transistors. The tunneling of Cooper pairs is influenced by charging effects in a similar way as that of single electrons. However, Cooper pairs can also tunnel coherently. The charge and the phase difference in a Josephson junction are quantum mechanical conjugate variables, and the junction is described by a macroscopic Hamiltonian. The eigenstates in general are superpositions of different charge states. Their properties can be probed by tunneling of normal electrons. We discuss a model where in an NSS transistor the Andreev reflection in the NS junction is used as a spectroscopic tool to detect the coherent Cooper-pair tunneling in the SS junction.

Many of the single-electron effects can be described within simple perturbation theory. A necessary requirement is that the resistance of the tunnel barriers is high compared with the quantum resistance $R_{\rm K} = h/e^2 = 25.81281...\ {\rm k}\Omega$. In order to describe junctions with lower tunnel resistance a more general formulation is required. A systematic description of tunneling in systems with strong charging effects is provided by a path-integral approach. It is a generalization of the formulation developed for dissipative quantum mechanics and reviewed Chapter 4 of this volume. We first present (Section 3.6) the imaginary-time path-integral method, which is appropriate for the description of equilibrium properties, e.g. the Josephson current through SNS transistors or the influence of charging on the proximity effect. On the other hand, we will also present and analyze in a real-time approach the time evolution of the density matrix (Section 3.7). In this approach we can describe systematically higher-order correlated tunneling processes, including "inelastic resonant tunneling". These processes give rise to a renormalization of system parameters and to life-time broadening effects.

Single-electron effects have been studied now for more than a decade, and a large number of papers have been devoted to this subject. Where available we quote review articles and collections of papers, where further references can be found. The first article to be mentioned is the one by Averin and Likharev [1], who developed the perturbation theory of single-electron tunneling and described several applications for current-biased junctions. Later it became clear that in most experiments voltage-biased junctions or systems of junctions were used. Initial scepticism against the new theoretical concepts was quickly overcome when experiments were successful. After an early experiment by Fulton and Dolan, the important breakthroughs were achieved in Delft by Mooij and Geerligs and in Saclay by Devoret, Estève and further members of these groups. Their early work is well summarized in the book *Single Charge Tunneling*

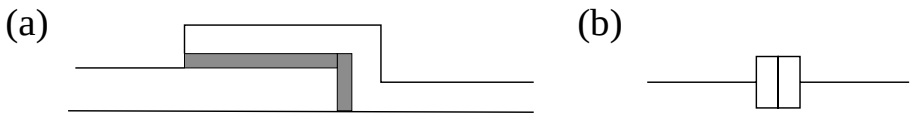

Fig. 3.1: (a) An overlap junction with an oxide layer, (b) schematic diagram for a tunnel junction.

[2], which contains review articles describing (i) the theory of single-electron tunneling under the influence of an electrodynamic environment by Ingold and Nazarov, (ii) some higher-order tunneling processes by Averin and Nazarov, (iii) Coulomb-Blockade effects in semiconducting nanostructures by van Houten, Beenakker and Staring, and (iv) properties of junction arrays by Mooij and the author. A collection of research articles was published simultaneously as a devoted issue of Zeitschrift für Physik [3].

Although much of the theoretical work on single-electron tunneling included also the effects of superconductivity, it took longer until the experimental situation became clear. Parity effects related to the presence of a single excitation in a superconducting island are a particular interesting example. In this context the experimental work of the groups in Saclay and Harvard should be mentioned; the theory was advanced by Averin and Nazarov, Glazman and Hekking, and others. The concepts have entered modern textbooks like that of M. Tinkham [4]. A collection of articles representing the state of 1994 is contained in the proceedings of the conference *Mesoscopic Superconductivity* [5]. The path-integral formulation of tunneling in systems with strong charging effects was developed in a collaboration of Ambegaokar, Eckern and the author [6] and is summarized in the review article with Zaikin [7]. It has been applied to describe several effects in mesoscopic superconductors in Refs. [8, 9]. A systematic description of tunneling beyond perturbation theory, incl. cotunneling and inelastic resonant tunneling is presented in Ref. [10].

3.2 Charging energy and single-electron devices

In this Section we introduce the concept of a capacitive charging energy and describe some of the circuits which show single-electron effects. We concentrate on metallic systems with a large electron density of states. The number of electrons in an "island", i.e. in a part of the system which is electrically isolated from the rest of the circuit, is integer. It may change in discrete units by tunneling. On the other hand, we have control variables, such as applied gate voltages, which change the polarization charge on the capacitors in a continuous way. Many of the measurable consequences of the single-electron effects depend on this interplay of discrete and continuous changes of the charge. For a further review and extensions of the material covered here the article by D. Estève in Ref. [2] is recommended.

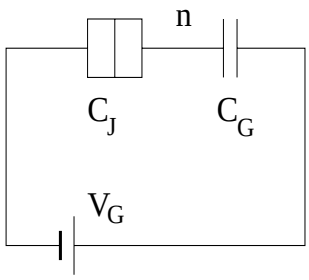

Fig. 3.2: The single-electron box.

3.2.1 The energy scale

Modern lithographic techniques allow the fabrication of narrow metallic lines with width down to several 10nm, as well as tunnel junctions in overlap regions of such lines, as illustrated in Fig. 3.1. Junctions with an area S=(100nm)^2 can be produced reliably. The oxide layer is roughly $d = 10$Å thick, and the dielectric constant of the oxide is $\epsilon \approx 10$. Using the classical expression for the capacitance we arrive at $C = \epsilon S/(4\pi d) \approx 10^{-15}$F. While it was not clear, a priori, whether the classical expression for the capacitance can be applied at such small length scales, it has been confirmed by the experimental observation of charging effects. The Coulomb gaps (see below) in the I-V characteristics are consistent with the simple estimate within a few percent.

The capacitance introduces an energy scale, the charging energy corresponding to a single-electron charge -e,

$$E_{\rm C} \equiv \frac{e^2}{2C} \ , \tag{3.1}$$

which characterizes all charging effects. It is of the order of $E_{\rm C} \approx 10^{-4}e$V if the capacitance is $C = 10^{-15}$F, which corresponds to a temperature $E_{\rm C}/k_{\rm B} \approx 1$K. This implies that in the sub-Kelvin regime the electronic states and transport properties are significantly affected by charging effects.

3.2.2 Single-electron box

We analyze now the charging energy of simple systems of tunnel junctions. It depends on the electron number in various parts of the system and the applied voltages. The first example is the single-electron box, shown schematically in Fig. 3.2. It consists of a small metallic island, coupled via a tunnel junction with capacitance $C_{\rm J}$ to an electrode and via a capacitor $C_{\rm G}$ to a gate voltage source $V_{\rm G}$. For $V_{\rm G} = 0$ the lowest energy state of the system is charge neutral. In this reference state the electrons on the island compensate the charge of the ions; there are $n = 0$ excess electrons on the island. If the gate voltage is turned on the number of excess electrons on the island can change due to tunneling across the junction in *discrete* steps to $n = \pm 1, \pm 2, ...$

While the total number of electrons on an island is integer, the charge is spatially distributed and in general shifted relative to the positive background. If a voltage is

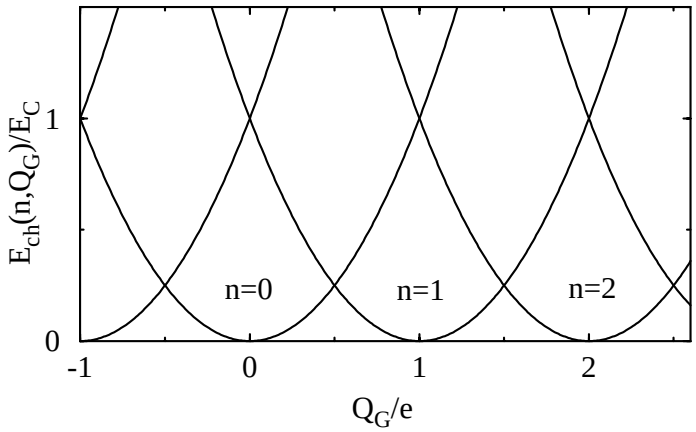

Fig. 3.3: The charging energy of a single-electron box as a function of the gate voltage for different numbers n of electron charges on the island.

applied the surface charges on the capacitor plates, which are of equal magnitude but opposite sign on the two sides of each junction, are in general non-quantized. They are determined by the integer n and the non-quantized applied voltage. We obtain the charging energy from the following elementary arguments: the total excess charge of the box splits into two parts on the left and right capacitor plate $-ne = Q_\mathrm{l} + Q_\mathrm{r}$. The corresponding voltage drops add to the applied voltage $V_\mathrm{G} = Q_\mathrm{l}/C_\mathrm{J} - Q_\mathrm{r}/C_\mathrm{G}$, and the charging energy is $Q_\mathrm{l}^2/2C_\mathrm{J} + Q_\mathrm{r}^2/2C_\mathrm{G}$. The relevant free energy is a Legendre transform of this energy, which also contains the work done by the voltage source $-V_\mathrm{G}Q_\mathrm{r}$. Elimination of Q_l and Q_r in favor of n and V_G yields, up to a contribution which does not depend on the variable n, the result

$$E_\mathrm{ch}(n, Q_\mathrm{G}) = \frac{(ne - Q_\mathrm{G})^2}{2C} \,. \tag{3.2}$$

Here $C = C_\mathrm{J} + C_\mathrm{G}$ is the total capacitance of the island. The effect of the voltage source is contained in the "gate charge" defined as $Q_\mathrm{G} = C_\mathrm{G}V_\mathrm{G}$.

The charging energy E_ch is plotted in Fig. 3.3 as a function of the gate charge for different numbers of excess electrons n. With increasing gate voltage, the electron number of the lowest energy state increases. It does so in discrete steps from n to $n+1$ at the degeneracy points $Q_\mathrm{G}/e = n+1/2$. Under the same conditions the voltage of the island $V_\mathrm{island} = \partial E_\mathrm{ch}/\partial Q_\mathrm{G}$ displays a sawtooth-like dependence on the applied voltage.

At finite temperatures the steps and sawtooth dependence are washed-out, as follows from the classical statistical average

$$\langle n(Q_\mathrm{G})\rangle = \frac{1}{Z_\mathrm{ch}} \sum_{n=-\infty}^{\infty} n\, \mathrm{e}^{-E_\mathrm{ch}(n,Q_\mathrm{G})/k_\mathrm{B}T} \,, \tag{3.3}$$

where Z_ch is an obvious normalization. The result is displayed in Fig. 3.4 for different temperatures. The stepwise increase has been observed experimentally, e.g. by the Saclay group (see results in Ref. [2]). Their measurement procedure will be discussed

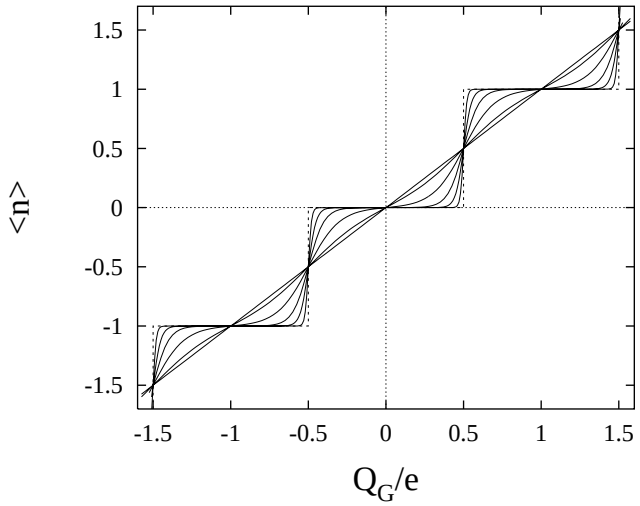

Fig. 3.4: The average number of electron charges $\langle n \rangle$ on the island of a single-electron box as a function of the gate charge (voltage) for different temperatures $T/E_{\rm C} = 0$ (dashed steps), 0.02, 0.05, 0.1, 0.2, 0.4, and 1 (nearly linear).

below. The experiments generally agree well with theoretical expectations, if one manages to control heating and the noise from the measurement setup, which usually is at a temperature higher than that of the cryostat.

3.2.3 Single-electron transistor

Another fundamental example is provided by the single-electron transistor shown in Fig. 3.5. Here an island is coupled via two tunnel junctions to a transport voltage source $V = V_{\rm L} - V_{\rm R}$ such that a current can flow. The island is, furthermore, coupled capacitively to a gate voltage $V_{\rm G}$. The charging energy of the system depends again on the (integer) number of electrons n on the island and the (continuous) voltages. Some algebra along the lines outlined for the electron box produces again $E_{\rm ch}(n, Q_{\rm G}) = (ne - Q_{\rm G})^2/2C$. For the transistor $C = C_{\rm L} + C_{\rm R} + C_{\rm G}$ is the total capacitance of the island, i.e. the sum of the two junction capacitances and the gate capacitance, and all three voltage sources define the gate charge $Q_{\rm G} = C_{\rm G}V_{\rm G} + C_{\rm L}V_{\rm L} + C_{\rm R}V_{\rm R}$.

In a tunneling process, increasing the island charge from n to $n+1$, the charging energy changes by

$$E_{\rm ch}(n+1, Q_{\rm G}) - E_{\rm ch}(n, Q_{\rm G}) = \left(n + \frac{1}{2} - \frac{Q_{\rm G}}{e}\right) \frac{e^2}{C} \; . \tag{3.4}$$

These energy differences are equally spaced and can be tuned by the gate voltage. The situation is illustrated in the energy scheme shown in Fig. 3.6. The differences in charging energy are plotted in the center. We further display the Fermi levels of the two leads which are shifted by the applied potentials $V_{\rm L/R}$.

For definiteness, we assume that the energy of the electrons in the left lead is higher than that in the right lead. Then, at low temperature, tunneling from the left lead to the island (transition from n to $n+1$) is possible if the energy in the left lead $eV_{\rm L}$ is

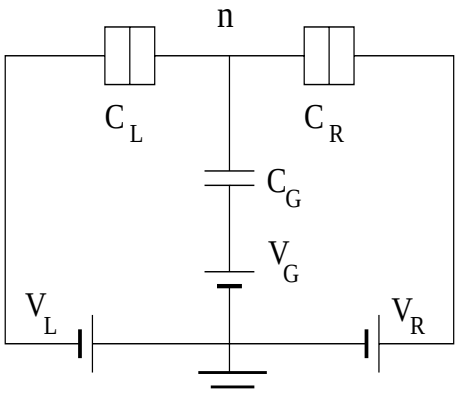

Fig. 3.5: The SET transistor.

high enough to compensate for the increase in charging energy of the island

$$eV_{\rm L} > E_{\rm ch}(n+1, Q_{\rm G}) - E_{\rm ch}(n, Q_{\rm G}) \ . \tag{3.5}$$

Similarly tunneling from the island (transition from $n+1$ to n) to the right lead is possible at low temperature only if

$$E_{\rm ch}(n+1, Q_{\rm G}) - E_{\rm ch}(n, Q_{\rm G}) > eV_{\rm R} \ . \tag{3.6}$$

Both conditions have to be satisfied simultaneously in order for a current to flow through the transistor. It is obvious from the figure that at low transport voltages, depending on the gate voltage $V_{\rm G}$ we may be either in a Coulomb blockade regime or have a finite current. By varying the gate voltage we produce the Coulomb oscillations, i.e. the e-periodic dependence of the conductance on $Q_{\rm G}$.

Further devices can be constructed (see e.g. Ref. [2]). We mention here the electron trap, which is similar to the electron box except that it contains at least two junctions in series. In contrast to the electron box the trap has metastable charge states. Two traps are combined to build the electron turnstile, which can serve as a current source. A suitable ac-gate voltage with frequency f allows the controlled transfer of a single-electron per cycle. Hence the current is $I = ef$. Finally we mention single-electron pumps, where a current is driven by two phase-shifted ac-voltages applied to different islands. In this case a current $I = ef$ is transported even at vanishing transport voltages. Both devices, in principle, can serve as a current standards, if one manages to minimize the effect of missed cycles, of thermal fluctuations, and of quantum fluctuations. This requires low frequencies, low temperatures, but also a design (many junctions) which minimizes higher order quantum tunneling processes.

Many properties of the SET transistor and its extensions can be understood by considering only the energy of the different charge configurations. However, a detailed understanding of the I-V characteristic requires knowledge of the tunneling rates of the electrons, which will be the next topic.

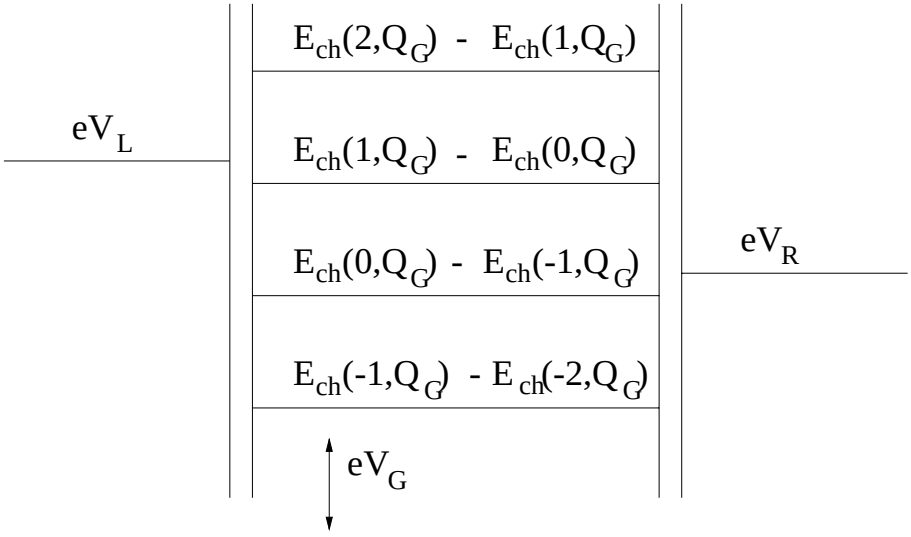

Fig. 3.6: The energy differences corresponding to the addition or removal of an electron charge are shown. They can be shifted by the gate voltage $V_{\rm G}$. The Fermi energies of the leads are shifted relative to each other by the transport voltage $V = V_{\rm L} - V_{\rm R}$.

3.3 Tunneling rates and *I*-*V* characteristics

In this Section, we introduce the Hamiltonian of the SET transistor. Using simple golden-rule arguments, we derive the rate for the transfer of a single electron charge across the tunnel barriers. It depends crucially on the change in the charging energy. The transition rates enter a master equation, from which we obtain the current-voltage characteristic. If the tunneling would increase the charging energy it is suppressed at low temperature, a phenomenon called "Coulomb blockade". This "orthodox theory" was developed by Averin and Likharev [1]. In the regime of the Coulomb blockade higher-order processes gain importance. We describe here "cotunneling" processes (see e.g. Averin and Nazarov in [2]).

3.3.1 The single-electron tunneling rate

For definiteness, we consider a SET transistor, shown in Fig. 3.5, which consists of a metallic island coupled via tunneling barriers to two leads and capacitively to an external gate voltage. Its Hamiltonian is

$$H = H_{\rm L} + H_{\rm I} + H_{\rm R} + H_{\rm ch} + H_{\rm t} \ . \tag{3.7}$$

Here, $H_{\rm L} = \sum_{k,\sigma} \epsilon_k c^\dagger_{k,\sigma} c_{k,\sigma}$ describes the noninteracting electrons with wave vector k in the left lead, with similar expressions for the island (with states denoted by q) and the right lead. We allow that the leads have different electrochemical potentials. The Coulomb interaction $H_{\rm ch}$ is assumed to depend only on the total charge on the island, as described in the previous Section,

$$H_{\rm ch} = \frac{(\hat{n}e - Q_{\rm G})^2}{2C} \ . \tag{3.8}$$

The number operator of excess electrons on the island is given by $\widehat{n} = \sum_{q,\sigma} c^\dagger_{q,\sigma} c_{q,\sigma} - N_+$, where the number of positively charged ions of the island has been subtracted. Charge transfer processes are described by the standard tunneling Hamiltonian, for instance tunneling in the left junction between the states k and q by

$$H_{\rm t,L} = \sum_{k,q,\sigma} T_{k,q} c^\dagger_{k,\sigma} c_{q,\sigma} + \text{h.c.} \,. \tag{3.9}$$

We determine the transition rates by golden-rule arguments. The rate of tunneling of an electron (one of many) from one of the states k in the left lead into one of the available states q in the island, changing the electron number from n to $n+1$, is

$$, _{\rm LI}(n) = \frac{1}{e^2 R_{\rm t,L}} \int_{-\infty}^{\infty} {\rm d}\epsilon_k \int_{-\infty}^{\infty} {\rm d}\epsilon_q f_{\rm L}(\epsilon_k)[1 - f_{\rm I}(\epsilon_q)] \delta(\delta E_{\rm ch} + \epsilon_q - \epsilon_k) \,. \tag{3.10}$$

The crucial point is that the energy, which is conserved as expressed by the δ-function, contains the energies of the electron states $\epsilon_{k/q}$, but also the *charging energy*. The latter depends on the electron number and the applied voltages $V_{\rm G}$ and $V_{\rm L/R}$. In the process considered it changes by

$$\delta E_{\rm ch} = E_{\rm ch}(n+1, Q_{\rm G}) - E_{\rm ch}(n, Q_{\rm G}) - eV_{\rm L} \,. \tag{3.11}$$

We further introduced the tunnel conductance of the junction

$$\frac{1}{R_{\rm t,L}} = \frac{4\pi e^2}{\hbar} N_{\rm I}(0) \Omega_{\rm I} N_{\rm L}(0) \Omega_{\rm L} |T|^2 \,. \tag{3.12}$$

It depends on the tunnel matrix elements $T_{k,q}$, which here can be considered as constants, as well as the densities of states at the Fermi level, $N_{\rm I/L}(0)$, and the volumes, $\Omega_{\rm I/L}$, of the island and lead. Equivalent expressions apply for the reverse process $, _{\rm IL}(n+1)$, changing the island charge from $n+1$ to n, and the other tunnel barrier.

In equilibrium the distribution functions $f_{\rm I/L}$ are Fermi functions, and the integrals in Eq. (3.10) can be performed explicitly: $\int d\epsilon f(\epsilon)[1-f(\epsilon - E)] = E/[\exp(E/k_{\rm B}T) - 1]$. Thus the "single-electron tunneling" (SET) rate is [1]

$$, _{\rm LI}(n) = \frac{1}{e^2 R_{\rm t,L}} \frac{\delta E_{\rm ch}}{\exp[\delta E_{\rm ch}/k_{\rm B}T] - 1} \,. \tag{3.13}$$

At low temperatures, $k_{\rm B}T \ll |\delta E_{\rm ch}|$, if the charging energy would increase in a tunneling process, the tunneling is suppressed, $, \to 0$. This phenomenon is called "Coulomb blockade" of electron tunneling. If the charging energy is decreased the rate is

$$, _{\rm LI}(n) = \frac{1}{e^2 R_{\rm t,L}} |\delta E_{\rm ch}| \quad \text{for} \;\; \delta E_{\rm ch} \le 0 \;\; , T \to 0 \,. \tag{3.14}$$

At finite temperatures all processes are allowed. The forward and backward rates between two states satisfy the detailed balance condition, $, _{\rm LI}(n)/, _{\rm IL}(n+1) = {\rm e}^{-\delta E_{\rm ch}/k_{\rm B}T}$.

A familiar limit of what is described above is a single voltage-biased tunnel junction where $\delta E_{\rm ch}$ is replaced by $-eV$. In this case (3.13) yields a linear current- voltage

relation, $I_t = e[,(V) - ,(-V)] = V/R_t$. We can also reverse the argument. The two requirements – (i) a linear characteristic in the voltage-biased case and (ii) detailed balance – uniquely determine the expression for the rate to be of the form (3.13) [1].

3.3.2 Master equation for sequential tunneling

Given the electron tunneling rates we can set up a master equation for the probability $p(n,t)$ to find the island in a state with n electrons. The probability changes by tunneling in the left and right junctions. Hence

$$\begin{aligned}\frac{\mathrm{d}}{\mathrm{d}t}p(n,t) = &- [,_{\mathrm{LI}}(n) + ,_{\mathrm{IL}}(n) + ,_{\mathrm{RI}}(n) + ,_{\mathrm{IR}}(n)]\,p(n,t)\\ &+ [,_{\mathrm{LI}}(n-1) + ,_{\mathrm{RI}}(n-1)]\,p(n-1,t)\\ &+ [,_{\mathrm{IL}}(n+1) + ,_{\mathrm{IR}}(n+1)]\,p(n+1,t)\ . \end{aligned} \tag{3.15}$$

The rates and probabilities also determine the current. In the left junction it is

$$I_{\mathrm{L}}(t) = -e\sum_n [,_{\mathrm{LI}}(n) - ,_{\mathrm{IL}}(n)]\,p(n,t)\ . \tag{3.16}$$

In most cases we apply dc-voltages and are interested in the dc-current. In this case we need only the stationary solution of the master equation, and the currents in the left and right junctions are equal $I = I_{\mathrm{L}} = I_{\mathrm{R}}$.

As an example we consider a transistor with symmetric bias $V_{\mathrm{L}} = -V_{\mathrm{R}} = V/2$. At low temperatures and low transport voltages (except at symmetry points) only two different charge states – and those transitions which connect both – have an appreciable probability. For instance, if $ne < Q_{\mathrm{G}} < (n+1)e$ we need to consider only $p(n)$ and $p(n+1)$ and the two transitions $,_{\mathrm{LI}}(n)$ and $,_{\mathrm{RI}}(n)$ increasing the island charge from n to $n+1$ electrons, as well as the two reverse transitions $,_{\mathrm{IL}}(n+1)$ and $,_{\mathrm{IR}}(n+1)$. The energy changes determining the rates $,_{\mathrm{LI}}(n)$ and $,_{\mathrm{IL}}(n+1)$ are

$$\delta E_{\mathrm{ch}} = \pm\left[(n+\frac{1}{2} - \frac{Q_{\mathrm{G}}}{e})\frac{e^2}{C} - \frac{eV}{2}\right]\ , \tag{3.17}$$

respectively, while for the transitions in the right junction eV is replaced by $-eV$. In the 2-state limit the stationary solution of the master equation is

$$p(n) = \frac{,_{\mathrm{IL}}(n+1) + ,_{\mathrm{IR}}(n+1)}{,_{\Sigma}} \quad ; \quad p(n+1) = 1 - p(n) \tag{3.18}$$

[1] Although the I-V characteristic may be linear, the system differs from an Ohmic resistor. For instance, the noise associated with the stochastic tunneling is shot noise. Assuming a Poissonian statistics we find for of a voltage-biased junction the power spectrum of current fluctuations

$$S_{\mathrm{I}}(\omega) \equiv \int \mathrm{d}t\ \left(\langle I(t)I(0)\rangle - \langle I\rangle^2\right)\mathrm{e}^{\mathrm{i}\omega t} = e^2[,(V) + ,(-V)] = \frac{eV}{R_t}\coth\left(\frac{eV}{2k_{\mathrm{B}}T}\right)\ ,$$

which differs from the Johnson-Nyquist noise of a resistor. Similarly, the current fluctuations in the junction of an electron box are [11] $S_{\mathrm{I}}(\omega) = (e^2/Z_{\mathrm{ch}})\sum_n [,_{\mathrm{LI}}(n) + ,_{\mathrm{IL}}(n)]\exp[-E_{\mathrm{ch}}(n)/k_{\mathrm{B}}T]$, with the rates given by (3.13). In both cases we wrote the classical form, the quantum mechanical form is obtained by shifting eV or δE_{ch} by $\pm\hbar\omega/2$.

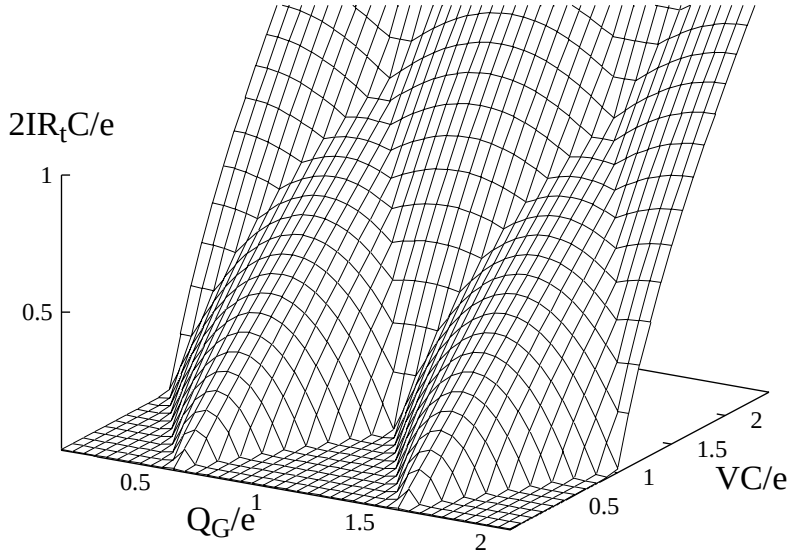

Fig. 3.7: The current of a symmetric transistor is shown as a function of gate and transport voltage. At low temperatures and low transport voltages $VC/e < 1$ only two charge states play a role, and the Coulomb oscillations are clearly demonstrated. At larger transport voltages, more charge states are involved.

where $,_\Sigma = ,_{\rm LI}(n) + ,_{\rm RI}(n) + ,_{\rm IL}(n+1) + ,_{\rm IR}(n+1)$. The current reduces to

$$I = -e\frac{,_{\rm LI}(n),_{\rm IR}(n+1) - ,_{\rm RI}(n),_{\rm IL}(n+1)}{,_\Sigma}\,. \tag{3.19}$$

This expression is readily analyzed by inspection of (3.17). At low temperatures the tunneling process in the left junction from n to $n+1$, with rate $,_{\rm LI}(n)$, is allowed when $Q_{\rm G} - (n+1/2)e \geq -VC/2$. On the other hand, the transition which carries on the charge to the right electrode with rate $,_{\rm IR}(n+1)$ is allowed when $Q_{\rm G} - (n+1/2)e \leq VC/2$. Both coexist in a window of width CV around $Q_{\rm G} = (n+1/2)e$. The other two processes are not allowed simultaneously, and in fact are suppressed in the window just mentioned. Therefore, at low temperature the current is

$$I = \frac{1}{4R_{\rm t}}\left[V - \frac{4e^2}{C^2V}\left(\frac{Q_{\rm G}}{e} - n - \frac{1}{2}\right)^2\right] \quad \text{for} \quad -\frac{VC}{2e} \leq \frac{Q_{\rm G}}{e} - n - \frac{1}{2} \leq \frac{VC}{2e}\,, \tag{3.20}$$

while it vanishes outside the window. For simplicity we have assumed in (3.20) that the two junctions have the same tunneling resistance $R_{\rm t} = R_{\rm t,L} = R_{\rm t,R}$.

At low temperatures, such that only two adjacent charges, n and $n+1$, play a role, $|E_{\rm ch}(n+1,Q_{\rm G}) - E_{\rm ch}(n,Q_{\rm G})| \approx k_{\rm B}T \ll E_{\rm C}$, we obtain from (3.19) the linear conductance ($V \to 0$)

$$G(T,Q_{\rm G}) = \frac{1}{2R_{\rm ass}}\frac{\delta E_{\rm ch}}{\sinh\left(\delta E_{\rm ch}/k_{\rm B}T\right)}\,. \tag{3.21}$$

It is peaked near the points of degeneracy where $\delta E_{\rm ch} = E_{\rm ch}(n+1,Q_{\rm G}) - E_{\rm ch}(n,Q_{\rm G})$ vanishes. The width of the peaks is proportional to the temperature. Even at the

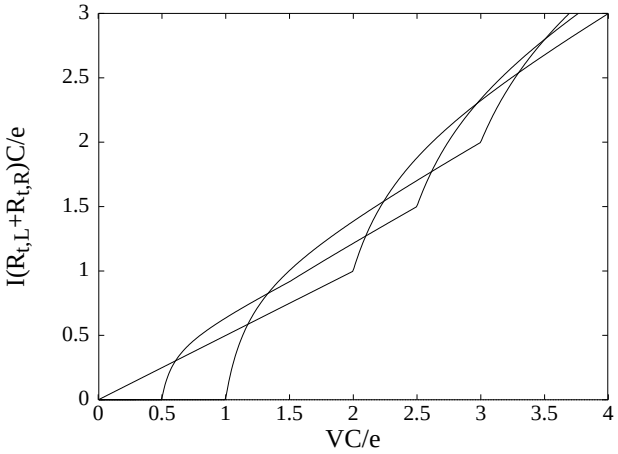

Fig. 3.8: Coulomb staircase: The current of an asymmetric transistor with different tunneling resistances in the two junctions $R_{\mathrm{t,R}} = 10R_{\mathrm{t,L}}$ is shown as a function of the transport voltage for $Q_{\mathrm{G}} = 0$ (pronounced Coulomb blockade), $Q_{\mathrm{G}}/e = 0.25$ (intermediate), and $Q_{\mathrm{G}}/e = 0.5$ (linear at low voltage).

maxima the conductance reaches only 1/2 of the assymptotic value $R_{\mathrm{ass}} = R_{\mathrm{t,L}} + R_{\mathrm{t,R}}$ corresponding to the series addition of the two junction resistors.

The current through a symmetric SET transistor is plotted as a function of the transport and gate voltages in Fig. 3.7. For gate voltages such that Q_{G}/e is close to an integer, the current vanishes below a threshold bias voltage $V_{\mathrm{th}}(Q_{\mathrm{G}} = ne) = e/C$. This is a manifestation of the Coulomb blockade. At non-integer values of Q_{G}/e the threshold voltage is lower $V_{\mathrm{th}}(Q_{\mathrm{G}}) = \min_n \{2|Q_{\mathrm{G}} - (n + 1/2)e|/C\}$. One finds a series of evenly spaced peaks centered around half-integer values of $Q_{\mathrm{G}}/e = n + 1/2$, each of parabolic shape as given by Eq. (3.20). These are the so-called "Coulomb oscillations".

The strong dependence of $I(Q_{\mathrm{G}}, V)$ on the gate voltage makes the SET transistor a highly sensitive "electrometer". Small changes of polarization charges by fractions of an electron charge influence a macroscopic measurement current. It has been used, for instance, to measure the charge in an electron box $\langle n(Q_{\mathrm{G}})\rangle$ discussed above.

For larger transport voltages, more charge states play a role even at low temperatures. In order to illustrate this, we consider a junction with symmetric bias $V_{\mathrm{L}} = -V_{\mathrm{R}} = V/2$ and $Q_{\mathrm{G}} = 0$, where the lowest energy state has $n = 0$ electrons in the island. At transport voltages exceeding a threshold $V_{\mathrm{th},0} = e/C$ tunneling sets in to a charge state with $n = 1$. Above this voltage, the electrochemical potential in the left lead is sufficient to compensate the increase in charging energy of the island. Since at the same time this state with $n = 1$ is unstable against a tunneling process in the right junction, a current is transported through the system. At the same voltage tunneling processes involving the state with $n = -1$ are possible. At still higher voltages further charge states $|n| \geq 1$ play a role. This leads to a series of threshold voltages $V_{\mathrm{th,n}} = (2n+1)e/C$, each marking where another pair of charge states becomes populated, opening a new channel for the conductance. The increase in conductance is limited due to the normalization condition for the $p(n)$. Still, for suitable parameters (significantly differing conductances or capacitances of the two junctions), the current increases in the shape of a staircase, as demonstrated in the plot of Fig. 3.8. The phenomenon was named accordingly "Coulomb staircase" [12].

3.3.3 Cotunneling processes

If sequential single-electron tunneling is suppressed by the Coulomb blockade, higher-order processes such as coherent "cotunneling" through several junctions become crucial (Averin and Nazarov in Ref. [2]). As a specific example, we consider a SET transistor, biased such that the current in lowest-order perturbation theory vanishes (see Fig. 3.7). At low temperatures sequential tunneling is exponentially suppressed in this regime since the energy of a state with an excess charge on the island lies above the Fermi levels of the leads. On the other hand, if a transport voltage is applied, a higher-order tunneling process transferring an electron charge coherently through the *total* system is energetically allowed. In this case the state with an excess electron charge in the island exists only virtually. Standard second-order (or fourth, depending on the counting) perturbation theory yields the rate

$$, _{\mathrm{i}\to\mathrm{f}} = \frac{2\pi}{\hbar}\left|\sum_{\psi}\frac{\langle i|H_{\mathrm{t}}|\psi\rangle\langle\psi|H_{\mathrm{t}}|f\rangle}{E_\psi - E_{\mathrm{I}}}\right|^2 \delta(E_{\mathrm{i}} - E_{\mathrm{f}}) \; . \tag{3.22}$$

The energy of the intermediate virtual state lies above the initial one, $E_\psi - E_{\mathrm{i}} > 0$, but it enters only into the denominator rather than into the exponent of the sequential tunneling rate. Hence the higher-order rate is nonzero even at very low temperatures.

When analyzing the process we have to pay attention to the following:

(i) There are actually two channels which add coherently. Either an electron tunnels first from the left lead onto the island, and then an electron tunnels from the island to the other lead. In this case the increase in charging energy of the intermediate state compared with the initial one is $\delta E_{\mathrm{L}} = E_{\mathrm{ch}}(n+1, Q_{\mathrm{G}}) - E_{\mathrm{ch}}(n, Q_{\mathrm{G}}) - eV_{\mathrm{L}}$. Or an electron tunnels first out of the island to the right lead and another electron from the left lead replaces the charge. In this case the increase in energy of the intermediate state is $\delta E_{\mathrm{R}} = E_{\mathrm{ch}}(n-1, Q_{\mathrm{G}}) + eV_{\mathrm{R}} - E_{\mathrm{ch}}(n, Q_{\mathrm{G}})$. Both amplitudes have to be added before the matrix element is squared.

(ii) The leads contain a macroscopic number of electrons. Therefore, with overwhelming probability the outgoing electron will come from a different state than the one which the incoming electron occupies. Hence, after the process an electron-hole excitation is left in the island, which explains why it is called "inelastic" cotunneling.

Transitions involving different excitations are added incoherently. The resulting rate for inelastic cotunneling is

$$\begin{aligned} , _{\mathrm{cot}} \;=\; & \frac{\hbar}{2\pi e^4 R_{\mathrm{t,L}} R_{\mathrm{t,R}}} \int_{k\in\mathrm{L}} \mathrm{d}\epsilon_k \int_{q\in\mathrm{I}} \mathrm{d}\epsilon_q \int_{q'\in\mathrm{I}} \mathrm{d}\epsilon_{q'} \int_{k'\in\mathrm{R}} \mathrm{d}\epsilon_{k'} f(\epsilon_k)[1-f(\epsilon_q)]f(\epsilon_{q'})[1-f(\epsilon_{k'})] \\ & \times \left[\frac{1}{\epsilon_q + \delta E_{\mathrm{L}} - \epsilon_k} + \frac{1}{\epsilon_{k'} + \delta E_{\mathrm{R}} - \epsilon_{q'}}\right]^2 \delta(eV + \epsilon_k - \epsilon_q + \epsilon_{q'} - \epsilon_{k'}) \; . \end{aligned} \tag{3.23}$$

At $T = 0$ the integrals can be performed analytically with the result

$$\begin{aligned} ,_{\rm cot} &= \frac{\hbar}{2\pi e^3 R_{\rm t,L} R_{\rm t,R}} V \left[\left(1 + \frac{2}{eV} \frac{\delta E_{\rm L} \delta E_{\rm R}}{\delta E_{\rm L} + \delta E_{\rm R} + eV} \right) \left(\sum_{\rm i=L,R} \ln \left(1 + \frac{eV}{\delta E_{\rm I}} \right) \right) - 2 \right] \\ &= \frac{\hbar}{12\pi e R_{\rm t,L} R_{\rm t,R}} \left(\frac{1}{\delta E_{\rm L}} + \frac{1}{\delta E_{\rm R}} \right)^2 V^3 \quad \text{for} \quad eV \ll \delta E_{\rm L}, \delta E_{\rm R}. \end{aligned} \tag{3.24}$$

At finite temperatures forward and backward processes occur. They obey a detailed balance relation $,_{\rm cot}(-V) = \exp(-eV/k_{\rm B}T),_{\rm cot}(V)$. The current then is

$$I(V) = \frac{\hbar}{12\pi e^2 R_{\rm t,L} R_{\rm t,R}} \left(\frac{1}{\delta E_{\rm L}} + \frac{1}{\delta E_{\rm R}} \right)^2 \left[(eV)^2 + (2\pi k_{\rm B} T)^2 \right] V \ . \tag{3.25}$$

In the Coulomb blockade regime of a SET transistor the V^3 dependence of the cotunneling current has been observed. In systems with N junctions a corresponding N-th order process (or $2N$-th order, depending on the counting) leads to a current $I \propto V^{2N-1}$. As an example we consider $N = 4$ junctions with $C = 10^{-15}$F and tunneling resistance $R_{\rm t}$. In this case (see D. Esteve in Ref. [2]) $,_{\rm cot} = (2.5 \times 10^{-3}/{\rm s})\,(V/\mu{\rm V})^7\,({\rm k}\Omega/R_{\rm t})^4$. These cotunneling processes limit the accuracy of the single electron turnstile even under the most favorable situations, i.e. low T and low frequency, where thermally activated multi-electron transfer processes and missed cycles play little role.

The expression for the cotunneling rate diverges logarithmically when the intermediate and initial or final states are degenerate. This divergence is removed by life-time broadening effects, which will be derived systematically – together with further effects – in Section 3.7.

There exists also the process where *one* electron tunnels through the total system, leaving no excitations in the island. This process is called "elastic cotunneling". Its rate has a small prefactor $\propto 1/[\Omega_{\rm I} N_{\rm I}(0)]$ (inversely proportional to the number of states of the island) compared with the inelastic cotunneling rate. On the other hand, it yields a current which is linear in the applied voltage, which makes it important at very low voltages and temperatures $k_{\rm B}T, eV \ll [E_{\rm C}/\Omega N(0)]^{1/2}$.

3.3.4 Broadening of the steps

Even at $T = 0$ where thermal effects are frozen, tunneling of electrons leads to an uncertainty in their location. This leads to a broadening of the steps in $\langle n(Q_{\rm G}) \rangle$ in the electron box. This effect can be estimated in perturbation theory [13]. We start from the basis states $|n; ...\rangle^{(0)}$ with total charge n on the island and certain single-electron states of the lead and the island occupied or empty (indicated by the dots). Due to tunneling the states are modified. In lowest-order perturbation theory the corrections

$$\begin{aligned} |\psi_n^{(1)}\rangle &= \sum_{k,q} \Big[\frac{T_{q,k}}{\epsilon_q - \epsilon_k + E_{\rm ch}(n+1, Q_{\rm G}) - E_{\rm ch}(n, Q_{\rm G})} |n+1; q, \bar{k}\rangle^{(0)} \\ &\quad + \frac{T_{k,q}}{\epsilon_k - \epsilon_q + E_{\rm ch}(n-1, Q_{\rm G}) - E_{\rm ch}(n, Q_{\rm G})} |n-1; \bar{q}, k\rangle^{(0)} \Big] \ , \end{aligned} \tag{3.26}$$

arise due to tunneling from an electron state k of the lead (leaving it empty $\bar{k}$) into the state q of the island, increasing the charge to $n+1$, or reversely. The resulting change in the expectation value of the electron number, $\delta n(Q_{\rm G}) = \langle \psi_n^{(1)} | \hat{n} | \psi_n^{(1)} \rangle$, is

$$\delta n(Q_{\rm G}) = |T|^2 N_{\rm L} N_{\rm I} \int {\rm d}\epsilon_k \int {\rm d}\epsilon_q \Big\{ \frac{f(\epsilon_k)[1-f(\epsilon_q)]}{[\epsilon_q - \epsilon_k + E_{\rm ch}(n+1,Q_{\rm G}) - E_{\rm ch}(n,Q_{\rm G})]^2} - \frac{f(\epsilon_q)[1-f(\epsilon_k)]}{[\epsilon_k - \epsilon_q + E_{\rm ch}(n-1,Q_{\rm G}) - E_{\rm ch}(n,Q_{\rm G})]^2} \Big\} , \tag{3.27}$$

which for $T=0$ reduces to

$$\delta n(Q_{\rm G}) = \frac{R_{\rm K}}{8\pi^2 R_{\rm t}} \ln \frac{E_{\rm ch}(n-1,Q_{\rm G}) - E_{\rm ch}(n,Q_{\rm G})}{E_{\rm ch}(n+1,Q_{\rm G}) - E_{\rm ch}(n,Q_{\rm G})} . \tag{3.28}$$

The result displays several important properties: (i) the expansion parameter is the dimensionless tunneling conductance $R_{\rm K}/R_{\rm t}$, where the quantum resistance $R_{\rm K}$ serves as reference, (ii) tunneling of single electrons leads to logarithmic corrections, (iii) the perturbation theory fails at the points of degeneracy of the charging energy, $Q_{\rm G}/e = n + 1/2$. In the last Sections of this Chapter we will present the theoretical framework which describes tunneling beyond perturbation theory and regularizes these expressions.

3.4 Influence of the electromagnetic environment

So far we have assumed that the electron box or the SET transistor are driven by ideal voltage sources, and we have considered ideal measurement devices. On the other hand, in a real experiment the sources are outside the cryostat, some distance away from the single-electron device to which they are connected by leads. This introduces stray capacitances and Ohmic resistors as well as thermal fluctuations. We have to understand their influence on single-electron tunneling in order to describe a realistic situation – or to know how to set up an experiment close to ideal. We, therefore, will consider now a tunnel junction which is connected to an electric circuit described by a general impedance $Z(\omega)$. A detailed review of this problems has been given by Ingold and Nazarov in Ref. [2]. It is a specific example of the general problem how to describe dissipation in quantum mechanics, which has been addressed for instance by Caldeira and Leggett [14] and which is reviewed in Chapter 4 of this volume. In this approach the fluctuating linear circuit is modeled by an ensemble of harmonic oscillators.

3.4.1 The model Hamiltonian

The simplest example is a single tunnel junction in series with an impedance $Z(\omega)$ and both driven by a voltage source as shown in Fig. 3.9. The tunnel junction is modeled in the usual way by a tunneling Hamiltonian. It is coupled to an ensemble of harmonic oscillators to account for the effect of the impedance. Due to this coupling tunneling processes in general are accompanied by emission or absorption processes of "photons".

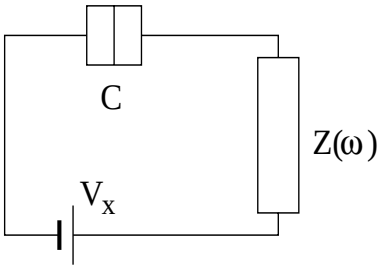

Fig. 3.9: A junction in an external circuit characterized by an impedance $Z(\omega)$.

We will calculate the tunneling current $I(V)$ as a function of the dc-voltage at the junction. Because of the voltage drop at the impedance the voltage at the junction

$$\widetilde{V}(t) = V + \delta V(t) \tag{3.29}$$

is reduced below the applied value, $V = V_{\rm x} - I(V)Z(0)$. Since this drop depends again on the current to be determined, we are left – even after we found $I(V)$ – with a self-consistency problem. Furthermore, the impedance produces current and hence voltage fluctuations at the junction $\delta V(t)$ with $\langle \delta V(t) \rangle = 0$.

Let us recall what is known about the fluctuations of a resistor, or in general of a linear circuit element with impedance $Z(\omega)$. For this purpose we ignore tunneling, which means that the junction is reduced to a capacitor C. Then the balance of currents in the circuit satisfies (after Fourier transformation)

$$[i\omega C + Z^{-1}(\omega)]\delta V(\omega) = \delta I(\omega)\,. \tag{3.30}$$

The power spectrum of the Gaussian current noise is given by the standard Johnson-Nyquist relation

$$\begin{aligned} \langle \delta I \delta I \rangle_\omega &\equiv \int_{-\infty}^{\infty} {\rm d}(t-t') {\rm e}^{{\rm i}\omega(t-t')} \frac{1}{2} \langle \{ \delta I(t), \delta I(t') \} \rangle \\ &= {\rm Re}\{Z^{-1}(\omega)\}\, \hbar\omega \coth\left(\frac{\hbar\omega}{2k_{\rm B}T}\right)\,. \end{aligned} \tag{3.31}$$

Hence the fluctuations of the voltage at the junction are governed by

$$\langle \delta V \delta V \rangle_\omega = {\rm Re}\{Z_{\rm t}(\omega)\}\, \hbar\omega \coth\left(\frac{\hbar\omega}{2k_{\rm B}T}\right)\,. \tag{3.32}$$

Here $Z_{\rm t}(\omega)$ is the impedance seen at the site of the junction, i.e. the effect of $Z(\omega)$ and the capacitance of the junction shunted in parallel,

$$Z_{\rm t}(\omega) = \left[{\rm i}\omega C + Z^{-1}(\omega)\right]^{-1}\,. \tag{3.33}$$

A microscopic description of the system consisting of the junction and the impedance is provided by the Hamiltonian

$$H = \sum_{k,\sigma} \left(\epsilon_k + e\widetilde{V}(t)\right) c^\dagger_{k,\sigma} c_{k,\sigma} + \sum_{q,\sigma} \epsilon_q c^\dagger_{q,\sigma} c_{q,\sigma} + \sum_{k,q,\sigma} T_{k,q} c^\dagger_{k,\sigma} c_{q,\sigma} + {\rm h.c.} + H_{\rm bath}\,. \tag{3.34}$$

The first terms describe the right and left electrodes and the tunneling. The last term, $H_{\rm bath}$, describes the degrees of freedom responsible for the fluctuations $\delta V(t)$. Since they result from a linear circuit element they are Gaussian and are in general described by an ensemble of harmonic oscillators. We set

$$H_{\rm bath} = \sum_j \left(\frac{p_j^2}{2m_j} + \frac{m_j}{2}\Omega_j^2 x_j^2 \right) \quad \text{and} \quad \delta\phi(t) = \sum_j c_j x_j(t) \; . \tag{3.35}$$

Here we introduced a phase as the time-integral of the voltage

$$\hbar\phi(t) \equiv \int^t {\rm d}t' e\widetilde{V}(t') = eV\,t + \hbar\delta\phi(t) \quad , \quad \hbar\delta\phi(t) = \int^t {\rm d}t' e\,\delta V(t') \; , \tag{3.36}$$

which will turn out to be the natural variable. The distribution of the oscillator frequencies Ω_j and the coefficients c_j have to be chosen appropriately in order to produce the correct power spectrum.

Using properties of the harmonic oscillators,

$$\langle x_j(t) x_{j'}(t') \rangle_{\rm bath} = \delta_{j,j'} \frac{\hbar}{2m_j\Omega_j} \left\{ \coth\left(\frac{\hbar\Omega_j}{2k_{\rm B}T}\right) \cos[\Omega_j(t-t')] - {\rm i}\sin[\Omega_j(t-t')] \right\} \; ,$$

we find for the Fourier transform of the symmetrized correlation function of $\delta\phi$

$$\frac{1}{2}\langle\{\delta\phi(t), \delta\phi(t')\}\rangle_{{\rm bath},\omega} = J(\omega) \coth\left(\frac{\hbar\omega}{2k_{\rm B}T}\right) \; . \tag{3.37}$$

The coefficient c_j and the frequencies of the oscillators enter only in the combination

$$J(\omega) \equiv \pi \sum_j \frac{c_j^2\hbar}{2m_j\Omega_j} \left[\delta(\omega - \Omega_j) - \delta(\omega + \Omega_j)\right] \; . \tag{3.38}$$

We can reproduce the Johnson-Nyquist correlation functions (3.32) by choosing

$$J(\omega) = \frac{e^2}{\hbar\omega} {\rm Re}\{Z_{\rm t}(\omega)\} \; . \tag{3.39}$$

Technically it is inconvenient to deal with time-dependent energies in the electrodes. Therefore, we perform a unitary transformation $H = U^\dagger H' U - {\rm i}\hbar U^\dagger \partial U/\partial t$, where

$$U = \exp\left[\frac{\rm i}{\hbar} \int^t {\rm d}t'\, e\widetilde{V}(t') \sum_{k,\sigma} c_{k,\sigma}^\dagger c_{k,\sigma} \right] \; . \tag{3.40}$$

In the resulting Hamiltonian H' the electrodes appear in unperturbed form

$$H' = \sum_{k,\sigma} \epsilon_k\, c_{k,\sigma}^\dagger c_{k,\sigma} + \sum_{q,\sigma} \epsilon_q\, c_{q,\sigma}^\dagger c_{q,\sigma} + \sum_{k,q,\sigma} T_{k,q}\, {\rm e}^{{\rm i}\phi(t)} \left(c_{k,\sigma}^\dagger c_{q,\sigma} + {\rm h.c.} \right) + H_{\rm bath} \; , \tag{3.41}$$

but the tunneling term acquired a time-dependent phase factor, depending on the integral of the voltage introduced by (3.36).

3.4.2 The single-electron tunneling rate

When evaluating the tunneling rates we have to take into account that a tunneling process (from state k in one electrode to q in the other) in general is accompanied by a transition in the bath ($X \to X'$) as well. Using the golden rule we find the rate for tunneling in one direction

$$\begin{aligned} \Gamma^{+}(V) &= \frac{1}{e^2 R_{\rm t}} \int \mathrm{d}\epsilon_k \int \mathrm{d}\epsilon_q f(\epsilon_k)[1-f(\epsilon_q)] \\ &\quad \times \sum_{X,X'} \rho_{\rm bath}(X) \left| \langle X' | \mathrm{e}^{\mathrm{i}\delta\phi} | X \rangle \right|^2 \delta(\epsilon_k + eV + E_X - \epsilon_q - E_{X'}) \,. \end{aligned} \tag{3.42}$$

Here $\rho_{\rm bath}(X)$ denotes the probability to find the bath in a state X. In thermal equilibrium and lowest-order in the coupling it is $\rho_{\rm bath}(X) = \langle X | \exp[-\beta H_{\rm bath}] | X \rangle / Z_{\rm bath}$. We write $\delta(\epsilon_k + eV + E_X - \epsilon_q - E_{X'}) = \int \frac{\mathrm{d}t}{2\pi\hbar} \exp\left[\frac{\mathrm{i}}{\hbar}(\epsilon_k + eV + E_X - \epsilon_q - E_{X'})t\right]$ and interpret the exponential of the bath energies as the time evolution operators of the bath. This allows us to express (3.42) as

$$\begin{aligned} \Gamma^{+}(V) = \frac{1}{e^2 R_{\rm t}} \int \mathrm{d}\epsilon_k \int \mathrm{d}\epsilon_q f(\epsilon_k)[1-f(\epsilon_q)] \int \frac{\mathrm{d}t}{2\pi\hbar} \mathrm{e}^{\mathrm{i}(\epsilon_k + eV - \epsilon_q)t/\hbar} \\ \times \sum_{X,X'} \rho_{\rm bath}(X) \langle X | \mathrm{e}^{\mathrm{i}\delta\phi(t)} | X' \rangle \langle X' | \mathrm{e}^{-\mathrm{i}\delta\phi(0)} | X \rangle \,. \end{aligned} \tag{3.43}$$

The second line of this expression can be expressed as a bath correlation function

$$\langle \mathrm{e}^{\mathrm{i}\delta\phi(t)} \mathrm{e}^{-\mathrm{i}\delta\phi(0)} \rangle_{\rm bath} = \mathrm{e}^{\langle [\delta\phi(t) - \delta\phi(0)]\delta\phi(0) \rangle_{\rm bath}} \equiv \mathrm{e}^{K(t)} \,. \tag{3.44}$$

We arrived at the second form using the Baker-Hausdorff formula and properties of a harmonic system. The correlation function $K(t)$, unlike the symmetrized correlation functions (3.37), depends on the order of the operators. It can be expressed as

$$K(t) = \int_{-\infty}^{\infty} \frac{\mathrm{d}\omega}{\omega} \frac{\mathrm{Re}\{Z_{\rm t}(\omega)\}}{R_{\rm K}} \left\{ \coth\left(\frac{\hbar\omega}{2k_{\rm B}T}\right) [\cos(\omega t) - 1] - \mathrm{i}\sin(\omega t) \right\} \,. \tag{3.45}$$

The tunneling rate in forward direction can now be written as

$$\Gamma^{+}(V) = \frac{1}{e^2 R_{\rm t}} \int_{-\infty}^{\infty} \mathrm{d}E \int_{-\infty}^{\infty} \mathrm{d}E' f(E)[1-f(E')] P(E + eV - E') \,, \tag{3.46}$$

where the function $P(E)$ is related to $K(t)$ by

$$P(E) = \frac{1}{2\pi\hbar} \int_{-\infty}^{\infty} \mathrm{d}t \exp[K(t) + \mathrm{i}Et/\hbar] \,. \tag{3.47}$$

This completes the derivation. The calculation of the tunneling rate is reduced to integrations. We will continue with a discussion and derive some limiting results.

3.4.3 General properties

The coupling to the environment (bath) is accounted for by the function $P(E)$ in the integral (3.46). In comparison to the usual expression for the tunneling rate of a voltage biased junction (see e.g. Eq. (3.10) with $\delta E_{\rm ch}$ replaced by eV), P replaces the energy conserving δ-function. This can be made apparent also by rewriting the rate (3.46) as a convolution

$$, {}^{+}(V) = \int \mathrm{d}E \, , {}^{+}_{Z=0}\left(V - \frac{E}{e}\right) P(E) = \frac{1}{e^2 R_{\rm t}} \int \mathrm{d}E \, \frac{E - eV}{\exp[(E-eV)/k_{\rm B}T] - 1} P(E) \; . \tag{3.48}$$

In the absence of the impedance and its fluctuations i.e. for $K(t) = 0$, $P(E)$ reduces to a δ-function, and we recover the standard result for the voltage-biased junction. In general, the function $P(E)$ describes the emission ($E > 0$) and absorption ($E < 0$) of energy during a tunneling process due to the coupling of the electrons to the oscillator bath.

The vanishing of $K(t = 0) = 0$ implies that the function $P(E)$ is normalized

$$\int_{-\infty}^{\infty} \mathrm{d}E P(E) = 1 \; . \tag{3.49}$$

We obtain a second sum rule by taking the derivative of $\exp[K(t)]$, with the result

$$\int_{-\infty}^{\infty} \mathrm{d}E E P(E) = \mathrm{i}\hbar K'(0) = \hbar \int_{-\infty}^{\infty} d\omega \frac{\mathrm{Re}\{Z_{\rm t}(\omega)\}}{R_{\rm K}} = E_{\rm C} \; . \tag{3.50}$$

At $T = 0$ the function $P(E)$ vanishes for negative energies, $P(E < 0) = 0$, and only the forward tunneling rate is nonzero. From the tunneling rates we obtain the current $I(V) = e, {}^{+}$,

$$I(V) = \frac{1}{e R_{\rm t}} \int_0^{eV} \mathrm{d}E \, (eV - E) P(E) \; , \tag{3.51}$$

which provides a convenient relation

$$\frac{\mathrm{d}^2 I}{\mathrm{d}V^2} = \frac{e}{R_{\rm t}} P(eV) \; . \tag{3.52}$$

At large voltages, such that eV is larger than the energies where $P(E)$ gives a noticeable contribution, the limits of integration in (3.51) can be extended to $\pm\infty$. In this case the sum rules derived above are sufficient to determine the current-voltage relation

$$I(V) = \frac{1}{R_{\rm t}} \left(V - \frac{e}{2C}\right) \; . \tag{3.53}$$

The shift of the I-V characteristic is a manifestation of the Coulomb blockade.

At finite temperatures $T \neq 0$ the function $P(E)$ obeys a detailed balance relation $P(E)/P(-E) = \mathrm{e}^{E/k_{\rm B}T}$. The current then is

$$I(V) = e(, {}^{+}(V) - , {}^{+}(-V)) = \frac{1}{e R_{\rm t}} \int_{-\infty}^{\infty} \mathrm{d}E \frac{1 - \mathrm{e}^{-\beta eV}}{1 - \mathrm{e}^{-\beta E}} E P(eV - E) \; . \tag{3.54}$$

Below we will present further analytic and numerical results. For the moment we only stress that the calculation of $I(V)$ is reduced to integrations. We have to recall, however, that in Eq. (3.29) we have split the voltage at the junction $\tilde{V}(t) = V + \delta V(t)$ into a dc part V and a fluctuating part with vanishing average. There remains the problem to determine the dc part, which differs from the applied voltage $V_{\rm x}$ due to the voltage drop at the junction. This in turn is proportional to the current $I(V)$, leading to the following self-consistency relation

$$I(V)Z(\omega = 0) + V = V_{\rm x} \; . \tag{3.55}$$

Along the same line we can also describe a current-biased junction with a parallel Ohmic resistor. Here the imposed current $I_{\rm x}$ is divided into a current through the junction $I(V)$ and a current through the resistor, which in turn depends on the voltage at the junction. Hence

$$I(V) + \frac{V}{R} = I_{\rm x} \; . \tag{3.56}$$

In both cases we combine the standard linear circuit description (Kirchhoff's laws) for resistors, capacitances, sources, ... with the "black-box" relation $I(V)$ for the junction, which is assumed to be the only nonlinear element in the circuit. The properties of the junction depend on the impedance $Z_{\rm t}(\omega)$ seen at the site of the junction. It is the same for both examples mentioned above. The current-biased junction with an Ohmic shunt resistor has been studied by Odintsov [15] and by Panyukov and Zaikin [16], who arrived at equivalent conclusions as described above.

At this stage we would like to comment on the range of validity of the treatment presented above. The transition rate was obtained in lowest-order perturbation theory. This requires that the tunneling conductance $1/R_{\rm t}$ is low, but the question remains what is the reference scale. Furthermore, it appears that no assumption was made about the value of the series impedance $Z(\omega)$. A systematic analysis of the problem where the tunneling and the Ohmic resistor are treated on an equal footing (see Section 3.6), yields the requirement $R_{\rm t} \gg Z(0)$. Obviously, in the extreme limit it is not crucial to solve the self-consistency relation (3.55). However, in intermediate situations only the self-consistent calculation produces results with the correct asymptotic behavior.

The analysis presented above can be generalized to more complex systems involving networks of junctions and general impedances. The basic point is that we treat the tunneling in lowest-order perturbation theory, i.e. for a tunneling process in one junction all the other junctions only act as capacitors. This means that the transition rate in each junction has the form presented above. However, it depends on the specific impedance $Z_{\rm t}(\omega)$ between the two sides of the considered junction, which in turn depends on the capacitances of all other junctions. The calculation of that impedance follows the classical electrodynamics rules.

3.4.4 The effect of an Ohmic resistor

As an important example we consider a tunnel junction in series with an Ohmic resistor $Z(\omega) = R$, defining the dimensionless conductance

$$\alpha_{\rm s} \equiv R_{\rm K}/R\,. \tag{3.57}$$

The resulting function $P(E)$ is plotted in Fig. 3.10 for different values of $\alpha_{\rm s}$ at $T = 0$. and the corresponding current-voltage characteristics in Fig. 3.11. The curves display a pronounced crossover. As $R/R_{\rm K}$ is increased the peak of $P(E)$ shifts from the origin to $E_{\rm C}$, and the I-V characteristics changes from a classical, linear dependence to a nonlinear one with a pronounced Coulomb gap.

In the limit of a low impedance environment, $R/R_{\rm K} \ll 1$, the function $P(E)$ reduces to $P(E) \to \delta(E)$. In this case we recover the classical linear I-V characteristic of a junction driven by a constant voltage source. In the opposite limit of a high impedance environment, $R/R_{\rm K} \gg 1$, the external voltage source and the series resistor act as a current source, which should lead to Coulomb blockade effects. Indeed at finite temperatures, $k_{\rm B}T \gg \hbar/RC$, where it is sufficient to replace $\mathrm{Re}\{Z_{\rm t}(\omega)\} = R/(1 + (\omega RC)^2) \to (\pi/C)\delta(\omega)$, we find $K(t) = -\pi/(CR_{\rm K})\,(\mathrm{i}t + k_{\rm B}Tt^2/\hbar)$. Hence, $P(E)$ is peaked around the Coulomb gap $E_{\rm C} = e^2/2C$,

$$P(E) = \frac{1}{\sqrt{4\pi E_{\rm C} k_{\rm B}T}} \exp\left[-\frac{(E - E_{\rm C})^2}{4E_{\rm C}k_{\rm B}T}\right]\,, \tag{3.58}$$

and the I-V characteristic shows a Coulomb gap. At very low temperatures, $k_{\rm B}T \ll \hbar/RC$, the width of the peak of $P(E)$ is proportional to $E_{\rm C}\sqrt{\alpha_{\rm s}}$.

We proceed by deriving further asymptotic results for $P(E)$ and the I-V characteristics. At low temperatures $K(t)$ can be expressed by Exponential Integrals

$$\frac{\mathrm{d}}{\mathrm{d}\tau}K(\tau) = \frac{1}{\alpha_{\rm s}}\left[\mathrm{e}^{-\tau}E_1(-\tau) - \mathrm{e}^{\tau}E_1(\tau)\right]\,. \tag{3.59}$$

Here we have introduced $\tau = t/RC$. In the long-time limit $\tau \to \infty$ we have

$$K(\tau) = -\frac{2}{\alpha_{\rm s}}\left[\ln(\tau) + \gamma + \mathrm{i}\frac{\pi}{2} + ...\right] \tag{3.60}$$

where $\gamma = 0.5772...$ is Euler's constant. From this we obtain $P(E)$ at low energies, up to a constant which is fixed by the normalization condition. Hence, we have

$$\begin{aligned} P(E \to 0+) \;&\propto\; \mathrm{e}^{-2\gamma/\alpha_{\rm s}} \int_{-\infty}^{\infty} \mathrm{d}\tau\, \tau^{-2/\alpha_{\rm s}} \mathrm{e}^{\mathrm{i}ERC\tau/\hbar} \\ &=\; \frac{\mathrm{e}^{-2\gamma/\alpha_{\rm s}}}{,\,(2/\alpha_{\rm s})} \frac{1}{E}\left[\frac{\pi}{\alpha_{\rm s}}\frac{E}{E_{\rm C}}\right]^{2/\alpha_{\rm s}}\,. \end{aligned} \tag{3.61}$$

Inserting the expansion into (3.51) we find for $T = 0$

$$I(V) = \frac{\mathrm{e}^{-2\gamma/\alpha_{\rm s}}}{,\,(2 + 2/\alpha_{\rm s})} \frac{V}{R_{\rm t}}\left[\frac{\pi}{\alpha_{\rm s}}\frac{e|V|}{E_{\rm C}}\right]^{2/\alpha_{\rm s}}\,. \tag{3.62}$$

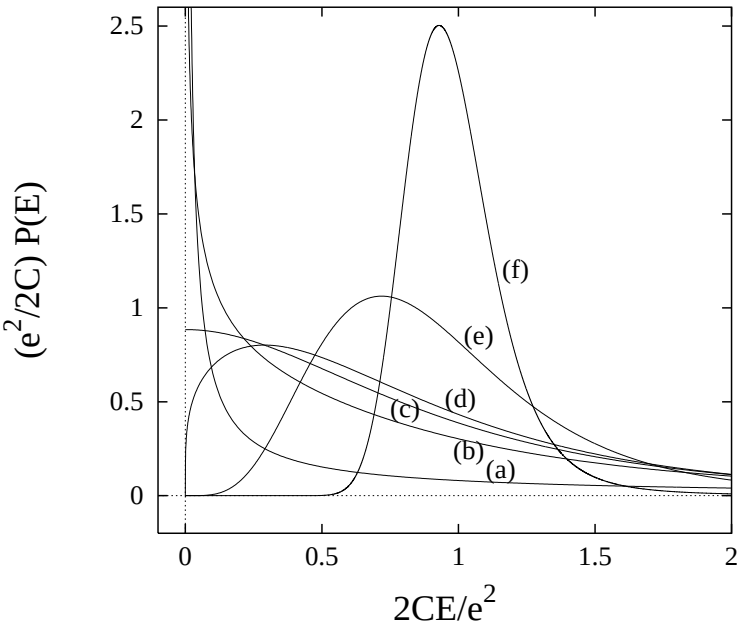

Fig. 3.10: The function P(E) at $T = 0$ for different values of the series resistor. From (a) to (f) $\alpha_s \equiv R_K/R = 20, 3.2, 2, 1.6, 0.4, 0.04$.

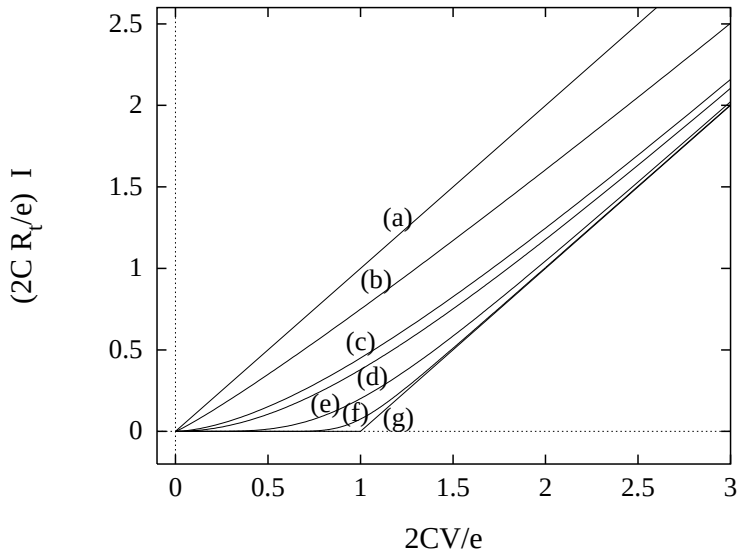

Fig. 3.11: I-V characteristic of a junction in an electric circuit at $T = 0$ for different values of the series resistor. From (a) to (g) $\alpha_s \equiv R_K/R = \infty, 20, 3.2, 2, 0.4, 0.04, 0$.

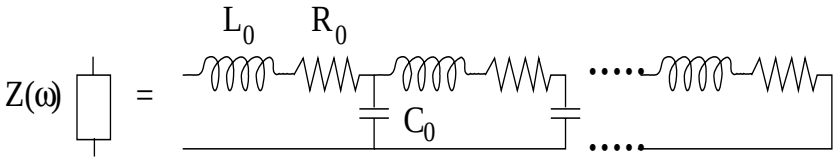

Fig. 3.12: RLC line

We note that at low temperature, as long as the series resistance does not vanish, $R \neq 0$, the differential conductance near $V = 0$ vanishes as a power law. At finite temperatures, $T \neq 0$, the conductance is finite. The linear conductance is [16]

$$\left.\frac{\mathrm{d}I}{\mathrm{d}V}\right|_{\mathrm{V}=0} \propto \frac{1}{R_{\mathrm{t}}}\left[\frac{\pi}{\alpha_{\mathrm{s}}}\frac{2k_{\mathrm{B}}T}{E_{\mathrm{C}}}\right]^{2/\alpha_{\mathrm{s}}} . \tag{3.63}$$

These examples show that a single tunnel junction only shows Coulomb blockade effects if shunted in series with a resistor exceeding the quantum resistance R_{K}. This is difficult to realize in an experiment since a high resistor close to the metal junction can be fabricated only by bringing different materials into good electric contact. Indeed single-electron effects and Coulomb blockade are easier studied in more complex systems, such as SET transistors discussed previously. In this case one junction effectively acts as a high resistor for the other junctions.

3.4.5 Other environments

Above we considered explicitly the effect of an Ohmic series resistor on the tunneling. The question arises, how other elements with a different frequency dependence of the impedance $Z(\omega)$ influence the tunneling. An example which is important from a practical point of view is a coaxial line, which can be modeled by an infinite line of inductances, resistors, and capacitors as shown in Fig. 3.12. When pursuing this question we quickly notice that we have done already most work. Most combinations of linear elements produce an impedance $Z(\omega)$, which is finite at low frequencies. For instance an LC-line has $Z(\omega \to 0) = (L_0/C_0)^{1/2}$, where L_0 and C_0 are the inductance and capacitance per building block. The interesting low-voltage part of the junction I-V characteristics depends precisely on this low-frequency impedance. Hence, most of the results presented above apply, provided we replace the resistance R by $Z(\omega = 0)$.

We can expect qualitatively different results only when the impedance does not approach a constant at low frequencies. Two examples can be mentioned: (i) A single LC resonator with resonance frequency $\Omega = \sqrt{LC}$ and $Z(\omega) \propto \delta(\omega \pm \Omega)$. This system is discussed in detail by Ingold and Nazarov in Ref. [2]. (ii) The RC line, i.e. a series of resistors and capacitors, shown in Fig. 3.12 with $L_0 = 0$. It has the impedance $Z_{\mathrm{RC}}(\omega \approx 0) = \sqrt{R_0/(i\omega C_0)}$.

We now study in more detail the effect of an RC-line. At low frequencies $Z_{\mathrm{t}}(\omega) = [i\omega C + Z_{\mathrm{RC}}^{-1}(\omega)]^{-1} \approx Z_{\mathrm{RC}}(\omega)$. Hence, $\mathrm{Re}\{Z_{\mathrm{t}}(\omega)\} \approx \sqrt{R_0/(2\omega C_0)}$, and in the long-time

limit

$$K_{\rm RC}(t) = \frac{2e^2}{h}\sqrt{\frac{R_0}{2C_0}}\int_0^\infty \frac{{\rm d}\omega}{\omega^{3/2}}\left({\rm e}^{-{\rm i}\omega t}-1\right) = -2\frac{R_0}{R_{\rm K}}\sqrt{\frac{\pi|t|}{R_0C_0}}[1+{\rm i}\ {\rm sgn}(t)]\ . \qquad (3.64)$$

Next we can evaluate

$$\begin{aligned} P_{\rm RC}(E) &= \frac{1}{\pi\hbar}\int_0^\infty {\rm d}t \exp\left[-2\frac{R_0}{R_{\rm K}}\sqrt{\frac{\pi t}{R_0C_0}}\right]\cos\left(\frac{Et}{\hbar}-2\frac{R_0}{R_{\rm K}}\sqrt{\frac{\pi t}{R_0C_0}}\right) \\ &= \sqrt{\frac{eV_0}{4\pi E^3}}\exp\left(-\frac{eV_0}{4E}\right) \quad \text{where} \quad eV_0 = 4\frac{R_0}{R_{\rm K}}\frac{e^2}{2C_0}\ . \end{aligned} \qquad (3.65)$$

The RC-line not only introduces a resistance scale but also an energy and voltage scale V_0. The function $P_{\rm RC}(E)$ has a maximum at $E \approx eV_0$. The resulting I-V characteristic shows a structure resembling the Coulomb gap discussed above. However, the energy scale does not depend on the junction but only on properties of the RC-line.

The RC-line sheds light on a fundamental problem. In all real systems the junction capacitance is shunted by stray capacitors arising from the leads. This raises the question whether the small junction capacitance C – with large charging energy $E_{\rm C} = e^2/2C$ and physical consequences on the tunneling – remains observable, or whether it is masked by the large stray capacitors. It has been conjectured that the tunneling electron sees only the stray capacitances within a certain 'horizon' in space, which hopefully is small. The question then is, what is the size l of this region, explored by the tunneling electron. In many cases the Ansatz $l = c\tau$ where c is the propagation velocity and $\tau \approx \hbar/\max\{eV, k_{\rm B}T\}$ appears to work [17]. The model calculation with spatially distributed capacitances, presented above, yields another limitation. Namely the effective capacitance is

$$C_{\rm eff} = \frac{R_{\rm K}}{4R_0}C_0\ . \qquad (3.66)$$

Notice that $R_{\rm K}/R_0$ is the number of building blocks needed to have a total resistance of order $R_{\rm K}$. From (3.66) we see that $R_{\rm K}/R_0$ is also the distance (in units of the building blocks) up to which the tunneling electron sees the spatially distributed capacitances. In summary, stray capacitances do influence the tunneling. However, they are effectively screened by a resistor of the order of the quantum resistance.

3.5 Charging effects and superconductivity

If the electrodes of the junction are superconducting, Cooper pairs can tunnel. At the same time quasiparticle tunneling is reduced due to the opening of the superconducting gap. This can make higher-order effects, such as the charge transfer due to Andreev reflection the dominant process. In low capacitance junctions Cooper-pair and Andreev tunneling are influenced by charging effects in much the same way as single-electron tunneling. In systems which contain small superconducting islands "parity effects"

may be observable. They arise since single-electron tunneling from the ground state, where all electrons near the Fermi surface are paired, leads to a state where one extra electron – the "odd" one – in the island is in an excited state. Its energy lies above that of the equivalent normal system by the gap Δ. Parity effects influence various physical properties, for instance the state of an electron box or the dissipative and Josephson currents through superconducting single-electron transistors. In this Section we discuss examples of these effects on the level of perturbation theory. A more systematic approach and further results will be presented in the next Section. For an introduction into superconductivity including some topics of this Section, Tinkham's book [4] is recommended. Recent work is presented in the proceedings of the workshop *Mesoscopic Superconductivity* [5] and the review article by Bruder [9].

3.5.1 Charging effects on quasiparticle tunneling

If the system, or part of it, is superconducting we have to describe the tunneling of quasiparticles , whose energy depends on the superconducting gap. The rate for tunneling is still given by the expression (3.10),

$$\begin{aligned} \Gamma_{\rm LI}(n) &= \frac{1}{e^2 R_{\rm t}} \int_{-\infty}^{\infty} {\rm d}E \int_{-\infty}^{\infty} dE' \\ &\quad \times \mathcal{N}_{\rm L}(E)\mathcal{N}_{\rm I}(E') f_{\rm L}(E)[1-f_{\rm I}(E')]\delta(\delta E_{\rm ch} + E' - E) \, , \end{aligned} \tag{3.67}$$

with the obvious modification that the energy integrals include the reduced densities of states of lead and island. In ideal systems they take the BCS form

$$\mathcal{N}_{\rm I/L}(E) = \Theta(|E| - \Delta_{\rm I/L}) \frac{|E|}{\sqrt{E^2 - \Delta_{\rm I/L}^2}} \, . \tag{3.68}$$

Although the integration can no longer be performed in closed form, the rate can be expressed in a transparent way

$$\Gamma_{\rm LI}(n) = \frac{1}{e} I_{\rm t}\left(\frac{\delta E_{\rm ch}}{e}\right) \frac{1}{\exp[\delta E_{\rm ch}/k_{\rm B}T] - 1} \, . \tag{3.69}$$

It depends on the change in charging energy given by Eq. (3.11). The function $I_{\rm t}(V)$ is the well-known quasiparticle tunneling characteristic (see e.g. Ref. [4] or curve (a) in Fig. 3.13), which is suppressed at voltages below the superconducting gap(s). Charging effects reduce the quasiparticle tunneling further. At zero temperature the rate is nonzero only if the gain in charging energy compensates the energy needed to create the excitations. i.e. it sets in with a step at $\delta E_{\rm ch} + \Delta_{\rm I} + \Delta_{\rm L} \leq 0$ if both electrodes are superconducting, or proportional to the square root of $|\delta E_{\rm ch} + \Delta_{\rm I/L}|$, if the argument is negative, in NS junctions. The rates approach the normal state result for large energy differences.

Fluctuations of the electrodynamic environment can be taken into account similar as in the normal state. The δ-function in Eq. (3.67) has to be replaced by the function $P(E)$ introduced in the previous Section. The resulting I-V characteristics [18], are plotted in Fig. 3.13. They show much structure at the sum of gap and charging energy.

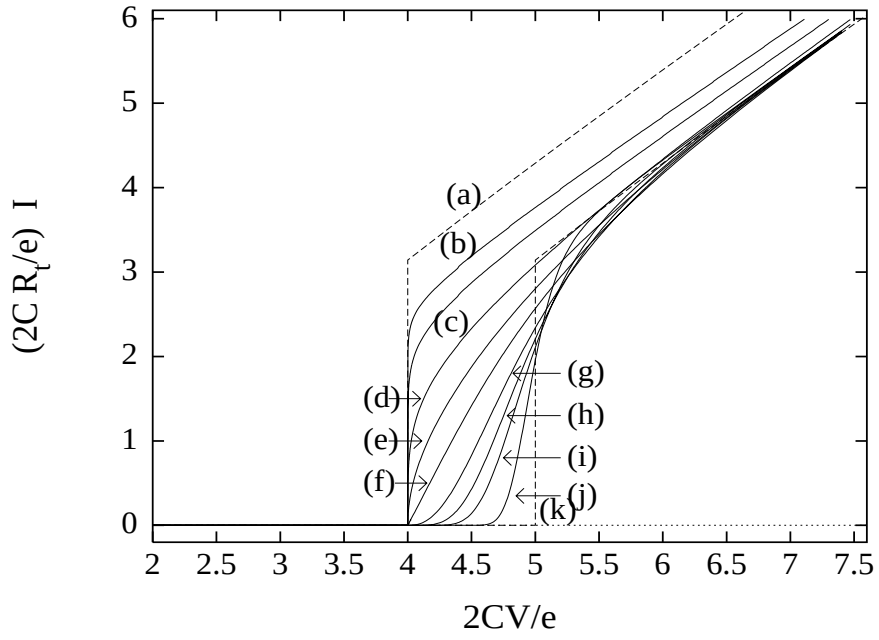

Fig. 3.13: I-V characteristic of a superconducting junction in an electric circuit for different values of the series resistor. From (a) to (k) $\alpha_{\rm s} \equiv R_{\rm K}/R = \infty, 40, 20, 8, 4, 2, 0.8, 0.4, 0.2, 0.04, 0$. The superconducting energy gap is $\Delta = 2E_{\rm C}$.

3.5.2 Two-electron tunneling, Andreev reflection

In the regime where quasiparticle tunneling is suppressed by the superconducting gap higher-order processes involving multi-electron tunneling play a role. Cooper-pair tunneling is such a process. We will discuss it later. If only one of the electrodes is superconducting there is still the process of 2-electron tunneling, denoted as Andreev reflection . In this process an electron approaching from the normal side with energy below the gap is reflected as a hole, while a Cooper pair propagates into the superconductor. (Andreev considered a normal metal and a superconductor in good metallic contact. But his physical picture can be generalized to tunnel junctions.)

For definiteness we consider a SET transistor with a superconducting island and normal leads (NSN). In order to describe tunneling in this system we have to rewrite the tunneling Hamiltonian in terms of the Bogoliubov creation and annihilation operators for the excitations in the superconducting island

$$H_{\rm t,L} = \sum_{k,q,\sigma} T_{k,q}[u_{q,\sigma}\gamma^\dagger_{q,\sigma} + v^*_{q,\sigma}\gamma_{-q,-\sigma}]c_{k,\sigma} + \text{h.c.}\ . \tag{3.70}$$

Here, $u_{q,\sigma}$ and $v_{q,\sigma}$ are the standard BCS coherence factors with magnitudes $\sqrt{\frac{1}{2}(1 \pm \frac{\epsilon_q}{E_q})}$, and $E_q = \sqrt{\epsilon_q^2 + \Delta^2}$ is the energy of the quasiparticles.

Andreev reflection is a second-order coherent process. In the first part of the transition one electron is transferred from an initial state, e.g. $k\uparrow$ of the normal lead, into an intermediate excited state $q\uparrow$ of the superconducting island. In the second part of the coherent transition an electron tunnels from $k'\downarrow$ into the partner state $-q\downarrow$

of the first electron, such that both form a Cooper pair. The final state contains two excitations in the normal lead and an extra Cooper pair in the superconducting island. The amplitude for this process, to which we add the amplitude of the process in reverse order, is then given by [19]

$$A_{k,k'} = \sum_q T_{k,q} T_{k',-q} u_q v_q \left(\frac{1}{\delta E_{\mathrm{ch},1} + E_q - \epsilon_k} + \frac{1}{\delta E_{\mathrm{ch},1} + E_q - \epsilon_{k'}} \right) . \tag{3.71}$$

Here spin indices have been suppressed. The change in the charging energy $\delta E_{\mathrm{ch},1} \equiv E_{\mathrm{ch}}(n+1, Q_{\mathrm{G}}) - E_{\mathrm{ch}}(n, Q_{\mathrm{G}}) - eV$ corresponds to the virtual intermediate state where *one* electron has tunneled from the lead (at voltage V) to the island. Finally, the rate for the Andreev reflection process is

$$, \,{}^{\mathrm{A}}_{\mathrm{LI}} = \frac{2\pi}{\hbar} \sum_{k,k'} |A_{k,k'}|^2 \, f_{\mathrm{L}}(\epsilon_k) f_{\mathrm{L}}(\epsilon'_k) \delta(\epsilon_k + \epsilon'_k + \delta E_{\mathrm{ch},2}) . \tag{3.72}$$

Here, the change in the charging energy $\delta E_{\mathrm{ch},2} = E_{\mathrm{ch}}(n+2, Q_{\mathrm{G}}) - E_{\mathrm{ch}}(n, Q_{\mathrm{G}}) - 2eV$ corresponds to the real final state where *two* electron charges have been added to the superconducting island.

If we ignore the dependence of the tunneling matrix elements on the magnituude of the momenta the q-summation in (3.71) can be performed with the result

$$A_{k,k'} = \pi N_{\mathrm{I}}(0) a \left(\frac{\Delta}{\delta E_{\mathrm{ch},1}} \right) \langle T_{k,q} T_{k',-q} \rangle_q , \tag{3.73}$$

where

$$a(x) \equiv \frac{4}{\pi} \frac{x}{\sqrt{x^2 - 1}} \arctan \sqrt{\frac{x-1}{x+1}} . \tag{3.74}$$

The quasiparticle energy E_q is at least Δ, and we assumed that the energy of the intermediate state lies above that of the initial state, $\Delta + \delta E_{\mathrm{ch},1} \gg \epsilon_k, \epsilon_{k'} \approx 0$. Andreev reflection is most important if the gap Δ is much larger than the relevant energy differences $|\delta E_{\mathrm{ch},1}|$. In this limit the function (3.74) reduces to $a(\Delta/\delta E_{\mathrm{ch},1} \gg 1) \approx 1$. We, therefore, drop in the following the weak energy dependence contained in the function a. It has to be taken into account when the energy of the virtual state coincides with that of the initial state, since a diverges in this case. In the opposite limit, $\Delta + \delta E_{\mathrm{ch},1} < 0$, single electrons tunnel, and Andreev reflection can be neglected.

If $a \approx 1$, the integrations in (3.72) can be performed, resulting in

$$, \,{}^{\mathrm{A}}(n, Q_{\mathrm{G}}) = \frac{G_{\mathrm{A}}}{4e^2} \frac{\delta E_{\mathrm{ch},2}}{\exp(\delta E_{\mathrm{ch},2}/k_{\mathrm{B}}T) - 1} . \tag{3.75}$$

Note that this rate coincides in the functional dependence with that for single-electron tunneling in a normal junction, Eq. (3.13), except that:

(i) The charge transferred in an Andreev reflection is $2e$, and the charging energy changes accordingly. An important conclusion is that Andreev reflection is also subject to Coulomb blockade in a way similar to normal-state single-electron tunneling [20].

(ii) The effective conductance is of second-order

$$G_{\rm A} = \frac{1}{4}\frac{R_{\rm K}}{N_{\rm ch} R_{\rm t}^2} \ . \tag{3.76}$$

(iii) We introduced the number of independent parallel channels

$$\frac{1}{N_{\rm ch}} = \frac{\langle |\langle T_{k,q} T_{k',-q}\rangle_q|^2\rangle_{k,k'}}{\left(\langle |T_{k,q}|^2\rangle_{k,q}\right)^2} \ , \tag{3.77}$$

which depends on the correlations between the tunnel matrix elements. In the second-order Andreev process the matrix elements appear in a combination as shown in the numerator of Eq. (3.77), differing from the square of the expression determining the normal state conductance $1/R_{\rm t}$ given in the denominator of Eq. (3.77) [2]. For the moment we consider $N_{\rm ch}$ as a fit parameter. Even in small junctions it turns out (from a comparison of Andreev and normal state conductance) to be much larger than one. Notice both, the normal state conductance $1/R_{\rm t} = N_{\rm ch}/R_{\rm t,0}$ and the Andreev conductance $G_{\rm A} \propto N_{\rm ch} R_{\rm K}/R_{\rm t,0}^2$ are the result of $N_{\rm ch}$ parallel channels. If we express the second order Andreev conductance by the normal state conductance $1/R_{\rm t}$ the factor $N_{\rm ch}$ appears in the denominator.

Since the Andreev reflection rate depends on the charging energy similar as the normal-state single-electron tunneling rate we expect a similar dependence on gate and transport voltages as shown in Fig. 3.7, with the obvious rescaling of the conductance and charge. This is indeed what has been observed in the experiments of the Harvard group [22].

3.5.3 Parity effects in small superconductors

In a normal-metal electron box, if the applied gate voltage is swept, the electron number on the island increases in unit steps, and the voltage of the island shows a periodic saw-tooth behavior. The periodicity in the gate charge $Q_{\rm G}$ is e. If the island is superconducting, and the gap Δ is smaller than the charging energy $E_{\rm C}$, then at low temperatures the charge and the voltage show a characteristic long-short cyclic, $2e$-periodic dependence on the induced charge. The effect arises since single-electron tunneling from the ground state, where all electrons near the Fermi surface of the superconducting island are paired, leads to a state with one extra electron – the "odd" one – in an excited state [23]. In a small island, as long as charging effects prevent further tunneling, the odd electron does not find another excitation for recombination. Hence the energy of this state stays (at least metastable) above that of the equivalent

[2] The careful reader will notice that the expression (3.77) would be correct if we would not have performed an integration over $|q|$ in the derivation of the expression for a. Hence the present derivation is not rigorous. (A separation into magnitude and direction of the momenta, suggested in Ref. [19], does not account for the relevant difficulty.) A more careful discussion will be presented in Section 3.6, where we will find that the Andreev conductance depends on correlations in space, which extend over the range of the Cooperon propagator in the normal metal [21].

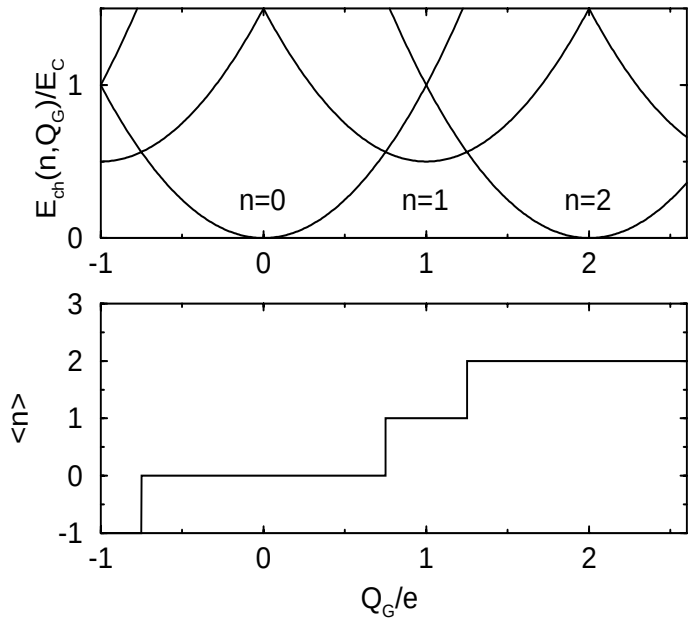

Fig. 3.14: The lowest energy state of a superconducting single-electron box as a function of the gate voltage shows a difference between even and odd numbers n of electron charges on the island. Accordingly the island charge is found in a broader range of gate voltages in the even state than in the odd state.

normal system by the gap energy. Only at larger gate voltages another electron can enter the island, and the system can relax to the ground state. This behavior repeats with periodicity $2e$ in $Q_{\rm G}$, as displayed in Fig. 3.14.

At low temperatures this even-odd asymmetry has been observed [24, 25, 26, 22], but at higher temperatures, above a crossover value $T_{\rm cr} \ll \Delta$, the e-periodic behavior typical for normal metal electron boxes is recovered. We can explain this crossover by analyzing the rate of tunneling of electrons between the lead and the island, paying particular attention to the fate of the "odd" electron [27]. Since at low temperature single-electron tunneling processes which cost energy are exponentially suppressed the further fate of the excited "odd" electron gains importance. This single excitation can tunnel out with a rate γ which is smaller by a factor $1/N_{\rm eff}$ than the rate , of the other $N_{\rm eff}$ electrons; in mesoscopic islands $N_{\rm eff}$ is typically of the order of 10^4 (see below). On the other hand, in an important range of parameters γ is not exponentially suppressed, since the excitation energy of the odd electron is regained if this electron tunnels out. Hence $\gamma \approx$, $\mathrm{e}^{\Delta/k_{\rm B}T}/N_{\rm eff}$. Parity effects are observable as long as this single-electron tunneling rate is relevant $\gamma \geq$, , from which we obtain the crossover temperature $k_{\rm B}T_{\rm cr} \approx \Delta/\ln N_{\rm eff}$. We will present now the arguments, analyze the rates in more detail, and use them in the next Subsection to derive the I-V characteristics of normal-superconducting NSN transistors.

We first consider an electron box with a superconducting island and a normal lead. If the distribution functions of lead and island are equilibrium Fermi functions, the rate of tunneling is given by Eq. (3.69). At low temperature the rate , $_{\rm LI}$ is finite only at voltages where the gain in charging energy (i.e. $\delta E_{\rm ch} < 0$) exceeds the energy of the excitations ($\epsilon_k \geq 0, E_p \geq \Delta$) created in the lead and island, i.e. for $\delta E_{\rm ch} + \Delta < 0$. It is

exponentially suppressed otherwise. The assumption of equilibrium Fermi distributions is sufficient when we start from the even state. For definiteness let us assume that we started from $n = 0$ and that the gate voltage is chosen such that $0 \leq Q_{\rm G} \leq e$. Hence, the relevant change in charging energy is $\delta E_{\rm ch} = E_{\rm ch}(1, Q_{\rm G}) - E_{\rm ch}(0, Q_{\rm G})$ and the rate of tunneling from an even to an odd state is

$$, ^{\rm eo} = , _{\rm LI}(n = 0, Q_{\rm G}) \; . \tag{3.78}$$

In the odd state the quasiparticle distribution differs from an equilibrium Fermi function. There is extra charge in the normal component. After thermalization the distribution of the excitations in the island can be described by a Fermi function, $f_{\delta\mu}(\epsilon) = [{\rm e}^{(\epsilon-\delta\mu)/k_{\rm B}T} + 1]^{-1}$, but with a shifted chemical potential $\mu_N = \mu_S + \delta\mu$ relative to the condensate [3]. The shift in chemical potential is fixed by the constraint to have *one* excess electron charge

$$1 = N_{\rm I}(0)\Omega_{\rm I} \int_{-\infty}^{\infty} {\rm d}E \mathcal{N}_{\rm I}(E)[f_{\delta\mu}(E) - f_0(E)] \; . \tag{3.79}$$

This reduces at low temperatures to

$$\delta\mu = \Delta - k_{\rm B}T \ln N_{\rm eff}(T), \tag{3.80}$$

where

$$N_{\rm eff}(T) = N_{\rm I}(0)\Omega_{\rm I}\sqrt{2\pi\Delta k_{\rm B}T} \tag{3.81}$$

is the number of states in the island available for quasiparticles near the gap [25]. Parity effects are observable as long as the shift of the chemical potential is observable $\delta\mu > k_{\rm B}T$. This (again) amounts to the requirement $T < T_{\rm cr}$, where the crossover temperature is

$$k_{\rm B}T_{\rm cr} = \Delta / \ln N_{\rm eff}(T_{\rm cr}) \; . \tag{3.82}$$

The tunneling rate back from the odd state (here $n = 1$) to the even state ($n = 0$) is given by the expression $, ^{\rm oe} = , _{{\rm IL},\delta\mu}(n = 1, Q_{\rm G})$ given by (3.67) with the island distribution function replaced by $f_{\delta\mu}(\epsilon)$. For $\exp(-\Delta/k_{\rm B}T) \ll 1$ the ratio of the rates of the two transitions is

$$, ^{\rm oe}/, ^{\rm eo} = {\rm e}^{[E_{\rm ch}({\rm odd}) + \delta\mu - E_{\rm ch}({\rm even})]/k_{\rm B}T} = {\rm e}^{\delta F/k_{\rm B}T} \; . \tag{3.83}$$

i.e. they obey a detailed balance relation, depending on a "free energy" difference, which in addition to the charging energy contains the shift of the chemical potential $\delta\mu$. This free energy difference coincides with that introduced in Ref. [25].

[3] A similar phenomenon was described 20 years ago by Tinkham and denoted as charge (or branch) imbalance [28]. In those experiments a nonequilibrium state was maintained by a balance of driving currents and relaxation processes. In the present parity-effect experiments the charge imbalance is preserved, at least in the sense of a metastable state, by the charging energy which prevents further electrons from tunneling and the following recombination.

For the following discussion it is useful to decompose the rate as

$$,^{\mathrm{oe}} = ,_{\mathrm{IL}}(1, Q_{\mathrm{G}}) + \gamma(Q_{\mathrm{G}}) \,, \tag{3.84}$$

where $,_{\mathrm{IL}}$ is given by the equilibrium form, analogous to (3.69), and

$$\gamma(Q_{\mathrm{G}}) = \frac{1}{2e^2 R_{\mathrm{t}}} \int_{-\infty}^{\infty} \mathrm{d}\epsilon_k \int_{-\infty}^{\infty} \mathrm{d}E \mathcal{N}_{\mathrm{I}}(E)$$

$$\times [f_{\delta\mu}(E) - f_0(E)] \quad [1 - f_0(\epsilon_k)] \delta(\epsilon_k - E - \delta E_{\mathrm{ch}}) \,, \tag{3.85}$$

describes the rate of tunneling of the odd, excited electron only. In the important range of parameters $\Delta + \delta E_{\mathrm{ch}} > k_{\mathrm{B}} T$ this rate reduces to

$$\gamma(Q_{\mathrm{G}}) = \frac{1}{2e^2 R_{\mathrm{t}} N_{\mathrm{I}}(0) \Omega_{\mathrm{I}}} \,, \tag{3.86}$$

whereas it is exponentially suppressed otherwise. Consistent with the simple picture outlined before we see that the odd electron tunneling rate γ contains a small prefactor $1/N_{\mathrm{I}}(0)\Omega_{\mathrm{I}}$ as compared with $,_{\mathrm{IL}}$. On the other hand, in an important range of gate voltages – since the energy of the excitation in the island is regained in the tunneling process – the rate γ is not exponentially suppressed. Hence it may be larger than $,_{\mathrm{IL}}$.

Above we described the range $0 \leq Q_{\mathrm{G}} \leq e$ where tunneling occurs between the island states $n = 0$ and $n = 1$. The range $e \leq Q_{\mathrm{G}} \leq 2e$ can be treated analogously. The tunneling now connects the states $n = 1$ and $n = 2$. In this case, except for the single-electron tunneling processes which create further excitations (described by $, $), one electron can tunnel into one specific state $(-k, -\sigma)$, the partner state of the excitation (k, σ) which is already present. Both condense immediately; the state with two excitations only exists virtually. The latter process is described again by $\gamma(Q_{\mathrm{G}})$. The symmetry implies $,^{\mathrm{eo/oe}}(Q_{\mathrm{G}}) = ,^{\mathrm{eo/oe}}(2e - Q_{\mathrm{G}})$. Since the properties of the system are $2e$-periodic in Q_{G}, we have provided a complete description for all values of the gate voltage.

In the following we will consider processes where the sweep rate of the gate voltage is small compared with the recombination rate of a pair of excitations. Therefore, we can concentrate at a given gate voltage on the even state (ground state and thermal distribution of pairs of excitations) and the odd state (one excess charge in an excited state plus thermal distribution of pairs of excitations). The sequential tunneling of charges between the island and the lead is described by a master equation for the occupation probabilities of the even and odd states $p_{\mathrm{e}}(Q_{\mathrm{G}})$ and $p_{\mathrm{o}}(Q_{\mathrm{G}})$,

$$\frac{\mathrm{d}p_{\mathrm{e}}(Q_{\mathrm{G}})}{\mathrm{d}t} = -,^{\mathrm{eo}}(Q_{\mathrm{G}}) p_{\mathrm{e}}(Q_{\mathrm{G}}) + ,^{\mathrm{oe}}(Q_{\mathrm{G}}) p_{\mathrm{o}}(Q_{\mathrm{G}}) \tag{3.87}$$

with $p_{\mathrm{e}}(Q_{\mathrm{G}}) + p_{\mathrm{o}}(Q_{\mathrm{G}}) = 1$. The equilibrium solution is $p_{\mathrm{e(o)}}(Q_{\mathrm{G}}) = ,^{\mathrm{oe(eo)}}(Q_{\mathrm{G}})/,_{\Sigma}(Q_{\mathrm{G}})$, where $,_{\Sigma}(Q_{\mathrm{G}}) = ,^{\mathrm{oe}}(Q_{\mathrm{G}}) + ,^{\mathrm{eo}}(Q_{\mathrm{G}})$. For $,^{\mathrm{oe}} \gg ,^{\mathrm{eo}}$ we have $\rho_{\mathrm{e}}(Q_{\mathrm{G}}) \approx 1$, i.e. the system occupies the even state, while for $,^{\mathrm{eo}} \gg ,^{\mathrm{oe}}$ the island is in the odd state.

The solution of the master equation, combined with symmetry arguments, determines the crossover value Q_{cr} of the gate charge where the system switches between the even and the odd state. The condition is $\rho_{\mathrm{e}} \approx \rho_{\mathrm{o}}$, i.e.

$$,^{\mathrm{oe}}(Q_{\mathrm{cr}}) \approx ,^{\mathrm{eo}}(Q_{\mathrm{cr}}). \tag{3.88}$$

At very low temperatures the switching point is determined by the lowest energy as shown in Fig. 3.14. At finite, but low temperature we find $Q_{\rm cr}(T) = \frac{e}{2} + \frac{C}{e}[\Delta - k_{\rm B}T \ln N_{\rm eff}(T)]$, where $N_{\rm eff}(T)$ was defined in (3.81). This means the short sections in Fig. 3.14 get longer until, above $T_{\rm cr}$, we have $Q_{\rm cr} = e/2$, and only the e-periodic behavior known from normal systems is recovered.

3.5.4 *I-V* characteristics of NSN transistors

The analysis presented above can be extended to describe even-odd effects in SET transistors with a superconducting island. As a specific example we first consider an NSN transistor where the energy gap is smaller than the charging energy scale $\Delta < E_{\rm C}$. In this system the important processes are single-electron tunneling processes in the left and right junction, causing transitions between even and odd states, with rates $,^{\rm eo/oe}_{\rm L}$ and $,^{\rm eo/oe}_{\rm R}$ which are obvious generalizations of Eq. (3.78) and (3.84). They depend on the change in charging energies as described in Eq. (3.17), and on the energies of the excitations created in the island.

These rates enter a master equation. At low T it is sufficient to consider only one even and one odd state of the island. From the master equation we find again the crossover gate voltage and temperature, but also the I-V characteristic of the transistor. In the limit considered ($\Delta < E_{\rm C}$) it is

$$I = e(,^{\rm eo}_{\rm L} p_{\rm e} - ,^{\rm oe}_{\rm L} p_{\rm o}) = e\frac{,^{\rm eo}_{\rm L},^{\rm oe}_{\rm R} - ,^{\rm eo}_{\rm R},^{\rm oe}_{\rm L}}{,^{\rm eo}_{\rm L} + ,^{\rm eo}_{\rm R} + ,^{\rm oe}_{\rm L} + ,^{\rm oe}_{\rm R}} \,. \tag{3.89}$$

At high temperatures $T > T_{\rm cr}$ the single-electron tunneling current (3.89) shows the Coulomb oscillations known from normal systems with parabola-shaped maxima at the points $Q_{\rm G} = e/2 + ne$ with integer n. At low temperature $T < T_{\rm cr}$ the current is limited by the odd electron tunneling rate γ in one of the junctions. In the window $Q_{\rm cr}(T) < Q_{\rm G} < e/2 + \Delta C/e + Q_{\rm cr}/2 < e$ it is

$$I_{\rm plateau} = e\gamma = \frac{1}{2eR_{\rm t}N_{\rm I}(0)\Omega_{\rm I}} \tag{3.90}$$

and exponentially small outside. A second current plateau exists in the window $e < 3e/2 - \Delta C/e - Q_{\rm cr}/2 < Q_{\rm G} < 2e - Q_{\rm cr}$. Both plateaus create a double structure which repeats 2e-periodically. For $\Delta + eV/2 > E_{\rm C}$ the two plateaus merge to form a 2e-periodic single plateau structure. An example is shown in Fig. 3.15 with parameters which are realistic for an experiment on parity effects. In this case the current (3.90) is of the order of 100fA.

In NSN transistors with a larger superconducting gap $\Delta > E_{\rm C}$ the odd states have a large energy. Hence a mechanism which transfers two electrons between the normal metal and the superconductor becomes important. Andreev reflection with rate (3.75) provides such a mechanism [19]. The master equation description can be generalized to include also this process. Because of the similarity of the rate for Andreev reflection to that of single electron tunneling it is clear that the shape of the I-V characteristic due to Andreev reflection also takes a similar form. At low temperatures a set of parabolic

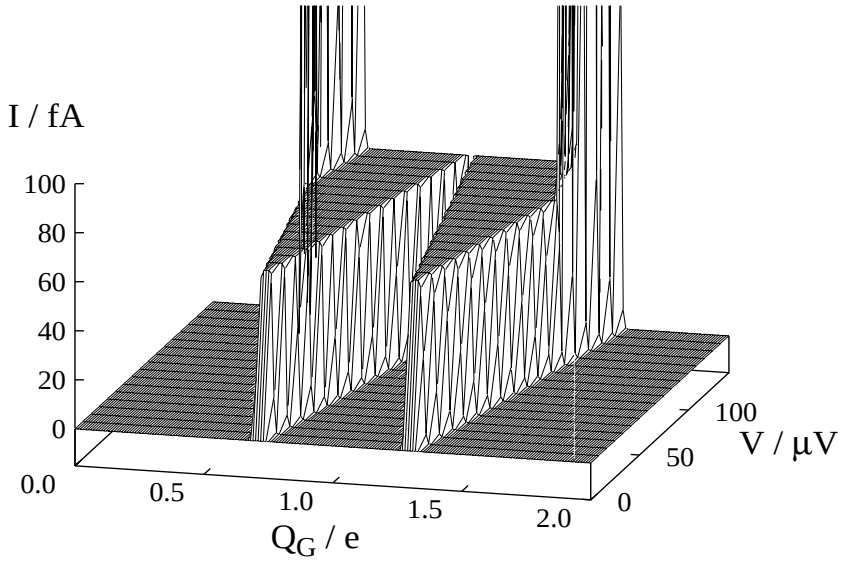

Fig. 3.15: Quasiparticle current in an NSN transistor with $\Delta < E_C$ as a function of gate and transport voltage. The parameters are $\Delta = 55\mu$eV, $E_C = 125\mu$eV, and $R_t = 25k\Omega$.

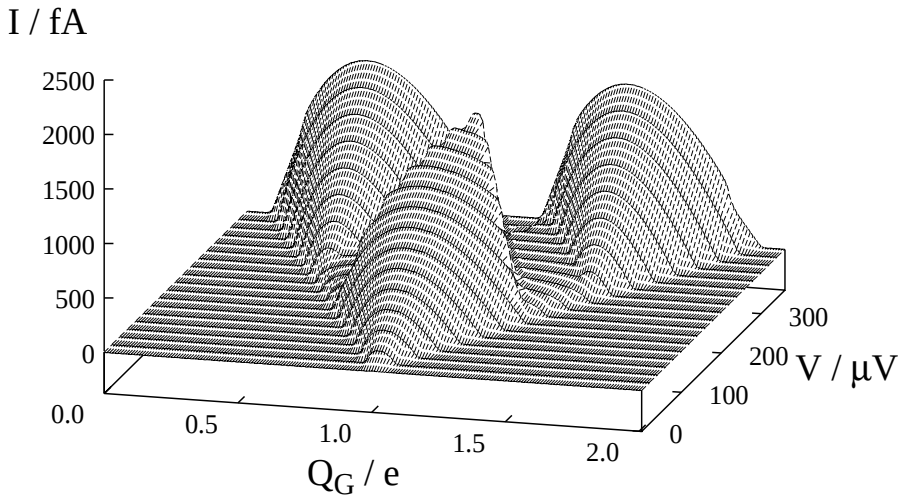

Fig. 3.16: The current $I(Q_G, V)$ through an NSN transistor with $\Delta > E_C$. The parameters are chosen to coincide with those of the experiments of Hergenrother et al., $E_C = 100\mu$eV, $\Delta = 245\mu$eV.

current peaks is found centered around the degeneracy points $Q_{\rm G} = \pm e, \pm 3e, \ldots$ [19]

$$I^{\rm A}(\delta Q_{\rm G}, V) = \frac{1}{4} G_{\rm A} \Big(V - 4\frac{\delta Q_{\rm G}^2}{VC^2} \Big) \Theta \Big(V - 4\frac{\delta Q_{\rm G}^2}{VC^2} \Big) \quad . \tag{3.91}$$

Here $\delta Q_{\rm G}$ is $\delta Q_{\rm G} = Q_{\rm G} - e$ for $Q_{\rm G}$ close to e, and similar near the other degeneracy points.

At larger transport voltages single-electron tunneling sets in, even in the limit $\Delta > E_{\rm C}$, and Andreev reflection becomes blocked; it gets "poisoned" [19]. The reason is that above a threshold voltage the odd state can be reached by a single-electron tunneling process. This occurs when $(e - Q_{\rm G})^2/2C - Q_{\rm G}^2/2C + \Delta \leq eV/2$, which requires sufficiently large transport voltages, $V \geq V_{\rm poison}$, where

$$V_{\rm poison} = \frac{2}{e} \left(E_{\rm C} - \frac{eQ_{\rm G}}{C} + \Delta \right) \ . \tag{3.92}$$

The rate for this transition, from the even to the odd state, is of the order of $,^{\rm eo} \sim G_n(V - V_{\rm poison})/e$. The state which is reached after such a single-electron tunneling process is not the ground state. It is energetically favorable that after the first tunneling process another electron tunnels into the partner state of the excitation which is present already. The rate for this process is given by γ, which in the considered range of parameters takes the value given in Eq. (3.86). Typically the rate for the second transition, from odd to even, is smaller than that of the first processes and, hence, creates the bottleneck in the sequence of SET processes. The same inequality also implies that above $V_{\rm poison}$ the system is most likely in the odd state, $p_{\rm o}/p_{\rm e} = ,^{\rm eo}/\gamma \gg 1$. Hence the current produced by the cycle is given by Eq. (3.90). (The current due to Andreev transitions between two odd states is smaller, $I_{\rm Andreev} \sim p_{\rm e} G_{\rm A} V$.)

Fig. 3.16 shows the current-voltage characteristic of an NSN transistor with $\Delta > E_{\rm C}$. At small transport voltage the 2e-periodic peaks due to Andreev reflection dominate; they get poisoned above a threshold voltage. The peaks at larger transport voltages arise from a combination of single-electron tunneling and Andreev reflection processes. The shape and size of the even-even Andreev peaks and some of the single-electron tunneling features at higher transport voltages agree remarkably well with the experiments of Hergenrother et al. [22]. In earlier experiments further odd-odd Andreev peaks have been observed. They cannot be explained simply by raising the electron temperature. Their origin, as has been pointed out by Hergenrother et al. [22], are single-electron transitions induced by the noise of the electromagnetic environment, which is at a higher temperature than the electron system.

3.5.5 Coherent Cooper-pair tunneling

In "classical" Josephson junctions Cooper pairs can tunnel free of dissipation between the superconducting electrodes. The coupling is described by the Josephson energy $-E_{\rm J} \cos\varphi$, which depends on φ, the phase difference across the barrier. The energy scale $E_{\rm J} = \hbar I_{\rm cr}/2e$ is related to the critical current of the junction, which in turn can be expressed by the tunneling resistance of the junction and the energy gap of the superconductor, $I_{\rm cr}(T = 0) = \pi\Delta/(2eR_{\rm t})$.

Charging introduces quantum effects: The phase difference and the charge on the electrodes, Q, are quantum mechanical conjugate variables. The dynamics of an ideal Josephson junction is governed by the Hamiltonian

$$H_0 = \frac{Q^2}{2C} - E_{\rm J}\cos\varphi \quad , \quad Q = \frac{\hbar}{\rm i}\frac{\partial}{\partial(\hbar\varphi/2e)} \; . \tag{3.93}$$

For simplicity we describe here a single junction. The generalization to multi-junction systems, including gate voltage sources is obvious. An important question is how dissipation due to the flow of normal currents and/or quasiparticle tunneling can be accounted for, which has been addressed e.g. in Refs. [14, 29, 6, 7]. So-called "macroscopic quantum effects" like macroscopic quantum tunneling of the phase, or quantum coherent oscillations are derived from the Hamiltonian (3.93). Macroscopic quantum tunneling has been observed in tunnel junctions with small capacitances of the order of 10^{-12} F. These values are orders of magnitude larger than those of the junctions where single-electron effects play a role.

We now turn to mesoscopic Josephson junctions or junction systems, where the number of electrons or Cooper pairs in small islands is a relevant degree of freedom. The charging energy has been discussed in detail above. The Josephson coupling describes the transfer of Cooper-pair charges in forward or backward direction, and can be written in a basis of charge states as

$$\langle n|E_{\rm J}\cos\varphi|n'\rangle = \frac{E_{\rm J}}{2}(\delta_{{\rm n}',{\rm n}+2} + \delta_{{\rm n}',{\rm n}-2}) \; . \tag{3.94}$$

Below we will first consider situations where Cooper pairs tunnel coherently. This shows features known from the phenomenon of resonant tunneling. It is non-dissipative and hence strongest in situations near degeneracy. We will show how in a superconducting electron box the steps in the expectation value of the charge on the island are broadened by Cooper-pair tunneling. In the next Subsection we will discuss, following Ref. [30], how coherent Cooper-pair tunneling can be probed by Andreev reflection and observed in the dissipative I-V characteristic of an NSS transistor. Further examples of coherent tunneling of Cooper pairs can be found in the literature. We mention the gate-voltage dependence of the critical current of SSS or SNS transistors [31, 32, 33]. Another example is the combination of coherent Cooper-pair tunneling and dissipative quasiparticle tunneling or transitions induced by the environment, which are responsible for the dissipative I-V characteristic of SSS transistors [34, 35, 25, 36].

We first consider an electron box with superconducting island and lead, assuming that the energy gap exceeds the charging energy and that the temperature is low, $\Delta > E_{\rm C} \gg k_{\rm B}T$. In this case, at low voltages quasiparticle tunneling is suppressed, and the island charge can change only by Cooper-pair tunneling in units of $2e$ as described by Eq. (3.94). The tunneling is strong near points of degeneracy. For instance for $Q_{\rm G} \approx e$ the states with $n = 0$ and $n = 2$ have similar charging energies, and we can restrict our attention to these two charge states. The coherent tunneling between both is described by the 2×2 Hamiltonian

$$H = \begin{pmatrix} E_{\rm ch}(0) & -E_{\rm J}/2 \\ -E_{\rm J}/2 & E_{\rm ch}(2) \end{pmatrix} \; . \tag{3.95}$$

This Hamiltonian is easily diagonalized. The eigenstates are

$$\psi_0 = \alpha|0\rangle + \beta|2\rangle \ , \qquad \psi_1 = \beta|0\rangle - \alpha|2\rangle \tag{3.96}$$

with coefficients

$$\alpha^2 = \frac{1}{2}\left[1 + \frac{\delta E_{\rm ch}}{\sqrt{\delta E_{\rm ch}^2 + E_{\rm J}^2}}\right] = 1 - \beta^2 \ , \tag{3.97}$$

and energies

$$E_{0/1} = \frac{1}{2}\left[E_{\rm ch}(0) + E_{\rm ch}(2) \mp \sqrt{\delta E_{\rm ch}^2 + E_{\rm J}^2}\right] \ . \tag{3.98}$$

Here we introduced the difference in charging energy $\delta E_{\rm ch} \equiv E_{\rm ch}(2) - E_{\rm ch}(0) = 4E_{\rm C}\,(Q_{\rm G}/e - 1)$. The coefficient α is close to unity if the charging energy of the state $|2\rangle$ lies above that of $|0\rangle$, i.e. for $\delta E_{\rm ch} > 0$, and vanishes in the opposite limit, while β has the complementary behavior.

The expectation value of the charge on the island in the ground state is given by

$$\langle\psi_0|n|\psi_0\rangle = 2\beta^2 \ . \tag{3.99}$$

It changes continuously near $Q_{\rm G} = e$ from 0 to 2 in a range of width of order $\Delta Q_{\rm G} \approx E_{\rm J}/E_{\rm C}$. This has recently been observed experimentally [37]. We note that the coherent mixing of different charge states due to Cooper-pair tunneling is described by elementary quantum mechanics (the diagonalization of a 2×2 matrix). In contrast, the perturbative description of single-electron tunneling presented in Section 3.3 diverges near the degeneracy point and requires a more careful analysis (see Section 3.7).

3.5.6 Andreev spectroscopy of Josephson tunneling

Next we consider an example of coherent Cooper-pair tunneling in an NSS transistor . Here Cooper pairs can tunnel coherently in the Josephson (SS) junction, which can be probed by the dissipative current due to Andreev reflection across the NS junction. Again we restrict ourselves to low temperatures, $k_{\rm B}T \ll E_{\rm J}$.

In the present example, where we describe coherent Cooper-pair tunneling in the SS junction in a situation with a nonzero transport voltage we have to account in the Hamiltonian for the work done by the voltage sources during the transitions. We, therefore, keep track also of the number of electrons $N_{\rm L}$ and $N_{\rm R}$ in the left and right electrode. A basis set of states is denoted by $|N_{\rm L}, n, N_{\rm R}\rangle$, and the corresponding charging energy (for symmetric bias $V_{\rm L} = -V_{\rm R} = V/2$) is

$$E_{\rm ch}(N_{\rm L}, n, N_{\rm R}) = \frac{(ne - Q_{\rm G})^2}{2C} - (N_{\rm R} - N_{\rm L})\frac{eV}{2} \ . \tag{3.100}$$

In a situation where only two charge states get appreciably mixed the eigenstates and energies of the corresponding 2×2 Hamiltonian are

$$\begin{aligned} \psi_0 &= \alpha|0,0,0\rangle + \beta|0,2,-2\rangle \ , \qquad \psi_1 = \beta|0,0,0\rangle - \alpha|0,2,-2\rangle \ , \\ E_{0/1} &= \frac{1}{2}\left[E_{\rm ch}(0,0,0) + E_{\rm ch}(0,2,-2) \mp \sqrt{\delta E_{\rm ch}^2 + E_{\rm J}^2}\right] \ . \end{aligned} \tag{3.101}$$

The coefficients coincide with those of the box discussed above, except for the obvious change of notation, and $\delta E_{\rm ch} = E_{\rm ch}(0,2,-2) - E_{\rm ch}(0,0,0)$.

In the low-bias regime, the dominant mechanism of transport in the NS junction of the transistor is Andreev reflection. Starting from a state $|0,0,0\rangle$ we are led by such a process to the state $|-2,2,0\rangle$. The Josephson coupling mixes this state with the state $|-2,0,2\rangle$. Hence we have to consider a second set of eigenstates

$$\psi_0' = \alpha|-2,0,2\rangle + \beta|-2,2,0\rangle \ , \qquad \psi_1' = \beta|-2,0,2\rangle - \alpha|-2,2,0\rangle \ . \tag{3.102}$$

The coefficients α and β are the same as for the other pair, but the corresponding energies are shifted $E_{0/1}' = E_{0/1} - 2eV$.

Andreev reflection causes transitions between the two sets of eigenstates $\psi_0 \to \psi_0'$. The rate for this process can be obtained along the lines described in the previous Subsection for an NSN transistor. An important modification arises as compared with Eq. (3.71), since the charge transfer operators pick from the initial state the component with zero charge on the island, which has amplitude α, and select from the final state the component with two extra charges, which has amplitude β. Hence the amplitude for a Andreev reflection process between the states ψ_0 and ψ_0' with two electrons tunneling from the states $k,\uparrow$ and $k',\downarrow$ of the normal electrode is

$$A_{k,k'}(\psi_0 \to \psi_0') = \alpha\beta \sum_q T_{k,q} T_{k',-q} u_q v_q \left(\frac{1}{E_0 - E_{k,q}} + \frac{1}{E_0 - E_{k',q}} \right) \ . \tag{3.103}$$

The energy of the virtual intermediate state $|-1_k, 1_q, 0\rangle$, with one electron added to the island leaving a quasiparticle in each electrode, is $E_{k,q} = E_{\rm ch}(-1,1,0) - \epsilon_k + E_q$, where ϵ_k and $E_q = [\epsilon_q^2 + \Delta^2]^{1/2}$ are the quasiparticle energies in the normal and superconducting electrode, respectively.

The summation in Eq. (3.103) can be performed, and the rate for the Andreev reflection process is obtained by the golden rule. After summation over the initial states k and k' one finds for low temperatures and $E_0' - E_0 = -2eV \leq 0$

$$, ^{\rm A}(\psi_0 \to \psi_0') = (\alpha\beta)^2 \, a_0^2 \, \frac{G_{\rm A}}{4e^2} \, 2eV \ . \tag{3.104}$$

The rate is proportional to the product

$$\alpha^2\beta^2 = \frac{1}{4} \frac{E_{\rm J}^2}{(\delta E_{\rm ch})^2 + E_{\rm J}^2} \ , \tag{3.105}$$

which displays a typical resonance structure. The Andreev conductance $G_{\rm A}$ and the function $a_0 = a\,(\Delta/[E_{\rm ch}(-1,1,0) - E_0])$ have been defined in Eq. (3.76) and (3.74). Here we assumed that the energy $\Delta + E_{\rm ch}(-1,1,0)$ of the intermediate state lies above E_0. If the superconducting gap Δ is much larger than the charging energies with scale $E_{\rm C}$ the function a reduces to $a \approx 1$. It diverges if the energy of the virtual state coincides with that of the initial state. In the other limit, where $\Delta + E_{\rm ch}(-1,1,0)$ lies below E_0, parity effects play a role (see below).

Andreev reflection processes can also lead to transitions between the other states introduced above, with rates

$$
\begin{aligned}
,^{\mathrm{A}}(\psi_0 \to \psi_1') &= \alpha^4 a_0^2 \frac{G_{\mathrm{A}}}{4e^2} [2eV - (E_1 - E_0)]\, \Theta[2eV - (E_1 - E_0)] \,, \\
,^{\mathrm{A}}(\psi_1 \to \psi_0') &= \beta^4 a_1^2 \frac{G_{\mathrm{A}}}{4e^2} [2eV + (E_1 - E_0)] \,, \\
,^{\mathrm{A}}(\psi_1 \to \psi_1') &= (\alpha\beta)^2 a_1^2 \frac{G_{\mathrm{A}}}{4e^2} 2eV \,. \qquad (3.106)
\end{aligned}
$$

The function a_1 is defined similar as a_0, but the energy of the initial state E_0 is replaced by E_1.

Below the threshold voltage $V < V_{\mathrm{th}}$, where

$$V_{\mathrm{th}} = (E_1 - E_0)/2e \,, \qquad (3.107)$$

the only transition at low temperatures is the Andreev reflection between the states ψ_0 and ψ_0'. The resulting current, $I_{\mathrm{res}} = -2e,^{\mathrm{A}}(\psi_0 \to \psi_0')$, shows a pronounced resonant structure due to the overlap of the functions α and β. The conductance is

$$G_{\mathrm{res}} = \frac{I_{\mathrm{res}}}{V} = G_{\mathrm{A}} \frac{a_0^2}{4} \frac{E_{\mathrm{J}}^2}{(\delta E_{\mathrm{ch}})^2 + E_{\mathrm{J}}^2} \quad \text{for } V < V_{\mathrm{th}} \,. \qquad (3.108)$$

At higher voltages the Andreev reflection can take the transistor to the excited state ψ_1'. A master equation yields the probabilities for the ground and excited states

$$p_0 = \frac{,^{\mathrm{A}}(\psi_1 \to \psi_0')}{,^{\mathrm{A}}(\psi_0 \to \psi_1') + ,^{\mathrm{A}}(\psi_1 \to \psi_0')} \,, \; p_1 = 1 - p_0 \neq 0 \;\text{ for }\; V > V_{\mathrm{th}} \,. \qquad (3.109)$$

The current then is

$$I = -2e[,^{\mathrm{A}}(\psi_0 \to \psi_0') + ,^{\mathrm{A}}(\psi_0 \to \psi_1')]\, p_0 - 2e[,^{\mathrm{A}}(\psi_1 \to \psi_1') + ,^{\mathrm{A}}(\psi_1 \to \psi_0')]\, p_1 \,. \qquad (3.110)$$

For $\Delta > E_{\mathrm{C}} + E_{\mathrm{J}}/2$, near the resonance, the difference between a_0 and a_1 is small. In this case the current is a sum $I = I_{\mathrm{res}} + I_{\mathrm{th}}$, where I_{res} follows from (3.108), while the second contribution, which exists only above the threshold $V > V_{\mathrm{th}}$, is

$$
\begin{aligned}
I_{\mathrm{th}} = \frac{G_{\mathrm{A}} F_0^2}{16e} \frac{E_{\mathrm{J}}^4}{(\delta E_{\mathrm{ch}})^2 + E_{\mathrm{J}}^2} \frac{(2eV)^2 - (\delta E_{\mathrm{ch}})^2 - E_{\mathrm{J}}^2}{[(\delta E_{\mathrm{ch}})^2 + E_{\mathrm{J}}^2](2eV - \delta E_{\mathrm{ch}}) - E_{\mathrm{J}}^2 eV} \\
\times \Theta\left(2eV - \sqrt{(\delta E_{\mathrm{ch}})^2 + E_{\mathrm{J}}^2}\right) \,. \qquad (3.111)
\end{aligned}
$$

Also this current contribution has a resonant peak. A plot of the current-voltage-characteristic as a function of the gate and bias voltage is shown in Fig. 3.17.

When the superconducting gap is smaller than the charging energy $\Delta \leq E_0$, parity effects play a role. If the gate voltage is such that the energy of the initial state coincides

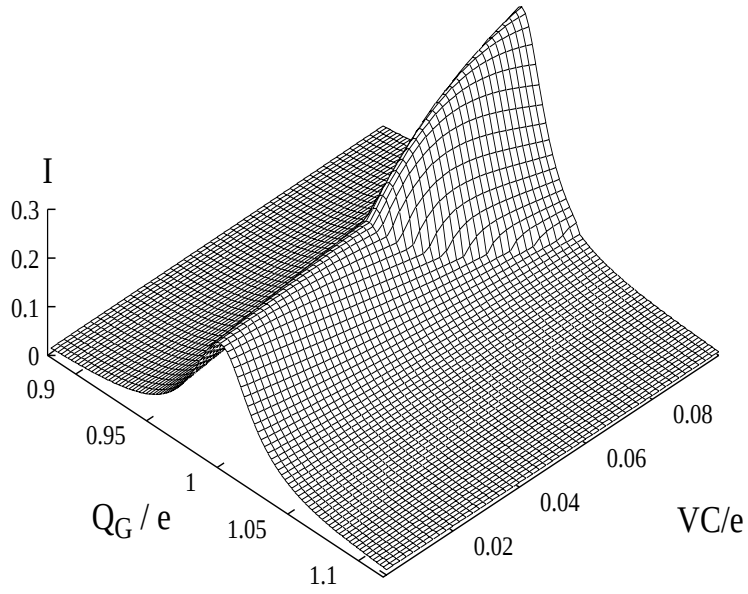

Fig. 3.17: I-V characteristic of an NSS transistor. A resonant structure due to Cooper-pair tunneling is visible in the dissipative current due to Andreev reflection.

with that of the virtual intermediate state the function a_0 diverges. This happens for $Q_\mathrm{G} = e \pm \delta Q^*_\mathrm{G}$, where

$$\delta Q^*_\mathrm{G} = \frac{e}{2}\sqrt{\left(1-\frac{\Delta}{E_\mathrm{C}}\right)^2 - \left(\frac{E_\mathrm{J}}{2E_\mathrm{C}}\right)^2}\,.$$

Clearly, at these points the perturbative treatment of Andreev reflection is no longer sufficient. However, close to these points we expect a strong increase of the current. Inside the window $e - \delta Q^*_\mathrm{G} \leq Q_\mathrm{G} \leq e + \delta Q^*_\mathrm{G}$, the ground state of the transistor is an odd state with a single quasiparticle present in the island. In this regime the current is much lower than outside. However, it is difficult to derive a precise value, since a large number of channels contribute with similar weight.

Above a threshold voltage, when $(e-Q_\mathrm{G})^2/2C - eV/2 + \Delta \leq E_0$, the odd state can be reached in a SET process, and the Andreev reflection is again "poisoned" (compare the NSN transistor). Again the odd electron tunneling creates a bottleneck for the current, which is small $I_\mathrm{SET} = e\gamma = [2eR_\mathrm{t}N_\mathrm{I}(0)\Omega_\mathrm{I}]^{-1}$. Once SET is possible the current related to Andreev reflection processes is negligible.

3.5.7 Incoherent Cooper-pair tunneling

Finally we consider situations where a mechanism is present which destroys the phase coherence of the quantum mechanical time evolution. In this case Cooper-pair tunneling can be treated perturbatively as a stochastic process. A realization of such a system is a circuit consisting of a Josephson junction in series with a voltage source and an external impedance $Z(\omega)$. It is the same setup as shown in Fig. 3.9 except that the tunnel junction has superconducting electrodes. The electrodynamic environment

can again be described by a suitable oscillator bath (see Section 3.4). An incoherent Cooper-pair tunneling process is accompanied by a transition in the bath. In analogy to Eq. (3.42) the rate for this process can be written as [40]

$$, ^{+} = \frac{\pi}{2\hbar} E_{\mathrm{J}}^2 \sum_{\mathrm{X},\mathrm{X}'} \rho_{\mathrm{bath}}(X) \left| \langle X' | \mathrm{e}^{\mathrm{i}\varphi} | X \rangle \right|^2 \delta(E_X - E_{\mathrm{X}'}) \; . \tag{3.112}$$

Note that the phase in the superconductor, which is related to the voltage by Josephson's relation $\hbar\dot{\varphi} = 2eV$, differs from the phase $\hbar\dot{\phi} = eV$ introduced in Section 3.4 by a factor 2, which accounts for the difference in charge transferred in the two cases.

The trace over the bath degrees of freedom can be performed, with the result

$$, ^{+} = \frac{E_{\mathrm{J}}^2}{\hbar^2} \int_{-\infty}^{\infty} \mathrm{d}t \exp\left(\frac{2\mathrm{i}}{\hbar} e V_{\mathrm{x}} t\right) \langle \mathrm{e}^{\mathrm{i}\varphi(t)} \mathrm{e}^{-\mathrm{i}\varphi(0)} \rangle \; . \tag{3.113}$$

Proceeding as before we can express the forward tunneling rate for a Cooper pair as

$$, ^{+} = \frac{\pi}{2\hbar} E_{\mathrm{J}}^2 \widetilde{P}(2eV) \; , \tag{3.114}$$

where $\widetilde{P}(2eV)$ has been defined by

$$\widetilde{P}(E) = \frac{1}{2\pi\hbar} \int_{-\infty}^{\infty} \mathrm{d}t \exp\left[4K(t) + \mathrm{i}\frac{Et}{\hbar}\right] \; . \tag{3.115}$$

This function $\widetilde{P}(E)$ differs from $P(E)$ introduced in (3.47) by a factor 2^2 because of the difference in the charge transferred. Except for this, much of the discussion given in Section 3.4 applies here as well. The backward tunneling rate follows simply from $, ^{-}(V) = , ^{+}(-V)$, and the current is

$$I_{\mathrm{CP}}(V) = 2e[, ^{+}(V) - , ^{-}(V)] = \frac{\pi e E_{\mathrm{J}}^2}{\hbar} [\widetilde{P}(2eV) - \widetilde{P}(-2eV)] \; . \tag{3.116}$$

The result depends strongly on the impedance. At low voltages the expansion of $\widetilde{P}$ yields $I_{\mathrm{CP}} \sim V^{2/\alpha_{\mathrm{s}}-1}$. In a high impedance environment, $\alpha_{\mathrm{s}} \equiv R_{\mathrm{K}}/R \ll 1$ the supercurrent has a Gaussian peak at $V = e/C$,

$$I_{\mathrm{CP}}(V) = I_{\max} \exp\left[-\frac{\pi^2 (CV - e)^2 / 2C}{E_{\mathrm{C}} \alpha_{\mathrm{s}}}\right] \; . \tag{3.117}$$

This feature has been denoted as "Coulomb blockade of Cooper-pair tunneling". The predicted voltage dependence has been observed by Kuzmin et al. [41].

3.6 Effective-action description

In the next two sections we will consider several aspects of transport through systems of junctions in a path-integral formulation. It is a systematic approach to include

dissipation in quantum mechanics (compare Chap. 4 and the work of Caldeira and Leggett [14, 29]). It allows us to go beyond perturbation theory, if

$$\alpha_{\rm t} \equiv R_{\rm K}/(4\pi^2 R_{\rm t}) \tag{3.118}$$

is no longer small. (For later convenience a factor $1/4\pi^2$ is included in the definition of $\alpha_{\rm t}$.) The path-integral formulation displays in a transparent way the interplay of charging and tunneling phenomena. We will rederive the tunneling rate for single electrons, cotunneling and Andreev reflection, describe Cooper-pair tunneling, but also further effects like the proximity effect and resonant tunneling. We first will review the imaginary-time approach, starting from the work of Ref. [6, 7] and include extensions discussed in Ref. [8, 9]. This approach is appropriate if we are interested in equilibrium properties such as supercurrents or the proximity effect. But we will also be able to draw conclusions about the tunneling rates. In Section 3.7 we will then present a real-time path-integral formulation, which yields directly tunneling rates and currents and allows us to describe time-dependent and nonequilibrium phenomena.

3.6.1 The effective action in imaginary times

Our aim is to study transport through systems composed of normal metal or superconducting tunnel junctions. A typical geometry is the one known from the transistor consisting of leads and an island, which is coupled capacitively to a gate voltage. The electrostatic charging energy of the system is given by Eq. (3.2). Tunneling across the junctions is described by the tunneling Hamiltonian (3.9). We consider "wide" metallic junctions, which implies that there are many transverse channels. As a result "inelastic" higher-order tunneling processes, involving different electron states for each step, dominate over those higher-order processes which involve the same state repeatedly. Accordingly, in the effective-action description presented below only simple loop diagrams have to be retained.

We are interested in the influence of charging effects on the properties of the junction system. Since the tunneling of electrons changes the charge on the island, the voltages are fluctuating quantities. They are related by the Josephson relation to the phases of the superconducting order parameters in the electrodes, $\varphi_{\rm J}$ ($j = L, R$), and that of the island, φ, if they are superconducting. When the electrodes or island are normal we still *define* a phase as the integral of the voltage

$$\varphi(\tau) \equiv \int_0^\tau {\rm d}\tau' 2eV(\tau')/\hbar \ , \tag{3.119}$$

and similar for the electrodes. A voltage drop at a junction interface can be accounted for by phase factors $\exp\{\pm i[\varphi(\tau) - \varphi_{\rm J}(\tau)]/2\}$ multiplying the tunneling matrix elements.

For definiteness we study in the following a transistor with normal or superconducting electrodes and assume that the voltages of the electrodes are fixed. In this case only fluctuations of the phase of the island need to be considered. After elimination of the microscopic electronic degrees of freedom the partition function of the junction system can be expressed as a path integral over this phase [6, 7]

$$Z = \int {\rm d}\varphi(\tau) \exp\{-S[\varphi]/\hbar\} \ . \tag{3.120}$$

It is governed by an effective action, which in an expansion in the tunneling matrix elements can be written as

$$S[\varphi] = S_{\rm ch} + S_{\rm t} + S_{\rm J} + S_{\rm Andreev} + S_{\rm SNS} \ . \tag{3.121}$$

The first term in the action is the charging energy (3.2), rewritten in terms of the phase

$$S_{\rm ch} = \int_0^{\hbar\beta} {\rm d}\tau \left[\frac{C}{2} \left(\frac{\hbar}{2e} \frac{\partial \varphi}{\partial \tau} \right)^2 + i\, Q_{\rm G} \frac{\hbar}{2e} \frac{\partial \varphi}{\partial \tau} \right] \ . \tag{3.122}$$

The remaining contributions will be discussed below, term by term.

The question arises, whether the phase is to be viewed as an extended variable defined in the range $-\infty \leq \varphi \leq \infty$ or whether it is defined on a ring. Both interpretations are possible. The first describes a system where charges can change also in a continuous fashion, for instance because of the additional flow of Ohmic currents. The second describes a situation where the charges are quantized, for instance in the island of a SET transistor [7]. In the latter case the path integral for the partition function includes a summation over winding numbers $\varphi(\hbar\beta) = \varphi(0) + 4\pi M$, where $M = 0, \pm 1, \pm 2, ...$ (Because of the factor 2 in the definition of $\varphi(\tau)$ suggested by the analogy to superconductivity, the ring has circumference 4π.) The second term in the charging action (3.122) has a meaning only in the latter case.

3.6.2 Single-particle and Cooper-pair tunneling

The second term in (3.121) describes single-electron tunneling. It is [6, 7]

$$S_{\rm t,L} = \frac{\hbar}{4} \alpha_{\rm t} \int_0^{\hbar\beta} {\rm d}\tau \int_0^{\hbar\beta} {\rm d}\tau' G_{\rm L}(\tau - \tau') G_{\rm I}(\tau' - \tau) \cos \left[\frac{\phi_{\rm L}(\tau) - \phi_{\rm L}(\tau')}{2} \right] \ , \tag{3.123}$$

which depends on $\phi_{\rm L} = \varphi - \varphi_{\rm L}$, and similar for the right junction. In a diagrammatic language, which allows us to keep track of the different contributions to the action, $S_{\rm t}$ corresponds to the "bubble" diagram shown in Fig. 3.18 a. It contains the two diagonal quasiclassical Green functions, $G_{\rm L/I}(\tau) \equiv i/N(0) \int d^3\boldsymbol{p}\, G_{\rm L/I}(\boldsymbol{p}, \tau)$, of the left side and the island. Their Fourier transforms are given by $G(\omega_\nu) = \omega_\nu / [\omega_\nu^2 + \Delta^2]^{1/2}$. In normal metals $G(\tau) = 2i/\tau$, while in a superconductor it decays like $G(\tau) \propto \exp(-\Delta|\tau|)$.

At this stage we do not want to present a derivation of the expression for $S_{\rm t}$ (which is given in Refs. [6, 7]). Rather we stress the similarity and differences to the term describing dissipative currents through an Ohmic resistor derived by Caldeira and Leggett [14] from a harmonic oscillator bath:

(i) If both electrodes are normal the product of Green functions is proportional to $1/\tau^2$ and coincides with the kernel found for Ohmic dissipation (see Chap. 4). If one or both electrodes are superconducting the kernel depends on the superconducting gap(s), which accounts for the reduction of the subgap current below a linear voltage dependence in this case.

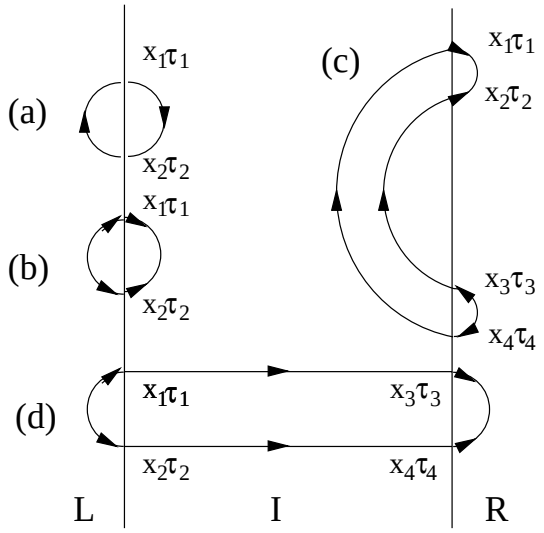

Fig. 3.18: Different processes contributing to the transport through a SET transistor: a) "bubble" diagram describing single-electron tunneling, b) Cooper-pair tunneling (if L and I are superconducting), c) "banana" diagram responsible for Andreev reflection (between a normal I and superconductor R), d) "sausage" diagram describing the correlated tunneling of a Cooper pair through both junctions (in an SNS transistor).

(ii) The second difference is the trigonometric dependence on the phase difference in contrast to a quadratic one of the Caldeira-Leggett action. Also this difference accounts for different physics. In the present problem the current is due to discrete single-electron tunneling rather than a continuous flow of charge through a resistor.

With suitable analytic continuation we can rederive from $S_{\rm t}$ the single-electron or quasiparticle tunneling rates (3.13) and (3.69). Since these results are well-known we do not discuss them here further. Rather we will demonstrate the limiting behavior, which applies for an ideal SS or SN junctions, where at low voltages, $eV \ll \Delta$, and low temperatures the quasiparticle tunneling is suppressed (vanishing subgap conductance). In this case, if the time evolution of the phase is slow on the scale given by the inverse energy gap $\hbar/\Delta$, the quasiparticle tunneling term $S_{\rm t}$ can be expanded to quadratic order in $\partial\phi/\partial\tau$. This implies that tunneling effectively renormalizes the charging energy and hence the capacitance $C_{\rm eff} = C + \delta C$. For an SS junction the result is $\delta C_{\rm SS} = (3\pi^2/16)\alpha_{\rm t} e^2/\Delta$ [6], for an ideal SN junction the equivalent result is $\delta C_{\rm NS} = 4\pi\alpha_{\rm t} e^2/\Delta$.

The next term in the action (3.121) is again of second order in the tunneling,

$$S_{\rm J,L} = \frac{\hbar}{4}\alpha_{\rm t}\int_0^{\hbar\beta} {\rm d}\tau \int_0^{\hbar\beta} {\rm d}\tau' F_{\rm L}(\tau-\tau')F_{\rm I}(\tau'-\tau)\cos\left[\frac{\phi_{\rm L}(\tau)+\phi_{\rm L}(\tau')}{2}\right] . \qquad (3.124)$$

It involves a product of two off-diagonal quasiclassical Green functions $F(\tau)$ with Fourier transform $F(\omega_\nu) = \Delta/[\omega_\nu^2 + \Delta^2]^{1/2}$. This term is appropriate for an SS interface and describes the Josephson tunneling. Diagrammatically, it corresponds again to a "bubble" diagram, shown in Fig. 3.18 b, where the two propagators are off-diagonal Green functions F. If the phases evolve slowly on the scale given by the inverse energy

gap the Josephson coupling can be simplified to

$$S_{\mathrm{J,L}} = -E_{\mathrm{J}} \int_0^{\hbar\beta} \mathrm{d}\tau \cos[\phi_{\mathrm{L}}(\tau)] \,, \tag{3.125}$$

and in this form is equivalent to the Hamiltonian (3.95).

3.6.3 Higher-order processes

In situations where quasiparticle tunneling is suppressed by the superconducting gap higher-order processes may be observable. An important example is the correlated tunneling of two electrons across a junction with a normal and a superconducting electrode. Such higher-order correlated processes require a careful analysis of the space correlations of the electron propagators. We, therefore, keep track of the location of the tunneling process and, accordingly, specify the tunneling Hamiltonian to describe tunneling at the junction interface ($z = 0$) only by choosing

$$T_{\boldsymbol{r},\boldsymbol{r}'} = \widetilde{T}\, \delta(\boldsymbol{r} - \boldsymbol{r}')\delta(z) \,. \tag{3.126}$$

Notice that this tunneling matrix element differs from the usual approximation, where $T_{k,q}$ is assumed to be independent of k and q and hence $T_{\boldsymbol{r},\boldsymbol{r}'} = T\,\delta(\boldsymbol{r})\delta(\boldsymbol{r}')$. Using (3.126) we can rederive the bubble diagram of Fig. 3.18 a. The comparison of results in both formulations yields the relation between the old and new matrix elements and the normal state tunneling conductance

$$|T|^2 = a\pi^2 \frac{\hbar^2 A}{p_F^2} |\widetilde{T}|^2 = \frac{h}{e^2 R_{\mathrm{t}} 8\pi^2 N_{\mathrm{I}}(0)\Omega_{\mathrm{I}} N_{\mathrm{L}}(0)\Omega_{\mathrm{L}}} \,. \tag{3.127}$$

Here A is the junction area and a a numerical coefficient of order one.

We can now study higher order terms. In NS junctions with vanishing quasiparticle current the leading term is the "banana" diagram, shown diagrammatically in Fig. 3.18 c. Two electron propagators on the normal-metal side are connected to off-diagonal propagators on the superconductor side (for definiteness we assume that the lead electrodes are superconducting while the island is a normal metal). This diagram describes Andreev scattering across the interface. It yields the fourth term in the action (3.121), which for the right junction becomes [20]

$$\begin{aligned} S_{\mathrm{A,R}} \;=\; & \int_0^{\hbar\beta} \mathrm{d}\tau_1 \int_0^{\hbar\beta} \mathrm{d}\tau_2 \int_0^{\hbar\beta} \mathrm{d}\tau_1' \int_0^{\hbar\beta} \mathrm{d}\tau_2' \int_A \mathrm{d}^2\boldsymbol{\rho}_1 \int_A \mathrm{d}^2\boldsymbol{\rho}_2 \int_A \mathrm{d}^2\boldsymbol{\rho}_1' \int_A \mathrm{d}^2\boldsymbol{\rho}_2' \\ & \times |\widetilde{T}|^4 F_{\mathrm{R}}(\boldsymbol{\rho}_2, \boldsymbol{\rho}_1; \tau_2 - \tau_1) G_{\mathrm{I}}(\boldsymbol{\rho}_1, \boldsymbol{\rho}_1'; \tau_1 - \tau_1') F_{\mathrm{R}}(\boldsymbol{\rho}_1', \boldsymbol{\rho}_2'; \tau_1' - \tau_2') G_{\mathrm{I}}(\boldsymbol{\rho}_2', \boldsymbol{\rho}_2; \tau_2' - \tau_2) \\ & \times \cos\left[\frac{\phi_{\mathrm{R}}(\tau_1) - \phi_{\mathrm{R}}(\tau_1') - \phi_{\mathrm{R}}(\tau_2') + \phi_{\mathrm{R}}(\tau_2)}{2}\right] . \end{aligned} \tag{3.128}$$

Here the modification of the tunneling Hamiltonian is apparent. The propagators connect the positions $\boldsymbol{\rho}$ in the junction plane where the tunneling processes occur. (They are now full Green functions, in contrast to the quasiclassical functions which

appeared in the expressions (3.123) and (3.124).) If we restrict ourselves to low voltages $eV \ll \Delta$ the short range of the off-diagonal Green functions $F(\boldsymbol{\rho}, \tau)$ in space and time and their normalization allow us to write

$$S_{\mathrm{A,R}} = \int_0^{\hbar\beta} \mathrm{d}\tau \int_0^{\hbar\beta} \mathrm{d}\tau' \int_A \mathrm{d}^2\boldsymbol{\rho} \int_A \mathrm{d}^2\boldsymbol{\rho}' \, |\widetilde{T}|^4 G_{\mathrm{I}}(\boldsymbol{\rho}, \boldsymbol{\rho}'; \tau - \tau') G_{\mathrm{I}}(\boldsymbol{\rho}', \boldsymbol{\rho}; \tau' - \tau) \times \cos\left[\phi_{\mathrm{R}}(\tau) - \phi_{\mathrm{R}}(\tau')\right] \; . \tag{3.129}$$

If the leads are made of dirty metals we perform an impurity averaging, introducing the Cooperon propagator introduced in Chap. 1, $K(\boldsymbol{\rho}, \boldsymbol{\rho}'; \tau - \tau') = \langle G_{\mathrm{I}}(\boldsymbol{\rho}, \boldsymbol{\rho}'; \tau - \tau') G_{\mathrm{I}}(\boldsymbol{\rho}', \boldsymbol{\rho}; \tau' - \tau) \rangle_{\mathrm{imp}}$. It satisfies a diffusion equation and depends on the geometry of the system. For illustration we consider a very small normal island in the absence of pair breaking effects such that electrons can propagate phase coherently between each pair of points. The integral of the Cooperon propagator then reduces to A^2/Ω_{I} and we find [20, 21]

$$S_{\mathrm{A,R}} = G_{\mathrm{A}} R_{\mathrm{K}} \int_0^{\hbar\beta} \mathrm{d}\tau \int_0^{\hbar\beta} \mathrm{d}\tau' \frac{1}{(\tau - \tau')^2} \cos\left[\phi_{\mathrm{R}}(\tau) - \phi_{\mathrm{R}}(\tau')\right] \; , \tag{3.130}$$

where G_{A} is given by (3.75) with $N_{\mathrm{ch}} = 1$. In general, the Cooperon propagator controls the range in space where electron propagation – and hence the higher-order tunneling processes – remain correlated. This allows us to evaluate the effective number of channels N_{ch} introduced by [19]. (The notation is suggested by the following picture: If g_0 denotes the dimensionless conductance per channel, then the total conductance is $g = N_{\mathrm{ch}} g_0$ and the effective (dimensionless) Andreev conductance $g_{\mathrm{A}} A \sim N_{\mathrm{ch}} g_0^2 = g^2/N_{\mathrm{ch}}$.) The problem has been analyzed in Ref. [21] for different junction geometries, including such geometries where interference effects in a magnetic field play a role.

The comparison of (3.129) and the quasiparticle term (3.123) reveals that in the low-voltage limit Andreev reflection and the associated charge transfer are very similar to ordinary single-electron tunneling in the normal state. The difference is that instead of e the charge $2e$ is transferred as can be seen from the missing factor $1/2$ in the argument of the cosine. This implies that two-electron tunneling is subject to the Coulomb blockade in much the same way as single-electron tunneling [20, 19].

3.6.4 Josephson current through SNS transistors

The last term in the action (3.121), illustrated by the "sausage" diagram in Fig. 3.18 d, describes the correlated tunneling of two electrons through both junctions. It is responsible for the Josephson coupling across an SNS structure (with tunnel barriers between the metals). For vanishing transport voltage $V_{\mathrm{L}} = V_{\mathrm{R}} = 0$ it is

$$\begin{aligned} S_{\mathrm{SNS}} = & \int_0^{\hbar\beta} \mathrm{d}\tau_1 \int_0^{\hbar\beta} \mathrm{d}\tau_2 \int_0^{\hbar\beta} \mathrm{d}\tau_1' \int_0^{\hbar\beta} \mathrm{d}\tau_2' \int_{\mathrm{A_L}} \mathrm{d}^2\boldsymbol{\rho}_1 \int_{\mathrm{A_L}} \mathrm{d}^2\boldsymbol{\rho}_2 \int_{\mathrm{A_R}} \mathrm{d}^2\boldsymbol{\rho}_1' \int_{\mathrm{A_R}} \mathrm{d}^2\boldsymbol{\rho}_2' \\ & \times |\widetilde{T}|^4 F_{\mathrm{L}}(\boldsymbol{\rho}_2, \boldsymbol{\rho}_1; \tau_2 - \tau_1) G_{\mathrm{I}}(\boldsymbol{\rho}_1, \boldsymbol{\rho}_1'; \tau_1 - \tau_1') F_{\mathrm{R}}(\boldsymbol{\rho}_1', \boldsymbol{\rho}_2'; \tau_1' - \tau_2') G_{\mathrm{I}}(\boldsymbol{\rho}_2', \boldsymbol{\rho}_2; \tau_2' - \tau_2) \\ & \times \cos\left[\frac{\varphi(\tau_1) - \varphi(\tau_1') - \varphi(\tau_2') + \varphi(\tau_2)}{2} - \varphi_{\mathrm{L}} + \varphi_{\mathrm{R}}\right] \; . \end{aligned} \tag{3.131}$$

The short range of the off-diagonal Green functions in space and time allows us to set $\tau_2 \approx \tau_1$, $\boldsymbol{\rho}_2 \approx \boldsymbol{\rho}_1$ and equivalent relations for the primed coordinates. Hence, (3.131) can be simplified to

$$S_{\rm SNS} = \int_0^{\hbar\beta} {\rm d}\tau \int_0^{\hbar\beta} {\rm d}\tau' \int_{\rm A_L} {\rm d}^2\boldsymbol{\rho} \int_{\rm A_R} {\rm d}^2\boldsymbol{\rho}' |\widetilde{T}|^4 G_{\rm I}(\boldsymbol{\rho},\boldsymbol{\rho}';\tau-\tau') G_{\rm I}(\boldsymbol{\rho}',\boldsymbol{\rho};\tau'-\tau) \times \cos\left[\varphi(\tau)-\varphi(\tau')-\varphi_{\rm L}+\varphi_{\rm R}\right] . \quad (3.132)$$

Impurity averaging introduces again the Cooperon propagator through the normal island.

The term $S_{\rm SNS}$ contributes to the free energy $\mathcal{F}$ of the system, from which we obtain the supercurrent

$$\begin{aligned} I_{\rm SNS}(\varphi_{\rm L}-\varphi_{\rm R}) &= \frac{2e}{\hbar\beta}\frac{\partial\mathcal{F}}{\partial(\varphi_{\rm L}-\varphi_{\rm R})} \\ &= \int_0^{\hbar\beta} {\rm d}\tau \int_0^{\hbar\beta} {\rm d}\tau' \int_{\rm A_L} {\rm d}^2\boldsymbol{\rho} \int_{\rm A_R} {\rm d}^2\boldsymbol{\rho}' \, |\widetilde{T}|^4 G_{\rm I}(\boldsymbol{\rho},\boldsymbol{\rho}';\tau-\tau') G_{\rm I}(\boldsymbol{\rho}',\boldsymbol{\rho};\tau'-\tau) \\ &\quad \times \langle \sin[\varphi(\tau)-\varphi(\tau')-\varphi_{\rm L}+\varphi_{\rm R}] \rangle_{\rm S_{ch}} . \end{aligned} \quad (3.133)$$

The supercurrent through a *classical* SNS structure without charging effects has been studied before by Aslamazov, Larkin, and Ovchinnikov [42]. Charging effects introduce the phase correlation function in Eq. (3.133). In an expansion in the tunneling matrix elements it is sufficient to evaluate the correlator $\langle \exp {\rm i}[\varphi(\tau)-\varphi(\tau')-\varphi_{\rm L}+\varphi_{\rm R}]\rangle_{\rm S_{ch}}$ with the charging energy $S_{\rm ch}$, given by Eq. (3.122). This is done most easily in the charge representation. The factor $\exp\{{\rm i}[\varphi(\tau)-\varphi_{\rm L}]\}$ describes the transfer of a Cooper pair in the left junction, increasing the island charge at time τ, while $\exp\{-{\rm i}[\varphi(\tau')-\varphi_{\rm R}]\}$ describes the transfer of another Cooper pair in the right junction decreasing the island charge at time τ' (see Fig. 3.19, which visualizes a more complicated process relevant for the proximity effect). Hence, for vanishing transport voltage, $V = 0$, we have

$$\langle {\rm e}^{{\rm i}[\varphi(\tau)-\varphi(\tau')]} \rangle_{\rm S_{ch}} = \frac{1}{Z_{\rm ch}} \sum_{n=-\infty}^{\infty} {\rm e}^{-\{\beta E_{\rm ch}(n,Q_{\rm G}) + [E_{\rm ch}(n\pm 2,Q_{\rm G}) + E_{\rm ch}(n,Q_{\rm G})](\tau-\tau')\}} , \quad (3.134)$$

where $Z_{\rm ch}$ is an obvious normalization. At low temperatures the sum is dominated by that $2e$ charge transfer process which costs the lowest energy difference $E_{\rm ch}\,(n \pm 2, Q_{\rm G}) - E_{\rm ch}\,(n, Q_{\rm G})$, and we have

$$\langle {\rm e}^{{\rm i}[\varphi(\tau)-\varphi(\tau')]} \rangle_{\rm S_{ch}} \approx \max\left\{\exp\left[-\left(E_{\rm ch}(n\pm 2,Q_{\rm G}) - E_{\rm ch}(n,Q_{\rm G})\right)(\tau-\tau')\right]\right\} . \quad (3.135)$$

If the island is small enough and the external time scales long enough the Cooperon propagator reduces again to a simple factor $A^2/\Omega_{\rm I}$. In this case we can generalize the result derived in Ref. [43] to obtain the following expression for the critical current

$$I_{\rm SNS}^{\rm crit} = \frac{2e}{\hbar}\frac{R_{\rm K}^2}{16 R_{\rm t,L} R_{\rm t,R}}\,\delta\epsilon\,\frac{1}{2}\sum_{\pm} \log\left[\frac{\Delta^2}{\pi^2 T^2 + (\delta E_{\rm ch}(Q_{\rm G}))^2}\right] , \quad (3.136)$$

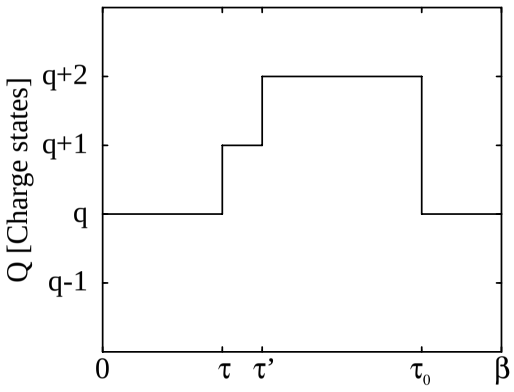

Fig. 3.19: Typical path in the charge representation. Single-particle tunneling events occur at times τ and τ' before the system returns to its original state by a 2e-charge transfer at time τ_0. The charge paths are periodic with period β.

where $\delta E_{\rm ch}(Q_{\rm G})$ is the energy difference dominating in Eq. (3.135), and $\delta\epsilon \propto 1/\Omega_{\rm I}N_{\rm I}(0)$ is the level spacing in the island. In the absence of charging effects, $\delta E_{\rm ch} = 0$ we recover the result of Ref. [42], which diverges at zero temperature indicating a breakdown of the perturbation theory. Charging effects reduce the supercurrent, and at the same time regularize the divergence.

To finish our systematic enumeration of fourth-order terms in the tunneling, we could discuss the inelastic and elastic cotunneling terms [44] using the same technique. Instead we will first comment on the influence of charging on the proximity effect and return to cotunneling processes in a real-time formulation of the next Section.

3.6.5 Proximity effect

The essence of the proximity effect is a nonvanishing pair amplitude $\langle\psi_{\rm N}\psi_{\rm N}\rangle$ in a normal metal which is in close neighborhood to a superconductor. If both are separated by a tunnel junction a nonvanishing pair amplitude arises because of tunneling. Since tunneling is affected by charging, the proximity effect is as well.

We obtain an expression for pair amplitude in the normal metal by adding a source term to the Hamiltonian, $H_\lambda = \int_0^\beta {\rm d}\tau \int d^3\boldsymbol{r}\lambda(\boldsymbol{r},\tau)\psi_{\rm N}(\boldsymbol{r},\tau)\psi_{\rm N}(\boldsymbol{r},\tau)$, and taking the functional derivative $\langle\psi_{\rm N}(\mathbf{r},\tau_0)\psi_{\rm N}(\mathbf{r},\tau_0)\rangle = -\,\delta\ln(Z)/\delta\lambda(\boldsymbol{r},\tau_0)|_{\lambda=0}$. Proceeding as before in an expansion in the tunneling we can express this contribution as

$$\langle\psi_{\rm N}(\boldsymbol{r},\tau_0)\psi_{\rm N}(\boldsymbol{r},\tau_0)\rangle = \frac{\alpha_{\rm t}\pi^2}{N_{\rm N}(0)}\int\frac{{\rm d}^3\boldsymbol{p}}{(2\pi)^3}\int_0^{\hbar\beta}{\rm d}\tau\int_0^{\hbar\beta}{\rm d}\tau' G(\boldsymbol{p},\tau)G(\boldsymbol{p},-\tau')F(\tau-\tau')$$
$$\times{\rm e}^{{\rm i}\varphi_{\rm S}}\left\langle\cos\left[\frac{\varphi(\tau)+\varphi(\tau')}{2}-\varphi(\tau_0)\right]\right\rangle_{S_{\rm ch}}. \qquad (3.137)$$

Diagrammatically, (3.137) is shown by the "proximity" diagram, (inset of Fig. 3.20). We assume that the phase $\varphi_{\rm S}$ of the superconductor remains constant in time. In com-

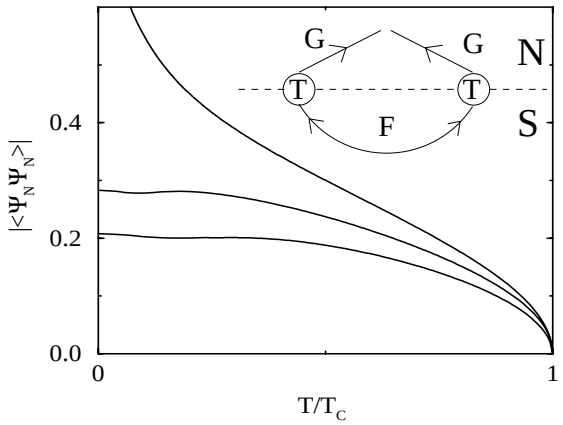

Fig. 3.20: Pair amplitude in a small island induced by the proximity effect. A normal island is coupled to a bulk superconductor. The gate voltage is chosen such that $Q_{\rm G} = 0$, and the parameters are $E_{\rm C}/\Delta = 0$ (upper curve), $E_{\rm C}/\Delta = 0.23$ (middle curve), and $E_{\rm C}/\Delta = 0.45$ (lower curve).

parison to the classical result for the proximity effect discussed by Azlamazov, Larkin, and Ovchinnikov [42] there appears a time dependent phase correlation function, which is averaged according to the dynamics of the system. Since we couple to an off-diagonal Green function the phases *add* in the exponent.

To lowest order in the tunneling the expectation value in Eq. (3.137) can be evaluated with the charging energy (3.122), which again is done most conveniently in the charge representation. The factor $\exp[i\varphi(\tau)/2]$ describes the transfer of one charge at time τ and $\exp[i\varphi(\tau')/2]$ of another one at time τ' before both of them are returned by $\exp[-{\rm i}\varphi(\tau_0)]$ at time τ_0, see Fig. 3.19. The result is

$$\left\langle \cos\left[\frac{\varphi(\tau)+\varphi(\tau')}{2}-\varphi(\tau_0)\right]\right\rangle_{\rm S_{ch}} \tag{3.138}$$

$$= \frac{1}{Z_{\rm ch}} \sum_{\rm n=-\infty}^{\infty} \mathrm{e}^{-[E_{\rm ch}(n)(\beta+\tau-\tau_0)+E_{\rm ch}(n+1)(\tau'-\tau)+E_{\rm ch}(n+2)(\tau_0-\tau')]}$$

for $\tau < \tau' < \tau_0$. Similar expressions hold for other relations between τ, τ' and τ_0.

Eq. (3.138) shows that the modification of the pair amplitude depends on the temperature and on the applied gate voltage. Results displaying the influence of charging effect on the proximity effect are shown in Fig. 3.20 and Fig. 3.21. The gate voltages can be used to modulate the proximity effect and hence the supercurrent in suitable normal metal-superconductor systems [45].

Summarizing we can say that the effective action displays in a systematic and transparent way the interplay of charging and transport properties. The latter includes single-electron and Cooper-pair tunneling, but also several extensions as the proximity effect, Andreev reflection and the supercurrent through composite structures. We have reproduced several classical results. As long as the tunneling is weak, charging effects lead to extra phase correlation functions multiplying the classical expressions. Charging suppresses the currents and proximity effects, but at the same time the gate voltage can be used to modulate these effects.

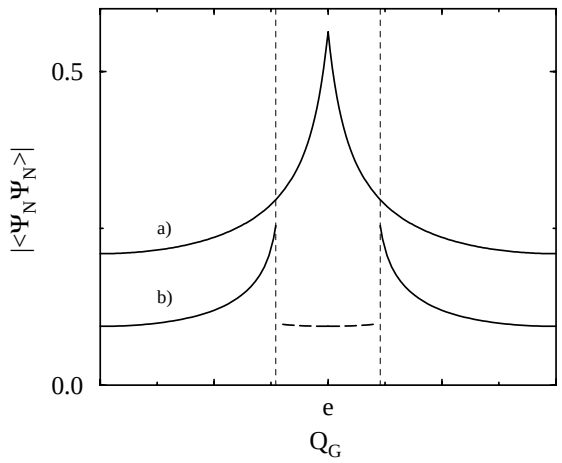

Fig. 3.21: Pair amplitude in a small island induced by the proximity effect as a function of the gate voltage, $Q_{\rm G}$. The island is superconducting and parity effects reduce the regime of the odd state of the island. The parameters are $E_{\rm C}/\Delta = 0.45$ (upper curve) and $E_{\rm C}/\Delta = 1.8$ (lower curve).

We considered here "wide" junctions, where a large number $N_{\rm ch} \gg 1$ of parallel channels contributes to the transport. As a result, higher order diagrams, such as the Andreev contribution, carry extra powers of $1/N_{\rm ch}$ as compared with higher powers of the simple-bubble diagrams $S_{\rm t}$ and $S_{\rm J}$. From a comparison of the Andreev conductance and the single-electron current in the experiments of Hergenrother et al. [22], we conclude that even in these small fabricated junctions $N_{\rm ch}$ is of order 10^3. Therefore, wide junctions with conductances as large as $1/R_{\rm K}$ are still described by the action presented above including only simple bubble diagrams. Only where the lowest-order effects are suppressed by a combination of Coulomb blockade, superconducting gap or parity effects or where further physical effects such as the Andreev current are of interest, the appropriate higher-order diagrams need to be considered.

For a renormalization group analysis of the effective-action description of normal junctions with large conductance we refer to the article [46]. As a result of strong tunneling various parameters get renormalized, and, e.g., the steps in $\langle n(Q_{\rm G})\rangle$ in the electron box are broadened. We will derive several of these results as well as several extensions in the real-time analysis of the following Section.

3.7 Real-time evolution of the density matrix

From the imaginary-time description presented in the preceding Section we derived equilibrium properties, such as the supercurrent or the pair amplitude in the proximity effect. For a systematic analysis of transition rates and I-V characteristics of driven systems with strong charging effects we present now a real-time path-integral formulation. We recover the classical (perturbative) description if the resistance $R_{\rm t}$ of a single barrier is much higher than the quantum resistance $R_{\rm K} = h/e^2$, i.e. for $\alpha_{\rm t} \equiv R_{\rm K}/(4\pi^2 R_{\rm t}) \ll 1$. In this regime, transport occurs in sequences of uncorrelated tunneling processes with

rates which can be obtained in lowest-order perturbation theory. When the dimensionless conductance α_t is not small, at very low temperatures or near resonances the classical description breaks down. Quantum fluctuations and higher-order coherent tunneling processes become important. We have discussed already cotunneling, where two electrons tunnel coherently in different junctions, thus avoiding the Coulomb blockade. Beyond this resonant tunneling, where electrons tunnel coherently back and forth between the island and the electrodes, plays a role. This phenomenon is well-known in situations where the electrons can be treated independent. Here we encounter two complications. One lies in the fact that the metallic system contains many electrons. With overwhelming probability different electron states are involved in the different transitions of the coherent process. The second arises since the Coulomb interaction is strong and, hence, cannot be accounted for in perturbation theory.

In this Section we study the time evolution of the density matrix and develop a systematic diagrammatic technique to identify the processes of sequential tunneling, inelastic cotunneling and resonant tunneling. A systematic formulation has been presented in Ref. [47] where after a separation of charge and fermionic degrees of freedom a many-body expansion technique has been used. Here we reformulate it in a real-time path-integral representation [10]. The latter is familiar from the work of Feynman and Vernon [48] and Caldeira and Leggett [49] who studied dissipation in quantum mechanics. Dissipation associated with tunneling of electrons was investigated in Refs. [6, 7]. An essential step in the present work is a transformation of the path-integral description of electron tunneling from a phase to a charge representation [7].

3.7.1 Phase representation

The time evolution of the density matrix involves a forward and a backward propagator, both of which can be expressed as path integrals. After elimination of bath or electronic degrees of freedom the two propagators are coupled. This has been described by Feynman and others [48, 49] for the case where a quantum degree of freedom is coupled to a harmonic bath. In Refs. [6, 7] the equivalent procedure for the case of a tunnel junction has been described, where the electronic degrees of freedom are eliminated.

For transparency we describe the formalism for a normal SET transistor with applied gate and transport voltages. The time evolution of its reduced density matrix can be expressed as a path integral over $\varphi(t)$, which is *defined* as the integral of the island voltage in analogy to Eq. (3.119) (in order to avoid confusion we retain the factor 2 in the definition). The phase is the conjugate variable of n, the number of excess electrons on the island. The phases of the reservoirs $\mathrm{r} = \mathrm{L}, \mathrm{R}$ are fixed by $\varphi_\mathrm{r} = 2eV_\mathrm{r}t$, without further fluctuations. Here and in the following we put $\hbar = k_\mathrm{B} = 1$. The two time-evolution operators require that we introduce two variables φ_σ with $\sigma = 1, 2$ for

the forward or backward branch [4]. Then we have

$$\rho(t_{\rm f};\varphi_{1\rm f},\varphi_{2\rm f}) = \int {\rm d}\varphi_{1\rm i}\,{\rm d}\varphi_{2\rm i} \int_{\varphi_{1\rm i}}^{\varphi_{1\rm f}} \mathcal{D}\varphi_1(t) \int_{\varphi_{2\rm i}}^{\varphi_{2\rm f}} \mathcal{D}\varphi_2(t) {\rm e}^{{\rm i}S[\varphi_1,\varphi_2]} \rho(t_{\rm i};\varphi_{1\rm i},\varphi_{2\rm i})\,. \tag{3.139}$$

The effective action is given by

$$S[\varphi_1,\varphi_2] = S_{\rm ch}[\varphi_1] - S_{\rm ch}[\varphi_2] + S_{\rm t}[\varphi_1,\varphi_2]\,. \tag{3.140}$$

The first two terms represent the charging energy

$$S_{\rm ch}[\varphi_\sigma] = \int_{t_{\rm i}}^{t_{\rm f}} {\rm d}t \left[\frac{C}{2}\left(\frac{\dot{\varphi}_\sigma}{2e}\right)^2 - Q_{\rm G}\frac{\dot{\varphi}_\sigma}{2e}\right]\,. \tag{3.141}$$

In systems with discrete charges, which can be tuned by a gate voltage $Q_{\rm G}$, the integrations over the phases φ_σ include a summation over winding numbers. For instance, in a trace we have $\varphi_{\sigma,\rm f} = \varphi_{\sigma,\rm i} + 4\pi m$; $m = 0, \pm 1, ...$ [7]. In this case the last term in $S_{\rm ch}$ does not vanish.

Electron tunneling in junction r, which is assumed to be a 'wide' junction with a large number of parallel channels, is described by [6, 7]

$$S_{\rm t,r}[\varphi_{1,\rm r},\varphi_{2,\rm r}] = 4\pi{\rm i} \sum_{\sigma,\sigma'=1,2} \int_{t_{\rm i}}^{t_{\rm f}} {\rm d}t \int_{t_{\rm i}}^{t} {\rm d}t'\, \alpha_{\rm r}^{\sigma,\sigma'}(t-t') \cos\frac{\phi_{\sigma,\rm r}(t) - \phi_{\sigma',\rm r}(t')}{2}\,, \tag{3.142}$$

where $\phi_{\sigma,\rm r} = \varphi_\sigma - \varphi_{\sigma,\rm r}$ is the appropriate phase difference. The tunneling term couples the forward and backward propagators. This arises in the step where the microscopic degrees of freedom are traced out. We notice at this stage that the effect of transport voltages can be absorbed by a shift of the arguments of the tunneling kernels in Fourier space $\omega \to \omega - eV_{\rm r}$. In this case the argument of the cos-function depends only on $\varphi_\sigma(t)$, and the kernels $\alpha_{\rm r}^{\sigma,\sigma'}$ are given in Fourier space by

$$\alpha_{\rm r}^{\sigma,1}(\omega) = (-1)^{\sigma+1}\alpha_{\rm r}^{-}(\omega) \qquad , \qquad \alpha_{\rm r}^{\sigma,2}(\omega) = (-1)^{\sigma}\alpha_{\rm r}^{+}(\omega) \tag{3.143}$$

and

$$\alpha_{\rm r}^{\pm}(\omega) = \pm\alpha_{\rm t,r}\frac{\omega - eV_{\rm r}}{\exp[\pm\beta(\omega - eV_{\rm r})] - 1}\,. \tag{3.144}$$

3.7.2 Charge representation

An important step for a systematic description of tunneling processes is the change from the phase to a charge representation , accomplished by

$$\rho(t_{\rm f};n_{1\rm f},n_{2\rm f}) \;\; = \;\; \sum_{\rm n_{1i},n_{2i}} \rho(t_{\rm i};n_{1\rm i},n_{2\rm i}) \int {\rm d}\varphi_{1\rm f}\,{\rm d}\varphi_{2\rm f}\,{\rm d}\varphi_{1\rm i}\,{\rm d}\varphi_{2\rm i}$$

[4] In order to make contact with the classical limit or the Wigner distribution the two variables $\varphi_1(t)$ and $\varphi_2(t)$ referring to the forward and backward paths, respectively, are frequently replaced by center of mass and relative coordinates, $\psi = (\varphi_1 + \varphi_2)/2$ and $\chi = \varphi_1 - \varphi_2$. The action in Ref. [5] has been written explicitly in terms of ψ and χ. For the present purpose it is more convenient to retain the original form.

$$\times \int_{\varphi_{1\mathrm{i}}}^{\varphi_{1\mathrm{f}}} \mathcal{D}\varphi_1(t) \int_{\varphi_{2\mathrm{i}}}^{\varphi_{2\mathrm{f}}} \mathcal{D}\varphi_2(t) \int \mathcal{D}n_1(t) \int \mathcal{D}n_2(t) \tag{3.145}$$

$$\times \exp\left[\sum_{\sigma=1,2} (-1)^\sigma \left(\mathrm{i}\, n_{\sigma,\mathrm{i}} \frac{\varphi_{\sigma,\mathrm{i}}}{2} - \mathrm{i}\, n_{\sigma,\mathrm{f}} \frac{\varphi_{\sigma,\mathrm{f}}}{2} + \mathrm{i}\, S_{\mathrm{ch}}[n_\sigma] - \mathrm{i} \int \mathrm{d}t\, n_\sigma \frac{\dot{\varphi}_\sigma}{2}\right)\right]$$

$$\times \exp\left[-2\pi \sum_{\mathrm{r}} \sum_{\sigma,\sigma'=1,2} \int_{t_\mathrm{i}}^{t_\mathrm{f}} \mathrm{d}t \int_{t_\mathrm{i}}^{t_\mathrm{f}} \mathrm{d}t' \alpha_{\mathrm{r}}^{\sigma,\sigma'}(t-t') \exp\left(\mathrm{i}\, \frac{\varphi_\sigma(t) - \varphi_{\sigma'}(t')}{2}\right)\right] .$$

The forward and backward propagators involve the charging energy $\exp(\pm \mathrm{i} S_{\mathrm{ch}}[n_\sigma])$, where $S_{\mathrm{ch}}[n] = \int_{t_\mathrm{i}}^{t_\mathrm{f}} \mathrm{d}t (ne - Q_\mathrm{G})^2/2C$.

To proceed we expand the tunneling part of the action $\exp(\mathrm{i}S_\mathrm{t})$ to arbitrary orders and integrate over φ_σ. Each of the exponentials $\exp[\pm \mathrm{i}\varphi_\sigma(t)/2]$ causes a change of the number of electrons on the island by ± 1 at time t on the forward or backward branch, $\sigma = 1$ or 2, respectively. These changes occur in pairs and are connected by tunneling lines representing $\alpha_{\mathrm{r}}^{\sigma,\sigma'}(t-t')$. The two correlated transitions can occur on the same or on different branches. The terms of the expansion can be visualized by diagrams; an example is displayed in Fig. 3.22. It shows the closed time-path corresponding to the forward propagator from t_i to t_f (upper line) and the backward propagator from t_f to t_i (lower line). Vertices, describing tunneling, are connected in pairs by dashed tunneling lines either within one propagator or between the two propagators.

The latter are of particular interest. Imagine we started in a diagonal state with n charges $\rho(t_\mathrm{i}) = |n\rangle\langle n|$. Then a transition, described by $\exp(\mathrm{i}[\varphi_{1,\mathrm{r}}(t) - \varphi_{2,\mathrm{r}}(t')]/2)$ changes the charge on both branches by e due to tunneling in junction r, and the density matrix acquires a finite value also for states $|n+1\rangle$. After integrating over the two times t and t', limited by $t_\mathrm{i} \le t' \le t \le t_\mathrm{f}$, we find

$$\langle n+1|\rho(t_\mathrm{f})|n+1\rangle = (t_\mathrm{f} - t_\mathrm{i}) 2\pi \alpha_{\mathrm{r}}^{+}(\delta E_{\mathrm{ch}}(n)) , \tag{3.146}$$

where $\delta E_{\mathrm{ch}}(n) = E_{\mathrm{ch}}(n+1) - E_{\mathrm{ch}}(n)$ (notice that eV_r is absorbed in the definition of α_r). Obviously we can interpret the coefficient of the time difference as transition rate, and indeed we reproduce the well-known single-electron tunneling rate.

3.7.3 Diagrams and rules

The time evolution of the density matrix is visualized in Fig. 3.22. It is expressed by the sum of all topological distinct diagrams with directed tunneling lines. The diagrams are evaluated according to the following rules:

1. Assign charge states n and the corresponding charging energy to each segment of the propagators. Segments of the forward (backward) propagator between t' and $t > t'$ carry factors $\exp[\mp \mathrm{i} E_{\mathrm{ch}}(n)(t-t')]$.

2. Each vertex represents an exponential $\exp[\pm \mathrm{i}\varphi_\sigma(t)/2]$ of the tunneling contribution to the action. It changes the charge by $\Delta n = \pm 1$.

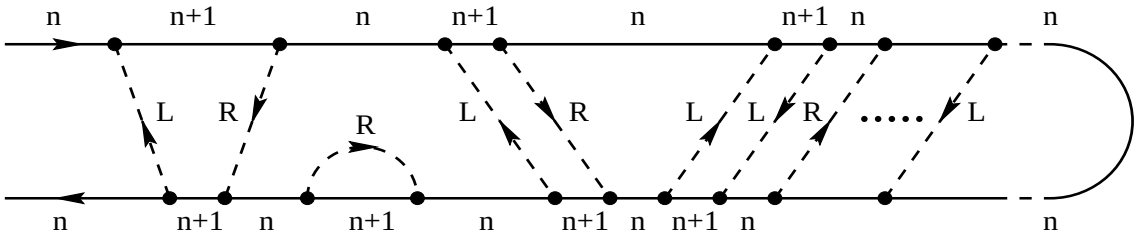

Fig. 3.22: Example of a diagram showing various tunneling processes: on the left sequential tunneling in the left and right junctions, then a term which preserves the norm, next a cotunneling process, and on the right resonant tunneling processes.

3. Pairs of vertices are connected by a directed tunneling line $\alpha_{\rm r}^{+}(t-t')\,[\alpha_{\rm r}^{-}(t-t')]$ for the electrodes ${\rm r} = {\rm L}, {\rm R}$, if the line of is running backward [forward] with respect to the closed time-path. The charge changes in units $\Delta n = +(-)1$ along the time-path by 1 if the tunneling line is directed towards (away from) the vertex.

4. Each diagram carries an prefactor $(-{\rm i})^M(-1)^m$, where M is the total number of vertices and m their number on the backward propagator.

5. Integrate over the internal times and sum over the reservoirs.

In order to calculate stationary transport properties it is convenient to change to an energy representation. For this purpose we order in each diagram the vertices from left to right and label them by $t_{\rm J}$, irrespective on which branch they are. We further set $t_{\rm i} = -\infty$ and $t_{\rm f} = t_{M+1} = 0$. We then encounter integrals of the type

$$\int_{-\infty}^{0} {\rm d}t_1 \ldots \int_{t_{M-1}}^{0} {\rm d}t_M \, {\rm e}^{\eta t_1} {\rm e}^{{\rm i}\Delta E_1 (t_2 - t_1)} \cdots {\rm e}^{-{\rm i}\Delta E_M t_M} = \frac{1}{-{\rm i}\Delta E_1 + \eta} \cdot \cdots \frac{1}{-{\rm i}\Delta E_M + \eta} \, .$$

Here ΔE_j is the difference of the energies of the upper and lower propagator and – if present – the frequency of the tunneling line within the segment limited by t_j and t_{j+1}. The convergence factor ${\rm e}^{\eta t_1}$ $(\eta \to 0^+)$ describes the adiabatic switching of the tunneling. The rules in energy representation read:

1. Draw all topological distinct diagrams. These are the same as in time space. In addition to the charging energy assigned to the propagators we assign a frequency ω to each tunneling line.

2. For each segment derived from $t_j \le t \le t_{j+1}$ with $j \ge 1$ we assign a resolvent $1/[\Delta E_j - {\rm i}\eta]$ where ΔE_j is the difference of the energies of the forward and backward propagator, plus the sum of the frequencies of the tunneling lines in the given segment. The latter have to be taken positive for lines from the left to the right and negative for lines from the right to the left.

3. The prefactor is given by $(-1)^{m+l}$, where m is the total number of vertices on the backward propagator and l the total number of resolvents.

4. For each coupling of vertices we write $\alpha_{\rm r}^{+}(\omega)\,[\alpha_{\rm r}^{-}(\omega)]$, if the tunneling line of reservoir r is going backward (forward) with respect to the closed time-path.

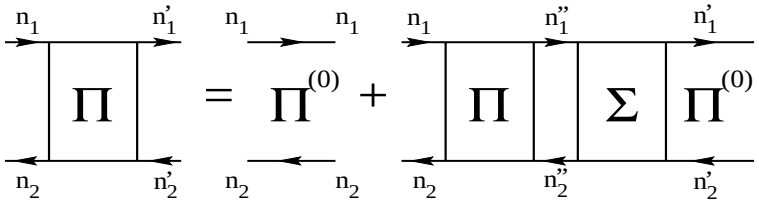

Fig. 3.23: The iteration of processes for Π, describing the time evolution of the density matrix.

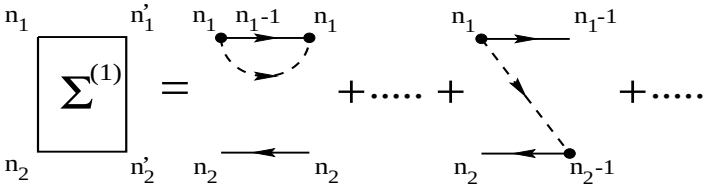

Fig. 3.24: Lowest-order approximation of the self-energy $\Sigma^{(1)}$, defined to contain no overlapping tunneling lines. Only one representative of each class is shown, the remaining ones are obtained by changing the direction of the arrows and exchanging the position on the forward and backward propagator.

5. Integrate over the frequencies of tunneling lines and sum over the reservoirs.

We denote the sum of all diagrams by $\Pi^{n_1,n_1'}_{n_2,n_2'}$, where the indices indicate the left and right charge states on the two branches, $\sigma = 1, 2$. They can be expressed as an iteration in the style of a Dyson equation, illustrated in Figs. 3.23 and 3.24, by the free propagator $\Pi^{(0)\,n_1}_{n_2}$ and an irreducible self-energy part $\Sigma^{n_1,n_1'}_{n_2,n_2'}$, defined as the sum of all diagrams where any vertical line cutting through them crosses at least one tunneling line. Hence

$$\Pi^{n_1,n_1'}_{n_2,n_2'} = \Pi^{(0)\,n_1}_{n_2}\delta_{n_1,n_1'}\delta_{n_2,n_2'} + \sum_{n_1'',n_2''} \Pi^{n_1,n_1''}_{n_2,n_2''}\,\Sigma^{n_1'',n_1'}_{n_2'',n_2'}\,\Pi^{(0)\,n_1'}_{n_2'} \;. \tag{3.147}$$

We start from a density matrix which is diagonal, $\rho(t_{\rm i}, n_1, n_2) = p^{(0)}(n_1)\delta_{n_1,n_2}$. This means it remains diagonal except during transitions described by Σ. In this case we can drop the upper indices and write, for instance, $\Sigma_{n,n'} \equiv \Sigma^{n,n'}_{n,n'}$. We identify the solution of Eq. (3.147) – after multiplication with $p^{(0)}(n)$ from the left – as the stationary distribution function $\sum_n p^{(0)}(n)\Pi_{n,n'} = p^{\rm st}(n')$. Hence

$$p^{\rm st}(n') = p^{(0)}(n') + \sum_{n''} p^{\rm st}(n'')\Sigma_{n'',n'}\Pi^{(0)}_{n'} \;. \tag{3.148}$$

The last term in this form, $\Pi^{(0)} \propto 1/i\eta$, describes a propagation in a diagonal state with $\Delta E = 0$. Hence we have $\sum_{n'} p^{\rm st}(n')\Sigma_{n',n} = 0$, and using symmetry arguments we can show that $\sum_{n'} \Sigma_{n,n'} = 0$. We thus arrive at

$$0 = -p^{\rm st}(n) \sum_{n'\neq n} \Sigma_{n,n'} + \sum_{n'\neq n} p^{\rm st}(n')\Sigma_{n',n} \;, \tag{3.149}$$

i.e. we recover the structure of a stationary master equation with transition rates given by $\Sigma_{n',n}$. In general the irreducible self-energy Σ yields the rate of all possible

correlated tunneling processes. We, furthermore, see that the stationary solution $p^{\rm st}(n)$ is independent of the initial distribution $p^{(0)}(n)$.

3.7.4 Simple examples, SET and cotunneling

For illustration, we evaluate all diagrams which contain no overlapping tunneling lines, as visualized on the left hand side of Fig. 3.22. After each transition the system is in a diagonal state of the density matrix and a probability can be assigned. These processes are also described by the master equation. In this simplest case the irreducible self-energy parts

$$\Sigma^{(1)}_{n,n\pm1} = 2\pi {\rm i} \sum_{\rm r} \alpha^{\pm}_{\rm r}(\pm\delta E^{\pm}_{\rm ch}) \qquad , \qquad \Sigma^{(1)}_{n,n} = -2\pi {\rm i} \sum_{\pm} \sum_{\rm r} \alpha^{\pm}_{\rm r}(\pm\delta E^{\pm}_{\rm ch}) \; , \tag{3.150}$$

where $\delta E^{\pm}_{\rm ch} = E_{\rm ch}(n \pm 1) - E_{\rm ch}(n)$, coincide with the single-electron tunneling rates derived within lowest-order perturbation theory above.

In situations where single-electron tunneling is suppressed by Coulomb blockade the lowest-order contribution to the current arises due to cotunneling. It is described by a diagram in Fig. 3.22 with tunneling processes in the left and in the right junction, where the corresponding lines $\alpha_{\rm L}(t_{\rm L} - t'_{\rm L})$ and $\alpha_{\rm R}(t_{\rm R} - t'_{\rm R})$ overlap in time. This means there is no intermediate state where the density matrix is diagonal, which would describe sequential tunneling. Performing the integrations we find the cotunneling rate (3.23).

3.7.5 Resonant tunneling

The perturbative approach breaks down at low temperatures or for large values for the dimensionless conductance $\alpha_{\rm t}$. Specifically we will show that the classical master equation is valid only for $\alpha_{\rm t} \ln(E_{\rm C}/2\pi T) \ll 1$, whereas for larger values resonant tunneling processes become important.

To proceed, we have to find a systematic criterion which diagrams should be retained and summed. For this, we note that during a tunneling process the reservoirs contain an electron excitation. Two parallel tunneling lines imply two such excitations. Our criterion is that we take into account only those matrix elements of the total density matrix, i.e. reservoirs plus charge states, which differ at most by two excitations in the leads or (equivalently) in the island. Graphically, this means that any vertical line will cut at most two tunneling lines.

Furthermore, we will concentrate here on situations where only two charge states with $n = 0, 1$ need to be considered. This is sufficient when the temperature, the energy difference of the two charge states $\Delta_0 \equiv E_{\rm ch}(1) - E_{\rm ch}(0)$, and the bias voltage $eV = eV_{\rm L} - eV_{\rm R}$ are small compared with $E_{\rm C}$, which is the energy associated with transitions to higher states. The combination of the two restrictions implies that no diagram contains *crossing* tunneling lines. In this case we can evaluate the irreducible self-energy analytically.

In order to sum all diagrams which contain up to two parallel tunneling lines we introduce a diagram labeled by $\phi^{n_1,n'_1}_{n_2,n'_2}({\rm r},\omega)$ (see Fig. 3.25). It has an open tunneling

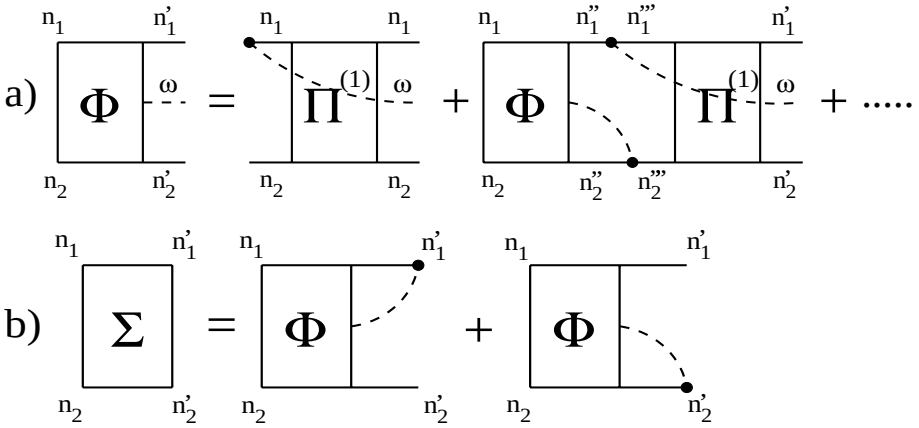

Fig. 3.25: a) Self-consistent equation for $\phi_n(\mathrm{r},\omega)$. A summation over the electrodes r and the direction of the tunneling lines is implied. b) Representation of the self-energy $\Sigma_{n,1}$ within our approximation.

line associated with tunneling in the junction r carrying the frequency ω. Consequently it remains in an off-diagonal state at one side. For the two-state problem we need only

$$\phi_n(\mathrm{r},\omega) \equiv \phi^{n,1}_{n,0}(\mathrm{r},\omega) \tag{3.151}$$

with $n = 0, 1$, for which we can formulate the iteration depicted diagrammatically in Fig. 3.25. It yields

$$\phi_n(\mathrm{r},\omega) = \pi(\omega)\left[\alpha^+_{\mathrm{r}}(\omega)\delta_{n,0} - \alpha^-_{\mathrm{r}}(\omega)\delta_{n,1} + \alpha_{\mathrm{r}}(\omega)\int \mathrm{d}\omega' \sum_{\mathrm{r}'} \frac{\phi_n(\mathrm{r}',\omega')^*}{\omega' - \omega - \mathrm{i}\eta}\right]. \tag{3.152}$$

Here we encounter the propagator $\pi(\omega) \equiv \Pi^{(1)}{}^{1,1}_{0,0}(\omega)$. It is given by the propagator Π, restricted to first order in the tunneling, starting and ending in an off-diagonal state. Furthermore, since the parallel tunneling line carries a frequency ω the energies of the upper and lower lines are shifted relative to one another. Notice that due to the restriction to a two-state problem there are no diagrams contained in $\Pi^{(1)}{}^{1,1}_{0,0}$ where a tunneling line connects the upper and lower propagator. We can express it by the first-order self-energy $\sigma(\omega) \equiv \Sigma^{(1)}{}^{1,1}_{0,0}(\omega)$, which is the off-diagonal version of the expression known from the first-order discussion, with the added complication of a parallel tunneling line with frequency ω.

The irreducible self-energy Σ is obtained from $\phi(\mathrm{r},\omega)$ by connecting the tunneling line with the appropriate direction to the upper and the lower propagator and adding both contributions (see Fig. 3.25). We get for $n = 0, 1$

$$\Sigma_{n,1} = -2\mathrm{i}\ \mathrm{Im}\int \mathrm{d}\omega \sum_{\mathrm{r}} \phi_n(\mathrm{r},\omega)\ , \tag{3.153}$$

while $\Sigma_{n,0}$ follows from the rule $\Sigma_{n,0} + \Sigma_{n,1} = 0$.

Applying our rules for the calculation of the diagrams we find

$$\pi(\omega) = \frac{1}{\omega - \Delta_0 - \sigma(\omega)} \qquad , \qquad \sigma(\omega) = -\int \mathrm{d}\omega' \frac{\alpha(\omega')}{\omega' - \omega - \mathrm{i}\eta}. \tag{3.154}$$

Here and for the following we introduce the notations $\alpha^{\pm}(\omega) = \sum_{\rm r} \alpha_{\rm r}^{\pm}(\omega)$, $\alpha_{\rm r}(\omega) = \alpha_{\rm r}^{+}(\omega) + \alpha_{\rm r}^{-}(\omega)$, $\alpha(\omega) = \alpha^{+}(\omega) + \alpha^{-}(\omega) = \sum_{\rm r} \alpha_{\rm r}(\omega)$, and $\alpha_{\rm t} = \sum_{\rm r} \alpha_{\rm t,r}$. The integral equation (3.152) is solved by

$$\Sigma_{0,1} = -\Sigma_{0,0} = 2\pi {\rm i}\, \frac{\lambda_+}{\lambda} \qquad , \qquad \Sigma_{1,0} = -\Sigma_{1,1} = 2\pi {\rm i}\, \frac{\lambda_-}{\lambda} \tag{3.155}$$

with

$$\lambda_{\pm} = \int {\rm d}\omega \alpha^{\pm}(\omega) |\pi(\omega)|^2 \qquad , \qquad \lambda = \int {\rm d}\omega |\pi(\omega)|^2 . \tag{3.156}$$

Inserting these quantities in the kinetic equation (3.149) we arrive at the stationary probabilities $P_0^{\rm st} = \lambda_-$ and $P_1^{\rm st} = \lambda_+$. Both are positive and normalized $P_0^{\rm st} + P_1^{\rm st} = 1$.

3.7.6 The current

The expression for the current at time t in the junction r can be written as

$$I_{\rm r}^{\rm st}(t) = 4\pi {\rm i} e \int_{-\infty}^{t} {\rm d}t' \sum_{\sigma} \alpha_{\rm r}^{1,\sigma}(t-t') \langle \sin[\varphi_1(t) - \varphi_\sigma(t')] \rangle \,, \tag{3.157}$$

where the expectation value is taken with the reduced density matrix discussed above, and $t = t_{\rm f}$. We, therefore, have to evaluate the two real-time correlation functions describing charge transfer processes at times t and t'

$$G^{>}(t,t') = -{\rm i} \left\langle {\rm e}^{-{\rm i}\varphi(t)} e^{{\rm i}\varphi(t')} \right\rangle \qquad , \qquad G^{<}(t,t') = {\rm i} \left\langle {\rm e}^{{\rm i}\varphi(t')} {\rm e}^{-{\rm i}\varphi(t)} \right\rangle . \tag{3.158}$$

In the stationary limit the current can be expressed by

$$I_{\rm r}^{\rm st} = -{\rm i}e \int {\rm d}\omega \left\{ \alpha_{\rm r}^{+}(\omega) G^{>}(\omega) + \alpha_{\rm r}^{-}(\omega) G^{<}(\omega) \right\} . \tag{3.159}$$

We, furthermore, introduce a spectral density for charge excitations

$$A(\omega) = \frac{1}{2\pi {\rm i}} [G^{<}(\omega) - G^{>}(\omega)] \,. \tag{3.160}$$

The correlation functions and spectral density can be evaluated in the approximation which we have used before, with the results

$$G^{(<)>}(\omega) =_{(-)}^{+} 2\pi {\rm i} \sum_{\rm r} \alpha_{\rm r}(\omega) f[{}_{(-)}^{+}(\omega - eV_{\rm r})] |\pi(\omega)|^2 \tag{3.161}$$

and

$$A(\omega) = \alpha(\omega)\, |\pi(\omega)|^2 \,. \tag{3.162}$$

The current can then be written as

$$I_{\rm r}^{\rm st} = \frac{e}{h} 4\pi^2 \int {\rm d}\omega \sum_{\rm r'} \frac{\alpha_{\rm r'}(\omega)\alpha_{\rm r}(\omega)}{\alpha(\omega)} A(\omega) [f(\omega - eV_{\rm r'}) - f(\omega - eV_{\rm r})] \,. \tag{3.163}$$

These results satisfy the conservation laws and sum rules. The current is conserved, $\sum_{\rm r} I_{\rm r}^{\rm st} = 0$, and vanishes in equilibrium when $V_{\rm r} = 0$. The spectral density is normalized $\int {\rm d}\omega\, A(\omega) = 1$, and the usual relationships between the correlation functions and the spectral density in equilibrium are reproduced. The classical result can be recovered if we use the lowest-order approximation in $\alpha_{\rm t}$ for the spectral density $A^{(0)}(\omega) = \delta(\omega - \Delta_0)$. We conclude with the observation that quantum fluctuations yield energy renormalization and broadening effects, which manifest themselves in the spectral density via the real and imaginary part of the self-energy $\sigma(\omega)$ given in Eq. (3.154). It will be evaluated in the next Section.

3.7.7 Charge fluctuations in the single-electron box

In equilibrium when $V_{\rm R} = V_{\rm L}$, the SET transistor is equivalent to the single-electron box. The energy difference $\Delta_0(Q_{\rm G}) = E_{\rm C}(1-2C_{\rm G}V_{\rm G})$ is tuned by the gate voltage. The average excess particle number can be obtained from (3.155) and (3.162) $\langle n(Q_{\rm G})\rangle = \int {\rm d}\omega f(\omega)A(\omega)$.

In the classical limit $A^{(0)}(\omega) = \delta(\omega - \Delta_0(Q_{\rm G}))$, and one obtains $\langle n^{\rm cl}(Q_{\rm G})\rangle = f(\Delta_0(Q_{\rm G}))$. It shows a step at $Q_{\rm G} = 1/2$, which is smeared only by temperature.

At larger values of $\alpha_{\rm t}$ or lower temperature we have to include the self-energy $\sigma(\omega)$ (3.154) in the spectral density (3.162). The two limits, $T = 0$ and $|\omega| \leq T$, can be analyzed analytically. In the first case, the spectral density has the form

$$A(\omega) \approx \frac{|\omega|}{\Delta_0} \frac{\widetilde{\Delta}(\omega)\widetilde{\alpha}(\omega)}{[\omega - \widetilde{\Delta}(\omega)]^2 + [\pi\widetilde{\Delta}(\omega)\widetilde{\alpha}(\omega)]^2} \;, \qquad T = 0 \tag{3.164}$$

where

$$\widetilde{\Delta}(\omega) = \frac{\Delta_0}{1 + 2\alpha_{\rm t}\ln(E_{\rm C}/|\omega|)} \frac{1}{1 + \pi^2\widetilde{\alpha}(\omega)^2} \;\;,\;\; \widetilde{\alpha}(\omega) = \frac{\alpha_{\rm t}}{1 + 2\alpha_{\rm t}\ln(E_{\rm C}/|\omega|)} \;. \tag{3.165}$$

The spectral density $A(\omega)$ has a maximum at the renormalized energy difference Δ, which is obtained from the self-consistent solution of

$$\Delta = \widetilde{\Delta}(\Delta) \;\;,\;\; \alpha = \widetilde{\alpha}(\Delta) \;. \tag{3.166}$$

It further has a broadening of order $\pi\Delta\alpha$. For $\pi\alpha \ll 1$ the broadening can be neglected. In this case our results coincide with the renormalization-group analysis of Refs. [46, 13, 50, 51].

At finite temperatures $|\omega| \leq T$, we get

$$A(\omega) \approx \frac{\Delta}{\Delta_0} \frac{\alpha\,\omega\,\coth(\omega/2T)}{[\omega - \Delta]^2 + [\pi\alpha\,\omega\,\coth(\omega/2T)]^2} \quad , \quad |\omega| \leq T \tag{3.167}$$

where

$$\Delta = \widetilde{\Delta}(T) = \frac{\Delta_0}{1 + 2\alpha_{\rm t}\ln(E_{\rm C}/2\pi T)} \;\;,\;\; \alpha = \widetilde{\alpha}(T) = \frac{\alpha_{\rm t}}{1 + 2\alpha_{\rm t}\ln(E_{\rm C}/2\pi T)} \;. \tag{3.168}$$

The broadening is of order $\pi\alpha_t T$. It adds in an important way to the thermal smearing contained in distribution functions if $\pi\alpha_t \geq 1$.

As a consequence of quantum fluctuations the step of the average charge in the electron box near the degeneracy points is washed out. We neglect broadening effects ($\pi\alpha \ll 1$) and assume that the energies of the ground state and the first excited state near the degeneracy point depend symmetrically on the distance, $E_C/4 \mp \Delta/2$. In this case the partition function is $Z \approx 2\,\exp[-E_C/4T]\,\cosh(\Delta/2T)$ and the average excess charge $\langle n\rangle$ becomes

$$\langle n\rangle = \frac{Q_G}{e} - T\frac{\partial}{\partial\Delta_0}\ln Z \approx \frac{\Delta_0-\Delta}{2\Delta_0} + \frac{\Delta}{\Delta_0}f(\Delta)\,. \tag{3.169}$$

In contrast to the result of perturbation theory (3.28) we find an anomalous but finite result. Depending on the temperature we have to choose the appropriate limiting form for Δ. At finite temperature the slope at $\Delta_0 = 0$ is $\partial\langle n\rangle/\partial\Delta_0|_{\Delta_0=0} = -\{4T[1+2\alpha_t\ln(E_C/2\pi T)]^2\}^{-1}$. It is reduced compared with the classical result $-1/4T$. This anomalous temperature dependence indicates coherent higher-order tunneling processes.

3.7.8 Conductance oscillations in the SET transistor

We will now demonstrate that the linear and nonlinear conductance of a transistor show pronounced deviations from the classical result, which are observable in an experiment. The linear conductance $G(V\to 0)$ of a transistor follows from (3.163)

$$G = -\frac{4\pi^2}{R_K}\int \mathrm{d}\omega\;\frac{\alpha_R(\omega)\alpha_L(\omega)}{\alpha(\omega)}A(\omega)f'(\omega). \tag{3.170}$$

Since the derivative of the Fermi function restricts the integration variable to the regime $|\omega| \leq T$ we can use the form (3.167) for the spectral function and perform the integration [47]. The maximum of the conductance at $\Delta_0 = 0$ and the width of the conductance peak are given by

$$G_{\max} = \frac{2\pi}{R_K}\frac{\widetilde{\alpha}_R(T)\widetilde{\alpha}_L(T)}{\widetilde{\alpha}(T)}\left[\frac{\pi}{2} - \arctan\left(\frac{(\pi\widetilde{\alpha}(T))^2-1}{2\widetilde{\alpha}(T)\pi}\right)\right]\,,$$

$$\gamma \approx \frac{1}{G_{\max}}\int \mathrm{d}\Delta_0\, G(\Delta_0) = \frac{\pi^3 T[1+2\alpha_t\ln(E_C/2\pi T)]}{\pi - 2\,\arctan\left(\frac{(\pi\widetilde{\alpha}(T))^2-1}{2\widetilde{\alpha}(T)\pi}\right)}\,. \tag{3.171}$$

Here $\widetilde{\alpha}_{L/R}(T)$ is given by (3.168) for the left and right junction and $\widetilde{\alpha}(T)$ depends on the sum of the conductances. We also introduced $\alpha_t = \alpha_{t,R} + \alpha_{t,L}$. In the regime $\alpha_t\ln(E_C/2\pi T) \ll 1$ the height and width of the conductance peak get modified as

$$G_{\max} \approx \frac{2\pi^2}{R_K}\frac{\alpha_{t,R}\;\alpha_{t,L}}{\alpha_t}\frac{1}{1+2\alpha_t\ln(E_C/2\pi T)}\quad,\quad \gamma \approx \frac{\pi^2}{2}T\left[1+2\alpha_t\ln\frac{E_C}{2\pi T}\right]\,. \tag{3.172}$$

For $\alpha_t \to 0$ we recover the classical result for sequential tunneling. The corrections depend logarithmically on temperature, indicating energy renormalization effects due

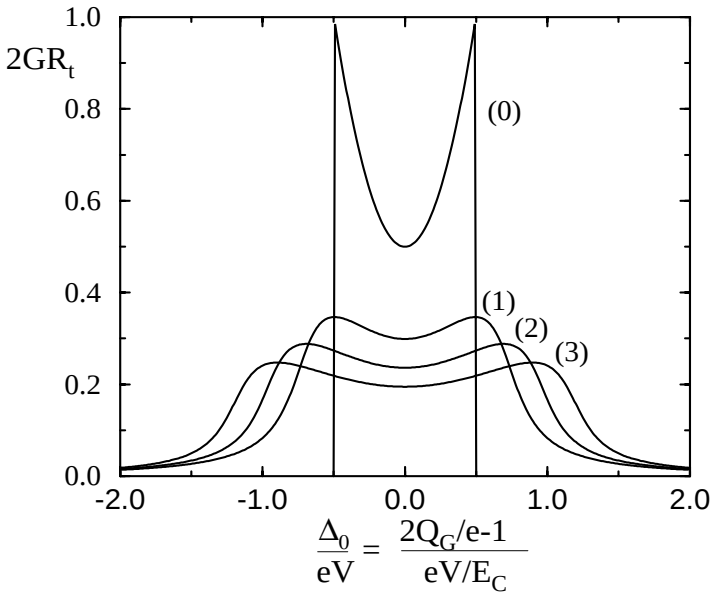

Fig. 3.26: The nonlinear differential conductance at $T = 0$ as function of the difference in charging energy between the two lowest branches $\Delta_0 = E_{\rm C}(1 - 2C_{\rm G}V_{\rm G})$, normalized to the transport voltage V. The parameters are $\alpha_{\rm t}^L = \alpha_{\rm t}^R = 0.05$ ($R_{\rm t,L} = R_{\rm t,R} = R_{\rm t}$), we consider a symmetric bias and chose (1) $eV/E_{\rm C} = 0.1$, (2) $eV/E_{\rm C} = 0.01$, (3) $eV/E_{\rm C} = 0.001$. For comparison, (0) shows the result for the classical case obtained from lowest-order perturbation theory.

to higher-order tunneling processes. For $T \to 0$ the maximum value as well as the broadening become $G_{\rm max} \sim 1/\ln T$ and $\gamma \sim T \ln T$. For $\alpha_{\rm t} \ln(E_{\rm C}/2\pi T) \sim 1$ finite life-time effects play a role, which are contained in (3.171). For a further discussion and comparison with experiment see Ref. [52].

A pronounced signature of quantum fluctuations is contained in the non-linear differential conductance $G(V) = \partial I^{\rm st}(V)/\partial V$. In this case the finite voltage provides an energy scale eV, and the renormalization and life-time effects are probed over a finite energy range even at zero temperature. The $T = 0$ result obtained from Eq. (3.163) is plotted in Fig. 3.26. For comparison we also show again the result obtained in perturbation theory. In this limit the conductance is nonzero only in the range $|\Delta_0| \leq eV/2$ with vertical steps at the edges. The result of Fig. 3.26 displays clearly the renormalization effects and, moreover, the finite life-time broadening due to the tunneling. Finite temperatures and Joule heating effects will wash out the effect. However, as long as the temperature remains lower than eV the quantum effects should be observable.

3.8 Outlook

Here we have described charging effects in normal-metal and superconducting tunnel junctions and discussed single-electron tunneling. We started from perturbation theory. We included higher-order processes where needed. This includes cotunneling in the regime of Coulomb blockade and Andreev tunneling in NS junction, where at subgap voltages single-electron tunneling is suppressed. We also described coherent and

incoherent tunneling of Cooper pairs, and we accounted for the effect of the electrodynamic environment. In the last two Sections we presented a systematic description of tunneling in metallic junctions beyond perturbation theory. Using the real-time description, the single-electron and cotunneling rates have been reproduced, but we also could go beyond and describe for instance inelastic resonant tunneling.

We have restricted ourselves to a discussion of the electron box and single-electron transistors. More complicated multi-junction systems are interesting too and important in various contexts. The electron turnstile which can serve as a current standard requires at least 4 junctions. Cotunneling processes which limit the accuracy of this standard are suppressed if one uses even more junctions. Arrays of junctions show collective behavior which depends on the competition between charging effects and tunneling. Another important extension which we had not the space to describe here are time-dependent perturbations. They produce e.g. side bands in the I-V characteristics.

Charging effects are also pronounced in the transport through semiconductor nanostructures, for instance through quantum dots in 2-dimensional electron systems. Here a new feature enters compared to the metallic case: In a small dot the electron states are quantized and the energy difference between different levels may become observable. In fabricated dots the charging energy is still the larger of the energies, but on top of the Coulomb oscillations further fine-structure related to the discrete energy levels and the occupation of excited states has been seen.

References

[1] D. V. Averin and K. K. Likharev, in *Mesoscopic Phenomena in Solids*, edited by B. L. Altshuler, P. A. Lee, and R. A. Webb (Elsevier, Amsterdam, 1991), p. 173.

[2] *Single Charge Tunneling*, NATO ASI Series, Vol. B 294, edited by H. Grabert and M. H. Devoret (Plenum Press, New York, 1992).

[3] Z. Phys. B **85** (1991).

[4] M. Tinkham, *Introduction to Superconductivity*, 2nd edition (McGraw Hill 1996).

[5] *Mesoscopic Superconductivity*, Proceedings of the NATO ARW, edited by F. W. J. Hekking, G. Schön, and D. V. Averin, Physica B **203** (1994).

[6] U. Eckern, G. Schön, and V. Ambegaokar, Phys. Rev. B **30**, 6419 (1984).

[7] G. Schön and A. D. Zaikin, Phys. Rep. **198**, 237 (1990).

[8] C. Bruder, R. Fazio, and G. Schön, Phys. Rev. B **50**, 12766 (1994);
page 240 in Ref. 4.

[9] C. Bruder, Superconductivity Review **1**, 261 (1996).

[10] J. König, H. Schoeller, G. Schön, and R. Fazio, in *Quantum Dynamics of Submicron Structures*, NATO ASI Series B **291**, edited by H. Cerdeira, B. Kramer, and G. Schön (Kluwer 1995), p. 221;
J. König, H. Schoeller, and G. Schön, Europhys. Lett. **31**, 31 (1995).

[11] E. Ben-Jacob, E. Mottola, and G. Schön, Phys. Rev. Lett. **51**, 2064 (1983).

[12] K. Mullen, E. Ben-Jacob, R. C. Jaklevic, and Z. Schuss, Phys. Rev. B **37**, 98 (1988).

[13] L. I. Glazman and K. A. Matveev, Sov. Phys. JETP. **71**, 1031 (1990);
K. A. Matveev, Sov. Phys. JETP **72**, 892 (1991).

[14] A. O. Caldeira and A. J. Leggett, Ann. Phys. (NY) **149**, 374 (1983).

[15] A. A. Odintsov, Zh. Eksp. Teor. Fiz. **94**, 312 (1988) [Sov. Phys. JETP **67**, 1265].

[16] S. V. Panyukov and A. D. Zaikin, J. Low Temp. Phys. **73**, 1 (1988).

[17] see e.g. J.P. Kauppinen and J.P. Pekola, Phys. Rev. Lett. **77**, 3889 (1996).

[18] G. Falci, V. Bubanja, and G. Schön, Z. Phys. B **85**, 451 (1991).

[19] F. W. J. Hekking, L. I. Glazman, K. A. Matveev, and R. I. Shekhter, Phys. Rev. Lett. **70**, 4138 (1993).

[20] F. Guinea and G. Schön, Physica B **152**, 165 (1988).

[21] F. W. J. Hekking and Yu. V. Nazarov, Phys. Rev. Lett. **71**, 1625 (1993).

[22] J. M. Hergenrother, M. T. Tuominen, and M. Tinkham, Phys. Rev. Lett. **72**, 1742 (1994);
J. M. Hergenrother, M. T. Tuominen, J. G. Lu, D. C. Ralph, and M. Tinkham, page 327 in Ref. 4.

[23] D. V. Averin and Yu. V. Nazarov, Phys. Rev. Lett. **69**, 1993 (1992).

[24] P. Lafarge, P. Joyez, D. Esteve, C. Urbina, and M. H. Devoret, Phys. Rev. Lett. **70**, 994 (1993).

[25] M. T. Tuominen, J. M. Hergenrother, T. S. Tighe, and M. Tinkham, Phys. Rev. Lett. **69**, 1997 (1992); Phys. Rev. B **47**, 11599 (1993).

[26] T. M. Eiles, J. M. Martinis, and M. H. Devoret, Phys. Rev. Lett. **70**, 1862 (1993).

[27] G. Schön and A. D. Zaikin, Europhys. Lett. **26**, 695 (1994);
G. Schön, J. Siewert, and A. D. Zaikin, page 340 in Ref. [5].

[28] M. Tinkham, Phys. Rev. B **6**, 1747 (1972);
A. Schmid and G. Schön, J. Low Temp. Phys. **20**, 207 (1975).

[29] U. Weiss, *Quantum Dissipative Systems*, Series in Modern Condensed Matter Physics, Vol. 2 (World Scientific, 1993).

[30] F. W. J. Hekking, L. I. Glazman, and G. Schön, Phys. Rev. B **51**, 15312 (1995).

[31] K.A. Matveev, M. Gisselfält, L. I. Glazman, M. Jonson, and R. I. Shekter, Phys. Rev. Lett. **70**, 2940 (1993).

[32] P. Joyez, P. Lafarge, A. Filipe, D. Esteve, and M. H. Devoret, Phys. Rev. Lett. **72**, 2458 (1994).

[33] K. A. Matveev, L. I. Glazman, and R. I. Shekter, Mod. Phys. Lett. B **8**, No 15 (1994).

[34] A. Maassen v. d. Brink, G. Schön, and L. J. Geerligs, Phys. Rev. Lett. **67**, 3030 (1991);
A. Maassen v. d. Brink, A. A. Odintsov, P. A. Bobbert, and G. Schön, Z. Phys. B **85**, 459 (1991).

[35] D. B. Haviland, Y. Harada, P. Delsing, C. D. Chen, and T. Claeson, Phys. Rev. Lett. **73**, 1541 (1994).

[36] J. Siewert and G. Schön, Phys. Rev. B **54**, 7421 (1996).

[37] M. H. Devoret, private communication.

[38] A. Widom, G. Megaloudis, T. D. Clark, H. Prance, and R. J. Prance, J. Phys. A **15**, 3877 (1982).

[39] K. K. Likharev and A. B. Zorin, J. Low Temp. Phys. **59** 347 (1985).

[40] D. V. Averin, Yu. V. Nazarov, and A. A. Odintsov, Physica B **165&166**, 945 (1990).

[41] L. S. Kuzmin, Yu. V. Nazarov, D. B. Haviland, P. Delsing, and T. Claeson, Phys. Rev. Lett. **67**, 1161 (1991).

[42] L. G. Aslamazov, A. I. Larkin, and Yu. N. Ovchinnikov, Sov. Phys. JETP **28**, 171 (1969).

[43] R. Bauernschmitt, J. Siewert, A. A. Odintsov, and Yu. V. Nazarov, Phys. Rev. B **49**, 4076 (1994).

[44] D. V. Averin and Yu. V. Nazarov, in Ref. [2].

[45] R. Fazio, C. Bruder, A. van Otterlo, and G. Schön, page 247 in Ref. [5].

[46] G. Falci, G. Schön, and G. T. Zimanyi, Phys. Rev. Lett. **74**, 3257 (1995).

[47] H. Schoeller and G. Schön, Phys. Rev. B **50**, 18436 (1994).

[48] R. P. Feynman and F. L. Vernon, Ann. Phys. (N.Y.) **24**, 118 (1963).

[49] A. O. Caldeira and A. J. Leggett, Physica A **121**, 587 (1983).

[50] S. V. Panyukov and A. D. Zaikin, Phys. Rev. Lett. **67**, 3168 (1991);
D. S. Golubev and A. D. Zaikin, Phys. Rev. B **50**, 8736 (1994).

[51] H. Grabert, Phys. Rev. B **50**, 17364 (1994);
X. Wang and H. Grabert, Phys. Rev. B **53**, 12621 (1996).

[52] J. König, H. Schoeller, and G. Schön, Phys. Rev. Lett. **78**, 4482 (1997); P. Joyez, V. Bouchiat, D. Esteve, C. Urbina and M. Devoret, Phys. Rev. Lett. **79**, 1349 (1997).